Evaluation of Hypoxia Induced Regulation of Nucleoside and Amino Acid Membrane Transporters in Breast Cancer

by

Daniel Krys

A thesis submitted in partial fulfillment of the requirements for the degree of

Master of Science

in

Cancer Sciences

Department of Oncology
University of Alberta

ABSTRACT

Positron Emission Tomography (PET) utilizes radioactively tagged molecules to identify cancerous tissue. In most cases, membrane transporters control entry of these molecules into human cancer cells. Hypoxia-inducible factor (HIF)-1 is the master homeostatic regulator during hypoxia in human cancer cells. Rapid cell proliferation, as seen in cancer, isolates regions of tumors from blood vessels. Oxygen diffusion becomes too distant, which induces hypoxia and activates the HIF-1 pathway and induces changes within those cells. Regulation of hypoxic responses and induction of malignant reprogramming is maintained by HIF-1. HIF-1 controls expression of hexose, nucleoside, and amino acid transporters and for this reason is partly responsible for increased proliferation and metabolism seen in cancer cells. Upregulated expression of multiple target genes such as membrane transporters like Glucose transporter 1 (GLUT1), the primary glucose transporter is necessary to facilitate the Warburg Effect. Recently we have also demonstrated regulation of GLUT5, the cell's primary fructose transporter, under hypoxia in breast cancer (BC). Currently, [^{18}F]-fluorodeoxyglucose ([^{18}F]FDG), a radiotracer transported into cells by GLUT1, is the "gold" standard and the only approved radiotracer for PET imaging of BC. [^{18}F]FDG uptake, is not consistent across BC subtypes therefore other radiotracers must be explored. We studied protein levels and functionality of human equilibrative nucleoside transporters 1 and 2, and amino acid transporters LAT1, x_c-, ASCT1, and ASCT2 under normoxic and hypoxic conditions using western blot experiments, flow cytometry, and/or confocal microscopy. Cellular uptake experiments were performed with 3'-deoxy-3'-L-[^{18}F]fluorothymidine ([^{18}F]FLT) for hENT1, 3,4-dihydroxy-6-(^{18}F)-fluoro-L-phenylalanine ([^{18}F]FDOPA) for LAT1, and (4S)-4-(3-^{18}F-fluoropropyl)-L-glutamate ([^{18}F]FPSG) for x_c-, in estrogen receptor positive (ER(+)) MCF7 and MDA-MB231 triple-negative BC (TNBC) cells.

In vitro [^{18}F]FLT uptake was higher in MDA-MB231 than in MCF7: 242 ± 9 % vs. 147 ± 18 % radioactivity/mg protein after 60 minutes under normoxia. Immunoblot analysis revealed higher hENT1 levels in MDA-MB231, and higher thymidine kinase 1 (TK1) in MCF7. Data indicated that [^{18}F]FLT uptake and hENT1 levels were not influenced significantly by hypoxia. *In vitro* inhibition experiments suggest involvement of both hENT1 and hENT2 [^{18}F]FLT uptake into MDA-MB231. *In vivo* PET imaging revealed comparable tumor uptake in MCF7 and MDA-MB231 tumors: SUV_{60min} 0.96±0.05 vs. 0.89±0.08 (n=3). LAT1 expression was higher in ER(+) MCF7 versus MDA-MB231 cells. [^{18}F]FDOPA cell uptakes revealed greater uptake in ER(+) MCF7 cells (467 ± 98 %) compared to TNBC MDA-MB231 cells (105 ± 54 %) under normoxic conditions at 30 min. ASCT1 and ASCT2 did not exhibit any differentiating protein levels in the BC cell lines. In MDA-MB231, system x_c- displayed high protein levels and high *in vitro* and *in vivo* uptakes with [^{18}F]FSPG. Hypoxia significantly increased [^{18}F]FDOPA uptake in MCF7 cells at 15 and 30 mins, and in MDA-MB231 cells at 30 and 60 mins. [^{18}F]FSPG uptake was increased in MDA-MB231 cells under hypoxia at 30 and 60 mins: 95 ± 34 % vs. 40 ± 9.8 % and 164 ± 37 % vs. 127 ± 33 %. *In vivo* PET imaging revealed greater tumor uptake of [^{18}F]FDOPA in MCF7 tumor models and [^{18}F]FSPG in MDA-MB231 tumor models.

Our study demonstrates that hypoxia has significant effects on amino acid transport as tested with [^{18}F]FDOPA and [^{18}F]FSPG in BC. Overall, there is increased transport of [^{18}F]FLT and of [^{18}F]FPSG in MDA-MB231 cells, while [^{18}F]FDOPA is increased in MCF7 cells. Higher hENT1 expression in MDA-MB231 seems to drive nucleoside transport, while higher TK1 expression in MCF7 seems to be responsible for [^{18}F]FLT retention in ER(+) tumors. We see minimal hypoxic regulation of protein levels of these transporters in both cell lines, but do see high activity of x_c- in MDA-MB231 and LAT1 in MCF7.

PREFACE

Parts of this thesis have been submitted/ will be submitted for publication as the following:

Chapter 2 of this Master Thesis. has been published as **Krys, D.,** Hamann I., Wuest, M., Wuest, F. **"**Effect of hypoxia on human equilibrative nucleoside transporters; hENT1 and hENT2 in breast cancer." to *FASEB J.* I was responsible for cell culture, western blot experiments, cell imaging, *in vitro* cell-uptake experiments, flow cytometry, analysis, contributed to the animal experiments, and wrote the manuscript; I. Hamann contributed to cell culture, Western blot experiments, and flow cytometry; M. Wuest performed all *in vivo* PET experiments and analysis, and wrote portions of and revised the manuscript; F. Wuest was responsible for the design of the study and critically reviewed the manuscript; and all authors read and approved the final manuscript and agreed to be accountable for the integrity of the work. All animal experiments were carried out in accordance with guidelines of the Canadian Council on Animal Care (CCAC) and approved (AC 15222) by the local Animal Care Committee of the Cross Cancer Institute (CCI).

Chapter 3 of this Master Thesis will be submitted as **Krys, D.,** Mattingly, S., Glubrecht, D., Wuest, M., Wuest, F. "Effect of hypoxia on amino acid transporters; ASCT1, ASCT2, LAT1, and x_c- in breast cancer, analyzed with [^{18}F]FDOPA and [^{18}F]FSPG". Unsubmitted. I was responsible for cell culture, Western blot experiments, *in vitro* cell-uptake experiments, analysis, contributed to the animal experiments, and wrote the manuscript; S. Mattingly for the preparation of [^{18}F]FSPG, the writing of the [^{18}F]FSPG radiosynthesis protocol, and supplemental information; D. Glubrecht for the entirety of the immunohistochemistry work; M.

Wuest performed all *in vivo* PET experiments and analysis, and wrote portions of and revised the manuscript; F. Wuest was responsible for the design of the study and critically reviewed the manuscript; and all authors read and approved the final manuscript and agreed to be accountable for the integrity of the work. All animal experiments were carried out in accordance with guidelines of the Canadian Council on Animal Care (CCAC) and approved (AC 15222) by the local Animal Care Committee of the Cross Cancer Institute (CCI).

ACKNOWLEDGEMENTS

Firstly, I would like to thank Dr. Frank Wuest for all his support over the past few years. Starting in his lab as an undergraduate summer research student was my first experience in research, and without his oversight and vision for this project that I began in the summer of 2015, I do firmly believe that I would not be at the same level in my career that I am today. Dr. Wuest has provided me with references, discussions, and has given me the opportunity to attend many conferences where I was able to present my research and network.

Aside from Dr. Frank Wuest, I have received immense assistance from many members of the Wuest lab group. Dr. Ingrit Hamann deserves great recognition for being my in-lab supervisor and helping me hone all of the skills that I gained throughout my research experience in the Wuest lab group. Dr. Melinda Wuest has helped immensely with project planning and helping me understand the data that I have collected. In addition to these two that were directly involved with my project, I would like to thank all the current and past members of the Wuest group who have made working in this lab such a great pleasure, with daily discussions at lunch, after work get-togethers, and in general any help I received with my project. Thanks goes out to: Marcus Litchfield, Cody Bergman, Dr. Susan Richter, Dr. Vincent Bouvet, Dr. Michael Wagner, Dr. Stephanie Mattingly, Jennifer Dufour, Alison Marshall, Samantha Leier, Simon Ferguson, Richard Yuen, and Jenilee Way.

In addition to my lab group, I would like to thank my Master thesis supervisors Dr. Elaine Leslie and Dr. Michael Sawyer. Dr. Leslie has been a supervisor for my project since the completion of my Physiology 467 project. I thank her for all her support and assistance with my project over the past 4 years.

I would also like to acknowledge all the funding I have received during my Master's Thesis. I gratefully thank the Dianne and Irving Kipnes Foundation for their generous support of the Wuest Laboratory group. I also acknowledge the Alberta Cancer Foundation (ACF) Antoine Noujaim Graduate Studentship, the Faculty of Medicine and Dentistry (FoMD) 75th Anniversary Award from the University of Alberta, the Faculty of Graduate Studies and Research (FGSR) for the dual awarding of the full Master's level Queen Elizabeth II Graduate Scholarship, the Government of Alberta Student Aid program, and the La Vie en Rose Scholarship for Breast Cancer Research awarded by the Cancer Research Institute of Northern Alberta (CRINA). I acknowledge travel funding I have received for research conferences from CRINA-ACF for the 2017 Canadian Cancer Research Conference and from the FGSR Marie Louise Imrie Graduate Student Award for travel to the 2018 Canadian Society for Molecular Biosciences (CSMB)-Membrane Proteins in Health and Disease Conference.

I thank Dr. John Wilson, David Clendening, and Blake Lazurko from the Edmonton Radiopharmaceutical Center for ^{18}F production and the preparation of [^{18}F]FDOPA. The authors thank Ali Akbari and Cody Bergman for preparation of [^{18}F]FLT. I am also grateful to Dan McGinn for supporting the animal work and Dr. Hans-Soenke Jans for technical help and support of the PET imaging experiments. I also thank Dr. Xuejun Sun and Geraldine Barron of the Cell Imaging Facility for their help with the cell imaging experiments.

Last but not least, I would like to thank my family. If not for their constant and unwavering support throughout my academic career, all of my achievements would have not been possible.

Table of Contents

List of Figures

List of Abbreviations

[^{64}Cu]ATSM	[^{64}Cu]Cu-diacetyl-bis(*N*4-methylthiosemicarbazone)
[^{18}F]FACBC	[^{18}F]-fluciclovine
[^{18}F]FAZA	[^{18}F]fluoroazomycin arabinoside
6-[^{18}F]FDF	6-deoxy-6-[^{18}F]fluoro-D-fructose
[^{18}F]FDG	2-deoxy-2-[^{18}F]fluoro-D-glucose
[^{18}F]FDOPA	3,4-dihydroxy-6-(^{18}F)-fluoro-L-phenylalanine
[^{18}F]FET	O-(2-^{18}F-fluoroethyl)-L-tyrosine
[^{18}F]FLT	3'-deoxy-3'-L-[^{18}F]fluorothymidine
[^{18}F]FPhPA	2-amino-5-(4-[^{18}F]fluorophenyl)pent-4-ynoic acid
[^{18}F]FSPG	(4S)-4-(3-^{18}F-fluoropropyl)-L-glutamate
AA	amino acids
Ab	antibody
ASCT	alanine, serine, cysteine transporter
ATP	adenosine triphosphate
BC	breast cancer
BCA assay	bicinchoninic acid assay

BCH	2-amino-2-norbornanecarboxylic acid
CA-IX	carbonic anhydrase IX
CT	computed tomography
EAA	excitatory amino acids
ER+	estrogen receptor positive
GLUT	facilitative glucose transporter
GSH	glutathione
FBS	fetal bovine serum
hENT	human equilibrative nucleoside transporter
FIH	factor inhibiting HIF-1 protein
HIF	hypoxia-inducible factor
HPLC	high performance liquid chromatography
IGF	Insulin-like growth factors
LAT	large amino acid transporter
LDHA	lactate dehydrogenase A
MCT4	monocarboxylate transporter 4
MRI	magnetic resonance imaging

$mTORC_1$	the mechanistic target of rapamycin complex 1
NBMPR	*S*-(4-nitrobenzyl)-6-thioinosine
NMR	Nuclear magnetic resonance
NRF2	NF E2 related factor 2
ODD	oxygen dependent degradation domain
PBS	phosphate-buffered saline
PDGF	platelet derived growth factor
PET	positron emission tomography
PHD-2	proline hydroxylase 2
PI3K	phosphoinositide 3-kinase
PR	progesterone receptor
ROI	region of interest
ROS	reactive oxygen species
SAHENTA	5′-S-[2-(6-aminohexanamido)]ethyl-6-N-(4-nitrobenzyl)-5′-thioadenosine
SUV	standardized uptake value
TAC	time-activity curve
TBS	Tris-buffered saline

TBST	Tris-buffered saline containing 0.05% Tween 20
TGF	transcription derived growth factor
TK1	thymidine kinase 1
TMR	tumor-to-muscle ratio
TNBC	triple-negative breast cancer
VEGF	vascular endothelial growth factor
VHL	von Hippel Lindau factor

CHAPTER 1

INTRODUCTION

1.1 Hypoxic Regulation of Cancer

1.11 Hypoxia

Cellular oxygen supply is necessary for maintaining cellular function. Humans maintain oxygenation of tissue through respiration and circulation of oxygenated blood. When a sufficient supply of oxygenated blood does not reach its intended target due to problems such as in pathophysiological situations of ischemia, or rapid cellular growth, significant changes are seen in cell microenvironments.

In cancer, and in particular solid tumors, rapid cellular growth can cause regions of hypoxia to develop. Due to such cellular proliferation seen in cancer, certain cells may become too distant for oxygen to diffuse to. Specifically, it has been determined that oxygen can diffuse a maximum of 100-180 μm from the end of the nearest capillary (1). Cellular mechanisms must change quickly in order to adapt to a decreased supply of oxygen. Cancer cells are able to quickly change from aerobic to anaerobic metabolism, which causes many changes within the tumour cells and their microenvironment. Without oxygen as a final electron acceptor in glycolysis, there are decreased amounts of ATP produced per each nutrient molecule (glucose, fructose, etc.). This results in the formation of acidic products such as lactic acid. To sustain function, more nutrient molecules must be shuttled in to compensate for the lack of oxygen and decreased ATP production generated through anaerobic metabolism.

The processes that allow tumour cells to survive in hypoxic environments are significantly different than the processes in healthy tissue. Whereas in instances of stroke or arterial blockage, tissues beyond such impasses can only survive for short periods of time, cancer cells are able to adapt and survive limited oxygen diffusion with mechanisms mainly mediated by the hypoxia-inducible factor (HIF)-1 (1).

1.12 HIF-1

HIF-1 is the master homeostatic regulator in human cells when exposed to decreased concentrations of oxygen. Due to its major role in responding to hypoxia in human cells, there have been many reviews highlighting these functions. One in particular, a review recently published by Kakkad *et al.* (2), discusses hypoxia, HIF-1, and the potential options for PET imaging of hypoxia in cancer.

HIF-1 in particular is a heterodimeric protein which consists of α and β subunits. The α subunit is oxygen-regulated, while the β subunit is constitutively expressed (2). The oxygen sensing property of HIF-1α plays an important role in the expression of proteins and mediating cellular metabolism in response to hypoxia. Through certain binding domains located on HIF-1, the protein is able to interact with a multitude of cellular targets. One of the most important sites for HIF-1 is the oxygen-dependent degradation domain (ODD) which interacts with proline-hydroxylase-2 (PHD-2) and factor inhibiting HIF-1 (FIH) proteins (2). These proteins ensure full repression of the HIF-1 signalling pathway by interacting with the oxygen-sensing HIF-1α subunit and marking it for degradation during normoxia via the von Hippel-Lindau (VHL) protein, which recruits E3 ubiquitin ligase (2). In hypoxic situations however, the PHD-2 and FIH proteins become inactive due to the lack of available oxygen. Without these two inhibitory proteins hydroxylating the ODD, HIF-1α is stabilized and is able to heterodimerize with the HIF-1β subunit in the nucleus, resulting in gene transcription (1).

Multiple PET radiotracers have been identified for their potential use in imaging hypoxia and the various indirect effects of HIF-1α on cellular processes. These cellular processes, as described in the subsequent sections of this introduction, are effector proteins from HIF-1α pathway activation, such as plasma membrane transporters of cancer cells. Currently, there are no radiotracers that are able to image HIF-1α levels directly, though our research group is currently

exploring this novel approach. Hypoxia, however can be imaged directly because of the changes to extracellular and intracellular microenvironments of cancer cells and other ischemic tissues. The reducing conditions produced by hypoxia are essential for the cellular trapping of [^{64}Cu]Cu-diacetyl-bis(*N*4-methylthiosemicarbazone) ([^{64}Cu]ATSM) (3) and ^{18}F-fluoroazomycin arabinoside (^{18}F-FAZA) (4), while in normoxic cells they are washed out. Hypoxic regions of tumors are highly resistant to radiation therapy as cells escape radiation-induced oxygen radical formation and subsequent DNA damage. Knowing this characteristic of a specific tumor this will allow physicians to better plan their patient's treatments.

1.2 Membrane Transporters in Cancer

Plasma membrane transporters are essential for the proper shuttling of nutrients needed for the survival of cells. In pathophysiological events such as cancer, the expression of plasma membrane transporters are altered, therefore fueling the progression and proliferation of cancer. In solid tumors, as is the case with breast cancer, membrane transporter's expression and function are regulated by different signalling pathways. As mentioned in the previous section, hypoxia and the related HIF-1α play major roles in membrane transporter regulation. Multiple review papers have discussed these and other factors that make membrane transporters an attractive target for therapy development and targeting by PET (5,6). The following section will highlight and give a brief summary of some of the major membrane transporter categories and their relationship with progression of breast cancer, regulation by hypoxia, and inroads made by PET researchers in imaging their expression and subsequent metabolic profiles.

1.21 Hexose Membrane Transporters

Upregulated hexose metabolism in cancer, which has been characterized by the "Warburg" effect, is widely seen as a driving mechanism in cancer proliferation (7,8). To facilitate the Warburg effect, many altered cellular pathways are needed, such as with HIF-1 and PI3K, which are central for the expression of cancer cell proteins (7). The hypoxia induced, transcription factor HIF-1α has been shown to activate the transcription of *SLC2A1* and *SLC2A3*, gene that encode GLUT1; the cell's primary glucose transporter, and GLUT3; a high affinity glucose transporter (4). In addition to these transporters, our research group has explored relationships between hypoxia and GLUT2; a glucose and fructose transporter, and GLUT5; the cell's primary fructose transporter. We have found that GLUT5 is regulated by hypoxia, while GLUT2 is not (9). In addition to transport proteins HIF-1α also activates transcription of genes that encode hexokinase, the first enzyme in the glycolytic pathway (10). Both Lactate dehydrogenase A (LDHA) and Monocarboxylate transporter 4 (MCT4) are needed for conversion of pyruvate to lactate and the shuttling of lactate out of the cell are regulated by HIF-1α (7,11).

The combination of the effects of dysregulated pathways that lead to altered expression of hexose membrane transporters in cancer make them attractive targets for therapy and PET imaging radiotracers. Specifically, one of the most widely used imaging molecules clinically is the glucose analogue 2-deoxy-2-[^{18}F]fluoro-D-glucose ([^{18}F]FDG). Currently, [^{18}F]FDG is the "gold" standard for PET imaging in BC, especially for tumor staging, detection of recurrent disease, and monitoring of treatment response (12). Though [^{18}F]FDG is considered the "gold" standard, there are many issues with false-positives and false-negatives, as often rheumatic diseases display high glucose metabolism (13) and certain cancers display low GLUT1 expression, which is essential for this radiotracer's uptake (14,15). Fructose metabolism is another interesting pathway in cancer that has been shown to be upregulated to sustain the cancer

cell's increased metabolism (9). In a previous study our lab has explored a radiolabelled fructose derivative, 6-deoxy-6-[^{18}F]fluoro-D-fructose (6-[^{18}F]FDF), which has been shown to be useful for imaging the GLUT5 expression profile in breast cancer (16).

1.22 Nucleoside Membrane Transporters

The hENT family of nucleoside transporter, mediates transport of nucleosides down their concentration gradients from which there are four; hENT1, hENT2, hENT3, and hENT4. hENT1 and hENT2 are the most highly expressed of these transporters, and are encoded by two different genes of the SLC29 family; *SLC29A1* and *SCL29A2* respectively (17). Both transporters are 456-residue proteins that share about 46% amino acid sequence similarity (18). The facilitated diffusion of purine and pyrimidine nucleosides are primary functions for both nucleoside transporters and are essential to normal cellular physiology. hENT1 mediates the transport of anti-cancer agents into the cell, such as gemcitabine and draflazine, more readily than other nucleoside transporters. hENT2 has a greater ability to transport anti-viral agents (18). The differences seen in the selectivity of nucleoside transport are due to variances in amino acid sequences (19).

The main function of nucleoside transporter is to move nucleosides from one body compartment to the other. Depending on the tissue type, nucleosides can be synthesized *de novo* or taken into cells through salvage pathways used for nucleotide synthesis (17). Once a nucleoside is present intracellularly, it can be metabolised and converted by intracellular enzyme-mediated pathways to a nucleotide (17), such as in the case of conversion of thymidine to deoxythymidine monophosphate with thymidine kinase 1 (TK1) (20,21). This conversion then allows for further cellular processes to occur such as the biosynthesis of nucleic acids for DNA replication,

phospholipid and oligosaccharide synthesis, and the use of nucleotides for cell signalling and salvage pathways (17).

Uncontrolled cellular proliferation, and the characteristic increase in synthesis and replication of DNA, is one of the major hallmarks of cancer. This property can be used to differentiate between healthy and cancerous tissue, as a decrease in the intracellular pool of nucleosides can be identified with an increased inward flux of nucleosides mediated by ENTs. To measure the flux of nucleoside transport we can use [^{18}F]3′-deoxy-3′-fluorothymidine ([^{18}F]FLT), a thymidine analog which becomes trapped intracellularly through phosphorylation by TK1 (22). Both hENT and human concentrative nucleoside transporter families contribute to the transport of [^{18}F]FLT (22).

Hypoxia may also have large effects on the transport of nucleosides into cells. The hypoxia/ HIF-1 dependent repression of hENT is well described (23–26). HIF-1 becomes activated once regions of tissue become hypoxic. In pathological terms, this may involve an arterial blockage or in cases such as tumorigenesis, insufficient blood perfusion. Once activated, HIF-1 binds to the hENT1 promotor sequence and represses transcription of the hENT1 gene (25). Overall, this results in decreased hENT1 mRNA and subsequently protein translation during hypoxia (23,25).

1.23 Amino Acid Transporters

Amino acids are essential to many cellular processes such as in protein synthesis and cellular metabolism. In cancer cells, utilization of amino acids is increased so that it may fuel extra protein synthesis due to increased cancer cell proliferation and growth, as well as the extra need for amino acids in metabolism. For this reason, certain amino acid membrane transporters have been identified as upregulated in cancer. Through research on breast cancer, amino acid

transporters ASCT2, LAT1, and x_c- have been shown to have altered expression or functionality, and subsequently have been subject to multiple review articles (27,28).

The alanine-serine-cysteine preferring transporter (ASCT), ASCT2/*SLC1A5*, other than the amino acids which make up its name, is also the primary transporter of glutamine in cancer cells (29,30). The x_c-/*SLC7A11* is an exchanger of extracellular cystine for intracellular glutamate. The primary role of system x_c- in cancer is preventing oxidative damage by increasing intracellular levels of glutathione (GSH), through the conversion of cystine to cysteine, and then subsequently to GSH (28,31). The third transporter that has altered functionality in BC is the L-amino acid transporter 1 (LAT1), which is responsible for transporting L-amino acids and large branched amino acids. LAT1/*SLC7A5* has additional roles in transporting excitatory amino acids (EAA) such as leucine, which are able to activate mTORC1, which then further promotes tumorigenic effects (32). These amino acid transporters have been highlighted as prime targets for PET imaging and radiotracer development. Radiotracers which are transported via these specific amino acid transporters, are [^{18}F]FACBC (33) and [^{18}F]FPhPA (34) for ASCT2; [^{18}F]FSPG (35) for x_c-; and [^{18}F]FDOPA (36) for LAT1.

Hypoxia has been shown to have effects on expression and function of amino acid transporters. Hu *et al.* (37) have shown that in hepatocellular carcinoma cells, HIF-1 triggers expression of membrane glutamate transporters as well as AMPA-type glutamate receptors. Aside from this example, there are many other amino acid transporters that are involved in cancer progression which also might be regulated by HIF-1. Additional research must be done to determine effects of hypoxia and HIF-1 on regulation of amino acid membrane transporters in cancer.

1.3 Hypothesis and Objectives

1.31 Hypothesis

This thesis aimed at testing two hypotheses…

1. The uptake of PET radiotracers by breast cancer cells will be dependent upon the respective cellular membrane transporter profiles.
2. Hypoxia modifies the expression and function of nucleoside transporters hENT1 and hENT2, and also of TK1; and of amino acid transporters ASCT1, ASCT2, LAT1, and x_c- in breast cancer cells.

1.32 Objectives

The goals of this thesis were achieved with…

1. Measurement of protein levels of select nucleoside and amino acid transporters in MCF10A, MCF7, and MDA-MB231 cells under normoxic and hypoxic conditions with Western blot, flow cytometry, immunohistochemistry, and/or confocal microscopy
2. Function measurement of the functionality of nucleoside and amino acid membrane transporters in MCF10A, MCF7, and MDA-MB231 cells under normoxic and hypoxic conditions with [^{18}F]FSPG, [^{18}F]FDOPA, [^{18}F]FLT in *in vitro/ in vivo* radiotracer uptake experiments

1.4 References

1. Ruan, K., Song, G., and Ouyang, G. (2009) Role of Hypoxia in the Hallmarks of Human Cancer. *J. Cell Biochem.* **107**, 1053-62.

2. Kakkad, S., Krishnamachary, B., Jacob, D., Pacheco-Torres, J., Goggins, E., Bharti, S.K., Penet, M.F., and Bhujwalla, Z.M. (2019) Molecular and functional imaging insights into the role of hypoxia in cancer aggression. *Cancer Metastasis Rev.* doi: 10.1007/s10555-019-09788-3.

3. Dehdashti, F. D., Rigsby, P. W. G., Mintun, M. A. M., Lewis, J. S., Siegel, B. A., and Welch, M. J. (2003) Assessing tumor hypoxia in cervical cancer by positron emission tomography with ^{60}Cu-ATSM: Relationship to therapeutic response—a preliminary report. *Int. J. Radiat. Onco.l Biol. Phys.* **55**, 1233–1238

4. Bollineni, V.R., Kerner, G.S., Pruim, J., Steenbakkers, R.J., Wiegman, E.M., Koole, M.J., de Groot, E.H., Willemsen, A.T., Luurtsema, G., Widder, J., Groen, H.J., and Langendijk, J.A. (2019) PET Imaging of Tumor Hypoxia Using 18F-Fluoroazomycin Arabinoside in Stage III – IV Non – Small Cell Lung Cancer Patients. *J. Nucl. Med.* **54**, 1175-1180

5. Lin, L., Yee, S.W., Kim, R.B., and Giacomini, K.M. (2015) SLC transporters as therapeutic targets : emerging opportunities. *Nat. Rev. Drug Discov.* **14**, 543-560

6. Rives, M., Javitch, J.A., and Wickenden, A.D. (2017) Potentiating SLC transporter activity : Emerging drug discovery opportunities. *Biochem. Pharmacol.* **135**, 1-11

7. Courtnay, R., Ngo, D.C., Malik, N., Ververis, K., Tortorella, S.M., and Karagiannis, T.C. (2015) Cancer metabolism and the Warburg effect: the role of HIF-1 and PI3K. *Mol. Biol. Rep.* **42**, 841-51

8. Liberti, M.V., and Locasale, J.W. (2016) The Warburg Effect: How Does it Benefit Cancer Cells? *Trends Biochem. Sci.* **41**, 11-218.

9. Hamann, I., Krys, D., Glubrecht, D., Bouvet, V., Marshall, A., Vos, L., Mackey, J. R., Wuest, M., and Wuest, F. (2018) Expression and function of hexose transporters GLUT1, GLUT2, and GLUT5 in breast cancer—effects of hypoxia. *FASEB J.* **32**, 5104–5118

10. Semenza, G.L. (2010) HIF-1 : upstream and downstream of cancer metabolism. *Curr. Opin. Genet. Dev.* **20**, 51-56

11. Semenza, G. L. (2016) The hypoxic tumor microenvironment: A driving force for breast cancer progression. *Biochim. Biophys. Acta - Mol. Cell Res.* **1863**, 382–391

12. Groheux, D., Cochet, A., Humbert, O., Alberini, J.L., Hindie, E., and Mankoff, D. (2016) ^{18}F-FDG PET/CT for Staging and Restaging of Breast Cancer. *J. Nucl. Med.* **57**, 17S–26S

13. Alvarez, J. V., Belka, G. K., Pan, T. C., Chen, C. C., Blankemeyer, E., Alavi, A., Karp, J. S., and Chodosh, L. A. (2014) Oncogene pathway activation in mammary tumors dictates FDG-PET uptake. *Cancer Res.* **74**, 7583–7598

14. Kubota, K., Yamashita, H., and Mimori, A. (2017) Clinical Value of FDG-PET/CT for the Evaluation of Rheumatic Diseases: Rheumatoid Arthritis, Polymyalgia Rheumatica, and Relapsing Polychondritis. *Semin. Nucl. Med.* **47**, 408–424

15. Adejolu, M., Huo, L., Rohren, E., Santiago, L., and Yang, W. T. (2012) False-positive lesions mimicking breast cancer on FDG PET and PET/CT. *AJR. Am. J. Roentgenol.* **198**, W304-W314

16. Wuest, M., Hamann, I., Bouvet, V., Glubrecht, D., Marshall, A., Trayner, B., Soueidan, O.M., Krys, D., Wagner, M., Cheeseman, C., West, F., and Wuest, F. (2018) Molecular Imaging of GLUT1 and GLUT5 in Breast Cancer : A Multitracer Positron Emission Tomography Imaging Study in Mice *Mol. Pharmacol.* **93,** 79-89

17. Young, J.D., Yao, S.Y.M., Baldwin, J.M., Cass, C.E., and Baldwin, S.A. (2013) The human concentrative and equilibrative nucleoside transporter families, SLC28 and SLC29. *Mol. Aspects Med.* **34**, 529-547.

18. Baldwin, S.A., Beal, P.R., Yao, S.Y., King, A.E., Cass, C.E., and Young, J.D. (2004) The equilibrative nucleoside transporter family, SLC29. *Pflugers Arch.* **447**, 735-743.

19. Nivillac, N.M.I., Wasal, K., Villani, D.F., Naydenova, Z., Hanna, W.J.B., and Coe, I.R. (2009) Disrupted plasma membrane localization and loss of function reveal regions of human equilibrative nucleoside transporter 1 involved in structural integrity and activity. *Biochim. Biophys. Acta.* **1788**, 2326-2334.

20. Zhang, C.C., Yan, Z., Li, W., Kuszpit, K., Painter, C.L., Zhang, Q., Lappin, P.B., Nichols, T., Lira, M.E., Affolter, T., Fahey, N.R., Cullinane, C., Spilker, M., Zasadny, K., O'Brien, P., Buckman, D., Wong, A., and Christensen, J.G. (2012) [(18)F]FLT-PET imaging does not always "light up" proliferating tumor cells. *Clin. Cancer Res.* **18**, 1303-1312.

21. Plotnik, D.A., Emerick, L.E., Krohn, K.A., Unadkat, J.D., and Schwartz, J.L. (2010) Different modes of transport for 3H-thymidine, 3H-FLT, and 3H-FMAU in proliferating and nonproliferating human tumor cells. *J. Nucl. Med.* 51, 1464-1471.

22. Paproski, R. J., Ng, A. M. L., Yao, S. Y. M., Graham, K., Young, J. D., and Cass, C. E. (2008) The Role of Human Nucleoside Transporters in Uptake of 3'-Deoxy-3'-fluorothymidine. Mol. Pharmacol. 74, 1372–1380.

23. Casanello, P., Torres, A., Sanhueza, F., González, M., Farías, M., Gallardo, V., Pastor-Anglada, M., San Martín, R., and Sobrevia, L. (2005) Equilibrative nucleoside transporter 1 expression is downregulated by hypoxia in human umbilical vein endothelium. *Circ. Res.* **97**, 16–24

24. Chaudary, N., Naydenova, Z., Shuralyova, I., and Coe, I.R. (2004) Hypoxia regulates the adenosine transporter, mENT1, in the murine cardiomyocyte cell line, HL-1. *Cardiovasc. Res.* **61**, 780-788.

25. Eltzschig, H. K., Abdulla, P., Hoffman, E., Hamilton, K. E., Daniels, D., Schönfeld, C., Löffler, M., Reyes, G., Duszenko, M., Karhausen, J., Robinson, A., Westerman, K. A., Coe, I. R., and Colgan, S. P. (2005) HIF-1–dependent repression of equilibrative nucleoside transporter (ENT) in hypoxia *J. Exp. Med.* **202**, 1493–1505

26. Morote-Garcia, J.C., Rosenberger, P., Nivillac, N.M.I., Coe. I.R., and Eltzschig, H.K. (2009) Hypoxia-inducible factor-dependent repression of equilibrative nucleoside transporter 2 attenuates mucosal inflammation during intestinal hypoxia. *Gastroenterology* **136**, 607-618.

27. Ulaner, G.A., and Schuster, D.M. (2018) Amino Acid Metabolism as a Target for Breast Cancer Imaging *PET Clin*. **13**, 437-444

28. Cha, Y.J., Kim, E.-S., and Koo, J.S. (2018) Amino Acid Transporters and Glutamine Metabolism in Breast Cancer. *Int. J. Mol. Sci.* **19**, 907

29. Jin, L., Alesi, G.N., and Kang, S. (2016) Glutaminolysis as a target for cancer therapy. *Oncogene*. **35**, 3619-3625

30. Schulte, M.L., Fu, A., Zhao, P., Li, J., Geng, L., Smith, S.T., Kondo, J., Coffey, R.J., Johnson, M.O., Rathmell, J.C., Sharick, J.T., Skala, M.C., Smith, J.A., Berlin, J., Washington, M.K., Nickels, M.L., and Manning, H.C. (2018) Pharmacological blockade of ASCT2-dependent glutamine transport leads to antitumor efficacy in preclinical models. *Nat. Med.* **24**, 194-202

31. Patel, S.A., Warren, B.A., Rhoderick, J.F., and Bridges, R.J. (2004) Differentiation of substrate and non-substrate inhibitors of transport system xc(-): an obligate exchanger of L-glutamate and L-cystine. *Neuropharmacology*. **46**, 273-284.

32. Wang, Q., and Holst, J. (2015) L-type amino acid transport and cancer : targeting the mTORC1 pathway to inhibit neoplasia. *Am. J. Cancer Res.* **5,** 1281-1294

33. Oka, S., Okudaira, H., Yoshida, Y., Schuster, D.M., Goodman, M.M., and Shirakami, Y. (2012) Transport mechanisms of trans-1-amino-3-fluoro[1-(14)C]cyclobutanecarboxylic acid in prostate cancer cells. *Nucl. Med. Biol.*; **39**, 109–119

34. Way, J.D., Wang, M., Hamann, I., Wuest, M., and Wuest, F. (2014) Synthesis and evaluation of 2-amino-5-(4-[(18)F]fluorophenyl)pent-4-ynoic acid ([(18)F]FPhPA): a novel (18)F-labeled amino acid for oncologic PET imaging. *Nucl. Med. Biol.* **41,** 660–669

35. Koglin, N., Mueller, A., Berndt, M., Schmitt-Willich, H., Toschi, L., Stephens, A.W., Gekeler, V., Friebe, M., and Dinkelborg, L.M. (2011) Specific PET imaging of xC- transporter activity using a ^{18}F-labeled glutamate derivative reveals a dominant pathway in tumor metabolism. *Clin. Cancer Res.* **17**, 6000-6011

36. Youland, R.S., Kitange, G.J., Peterson, T.E., Pafundi, D.H., Ramiscal, J.A., Pokorny, J.L., Giannini, C., Laack, N.N., Parney, I.F., Lowe, V.J., Brinkmann, D.H., and Sarkaria, J.N. (2013) The role of LAT1 in (18)F-DOPA uptake in malignant gliomas. *J. Neurooncol.* **111**, 11-18.

37. Hu, H., Takano, N., Xiang, L., Gilkes, D.M., Luo, W., and Semenza, G.L. (2014) Hypoxia-inducible factors enhance glutamate signaling in cancer cells. *Oncotarget* **5**, 8853-8868.

CHAPTER 2

Effect of hypoxia on human equilibrative nucleoside transporters hENT1 and hENT2 in breast cancer

Effect of hypoxia on human equilibrative nucleoside transporters; hENT1 and hENT2 in breast cancer

Daniel Krys, Ingrit Hamann, Melinda Wuest[1], Frank Wuest[*]

Chapter published in The FASEB Journal

Abstract: Elevated proliferation rates in cancer can be visualized with PET using 3'-deoxy-3'-L-[^{18}F]fluorothymidine ([^{18}F]FLT). This study investigates whether [^{18}F]FLT transport proteins are regulated through hypoxia. Expression and function of human equilibrative nucleoside transporters 1 (hENT1), 2 (hENT2), and thymidine kinase 1 (TK1) were studied under normoxic and hypoxic conditions, and assessed with [^{18}F]FLT-PET in estrogen receptor positive (ER(+)) MCF7, triple-negative MDA-MB231 breast cancer (BC) cells, and MCF10A cells; human mammary epithelial cells. Functional involvement of hENT2 [^{18}F]FLT transport was demonstrated in all cell lines. *In vitro* [^{18}F]FLT uptake was higher in MDA-MB231 than in MCF7: 242±9 % vs. 147±18 % radioactivity/mg protein after 60 minutes under normoxia. Hypoxia showed no significant change in radiotracer uptake. Protein analysis revealed higher hENT1 ($P<0.0963$) in MDA-MB231. Hypoxia did not change expression of hENT1, hENT2 or TK1. *In vitro* inhibition experiments suggested involvement of hENT1, hENT2, and hCNT's during [^{18}F]FLT uptake into all cell lines. *In vivo* PET imaging revealed comparable tumor uptake in MCF7 and MDA-MB231 tumors: Standardized Uptake Value at 60-min (SUV60min) 0.96±0.05 vs. 0.89±0.08 (n=3). Higher hENT1 expression in MDA-MB231 seems to drive nucleoside transport, while TK1 expression in MCF7 seems responsible for comparable [^{18}F]FLT retention in ER(+) tumors. Our study demonstrates that hypoxia does not significantly affect nucleoside transport as tested with [^{18}F]FLT in BC.

Keywords: Nucleoside transport, Hypoxia, Thymidine kinase 1, [^{18}F]FLT, Positron emission tomography

2.1 INTRODUCTION

Breast cancer (BC) is the most commonly diagnosed cancer in women. With recent innovations in early detection and targeted treatments based on novel prognostic biomarkers and molecular subtyping, the 5-year survival rate of BC patients has increased, along with a substantial decrease in mortality rates (1, 2). However, BC is still the second leading cause of cancer death in females. In these patients, it is not the primary tumour, but it's metastases at distant sites that are the main cause of death. Metastatic breast cancer still remains incurable, and median overall survival is only in the order of 2-3 years with currently available therapies (3).

In the clinic, there are multiple medical imaging technologies for the diagnosis of BC. Technologies such as ultrasound, computed tomography (CT), mammography, and magnetic resonance imaging (MRI) are frequently used to confirm presence of the disease (4). However, all these methodologies are based on the visualization of breast tumor morphology rather than functional and metabolic processes as championed by positron emission tomography (PET). Despite development of various hormone receptor-binding PET radiotracers such as 16α-[^{18}F]fluoroestradiol-17β ([^{18}F]FES) (5–7) for PET imaging of estrogen receptor-positive (ER(+)) BCs, glucose analogue 2-deoxy-2-[^{18}F]fluoro-D-glucose ([^{18}F]FDG) still remains the "gold" standard for PET imaging in BC, especially for tumor staging, detection of recurrent disease, and monitoring of treatment response (8). Use of [^{18}F]FDG as a radiofluorinated glucose analog in BC detection relies on the metabolic switch from oxidative phosphorylation in normal cells to anaerobic glycolysis, also referred to as the Warburg effect in cancer cells (9). [^{18}F]FDG uptake into BC cells is mainly mediated through the facilitative glucose transporter 1 (GLUT1), and its intracellular retention occurs through phosphorylation by hexokinase II (9). Despite its high sensitivity in BC imaging, [^{18}F]FDG also has several limitations. Firstly, GLUT1 expression levels can vary widely among BC patients, which leads to false-negative results (8, 10).

Moreover, inflammatory lesions also show high [^{18}F]FDG uptake which can lead to false-positive results (11, 12). As a consequence, there are still no recommendations in current clinical guidelines to use PET as a molecular imaging technique for primary diagnosis and monitoring of treatment response in BC patients. Alternatively, 3´-deoxy-3´-[^{18}F]fluorothymidine ([^{18}F]FLT) has been used for molecular imaging of proliferation in various types of cancer (13). An important advantage of [^{18}F]FLT over [^{18}F]FDG is its ability to better discriminate between tumor and inflammatory tissue.

[^{18}F]FLT is a radiofluorinated thymidine analogue whose primary uptake mechanism into cells occurs through the human equilibrative nucleoside transporter 1 (hENT1) (14). [^{18}F]FLT is also transported by concentrative nucleoside transporters (CNT). The hENT family of nucleoside transporter mediates passive diffusion of nucleosides down their concentration gradients. To date, hENT1 to hENT4 subtypes have been described (15). The human CNT family is composed of three known transporter subtypes; hCNT1, hCNT2 and hCNT3.

In contrast to hENTs, CNTs transport nucleosides against their concentration gradients via secondary active transport by interacting with either sodium or hydrogen ions (16). Upon cellular entry, [^{18}F]FLT is phosphorylated by thymidine kinase 1 (TK1) and the subsequent [^{18}F]FLT-triphosphate cannot be incorporated into the DNA (17). Intracellular trapping of [^{18}F]FLT as [^{18}F]FLT-triphosphate results in increased tumor-to-background ratios over time, which provides optimal imaging contrast in PET. Both processes, transport and phosphorylation, are upregulated in rapidly proliferating cancer cells.

Another important process which occurs during development of solid tumors involves changes in tumor vascularization and oxygen perfusion, which leads to various degrees of tumor hypoxia. Hypoxic regions of solid tumors adapt to the reduced oxygen supply by activating hypoxia-inducible factor (HIF) which consists of an oxygen-regulated HIF-1α subunit and the

constitutively expressed HIF-1β subunit (18). Beside its multiple roles in tumor cells, HIF-1α is also important in normoxic cells, e.g. in lymphocytes and spermatazoal flagella, and it has also been shown to have protective effects to low-dose radiation (19). However, under hypoxic conditions, expression of HIF-1α is strongly elevated in oxygen-deprived tumor regions. As a transcription factor, HIF-1α regulates expression of a variety of targets genes such as GLUT1, vascular endothelial growth factor (VEGF), platelet derived growth factor (PDGF), transcription growth factor (TGF), and carbonic anhydrase IX (CA-IX) (20, 21). Recently, we have demonstrated that other facilitative hexose transporter GLUT5, the main transporter for fructose, is also regulated by HIF-1α in BC, while GLUT2, a hexose transporter for both glucose and fructose, is not (22).

To date, very few studies have discussed potential regulation of nucleoside transporter expression by HIF-1α. In one study which focused on ischemia in cardiac endothelial cells and uterine tissue, the authors concluded that ischemia-induced HIF-1α expression led to a downregulation of nucleoside transporter protein hENT1 (23, 24). Downregulation of ENT1 and ENT2 mRNA after exposure to chronic hypobaric hypoxia over one week was reported in a different study which analyzed mammalian carotid bodies from juvenile rats (25).

The first goal of the present study was to explore whether HIF-1α alters expression and function of hENT1 and hENT2 in BC under hypoxic conditions using the ENT substrate [^{18}F]FLT and the hypoxia imaging agent [^{64}Cu]ATSM. Recently, protein expression levels of hENT1 were reported as a useful prognostic factor for gastric tumors (26), whereas hENT1 protein expression was described as highly variable in primary breast cancer patients (27). Moreover, a recent PET study in ENT1 KO mice and ENT1 deprived lung tumors still observed 60% of the control [^{18}F]FLT uptake values (28). A second goal of the present study was to analyze potential

differences in hENT1 and hENT2 expression and function in BC which could have an impact on the clinical use of [^{18}F]FLT for ER (+) and TNBC tumours using *in vivo* PET. In addition, the third goal of this study was to analyze the potential involvement of hENT2 for the uptake of [^{18}F]FLT into BC cells.

2.2 MATERIALS AND METHODS

2.21 Chemicals and radiosynthesis

All chemicals and reagents were obtained from Sigma-Aldrich (Sigma-Aldrich, Oakville, ON, Canada) unless otherwise stated.

Radiotracer 3'-deoxy-3'-L-[^{18}F]fluorothymidine ([^{18}F]FLT) was prepared at the cyclotron facility of the Cross Cancer Institute using a GE TracerLab FX automated synthesis unit (GE Healthcare, Little Chalfont, United Kingdom) according to the method developed by Machulla et al. using 5′-O-(4,4′-dimethoxytrityl)-2,3′-anhydrothymidine as the labeling precursor (29). [^{64}Cu]Cu-diacetyl-bis(N4-methylthiosemicarbazone) ([^{64}Cu]ATSM) was synthesized according to Dehdashti et al. starting from diacetyl bis(N4-methylthiosemicarbazone) (ABX GmbH, Radeberg, Germany) (30). Radioisotope ^{64}Cu was obtained from Washington University School of Medicine (St. Louis, MO, USA) as a [^{64}Cu]$CuCl_2$ solution in HCl.

2.22 Patient samples

Gene-expression microarray analysis was performed as described previously using primary samples from 176 treatment-naive patients with BC and 10 healthy breast-tissue samples collected from reduction mammoplasties through the Canadian Breast Cancer Foundation Tumor Bank (Northern Alberta Study Center, Cross Cancer Institute, Edmonton, AB, Canada) (31). Patient information was collected under Research Ethics Board Protocol ETH-02-86-17.

2.23 Cell cultures

The following cell lines were used in the study: MCF10A (American Type Culture Collection (ATCC) CRL-10317; ATCC, Manassas, VA, USA) is a human non-carcinogenic basal B cell line, derived from fibrocystic breast disease and obtained during a reduction mammoplasty. MCF7 (ATCC HBT-22) is an estrogen receptor (ER) and progesterone receptor (PR) positive breast cancer cell line, derived from luminal invasive ductal carcinoma, while MDA-MB231 (ATCC HTB-26) is a triple negative basal B breast cancer (TNBC) cell line. MCF7 and MDA-MB231 cells were grown in DMEM/F-12 (Gibco, ThermoFisher Scientific, Burlington, ON, Canada) with 10% fetal bovine serum (FBS) (Gibco) and 1% penicillin/streptomycin (Pen/Strep), while MCF10A cells were grown in DMEM/F-12 containing Clonetics® MEGM SingleQuots® (Lonza, Walkersville, MD, USA). For experiments, cells were seeded in their medium and grown for 24 h. Media was preconditioned for 2-3 h in our hypoxia chamber (Department of Pharmacy and Pharmaceutical Sciences, University of Alberta, Edmonton, AB, Canada) used at setting of 1% O_2 and 5% CO_2 at 37°C. Preconditioned media was used to exchange regular growth media for hypoxia experiments. These conditions were set and compared to cells under normoxic conditions for all following experiments (19).

2.24 Western blotting

For analysis of hENT1, hENT2, TK1, and β-actin, MCF10A, MCF7, and MDA-MB231 cells For analysis of GRPR and β-actin, MCF10A, MCF7, and MDA-MB231 cells were seeded in 60 mm dishes (Nunc™ Cell Culture/Petri Dishes, ThermoFisher Scientific) and had their media changed 24 h prior to collection. Cells in the dishes were washed with PBS, then suspended in lysis buffer (50mM Tris, 150 mM NaCl, 0.1% SDS, 0.5% sodium deoxycholate, 0.5% Triton X) containing protease inhibitor cocktail (ab65621, abcam, 1:500). Extracts were sonicated (10% amplitude, 5 s) on ice and centrifuged at 14,500 g for 10 min at 4°C to remove debris. Protein determination

in supernatants was conducted, using a BCA based protein assay (Pierce/Thermo Scientific, Rockford, IL, USA). Aliquots of supernatants were mixed with 1/4 volume of 4x Laemmli buffer (250 mM Tris/HCl, 8% (w/v) SDS, 40% glycerol, 200 mM dithiothreitol and 0.04% (w/v) bromophenol blue, pH 6.8) and heated for 5 min at 95°C. Protein extracts were loaded onto SDS-polyacrylamide gels and separated by electrophoresis. Proteins were transferred to nitrocellulose membranes by electroblotting and blocked for 1 h at room temperature in 5% (w/v) non-fat dry milk in Tris-buffered saline containing 0.05% (v/v) of Tween-20 (TBST). Membranes were incubated overnight at 4°C with the following primary antibodies: mouse monoclonal anti-ENT1 IgG_{2a} (clone F-12, sc-277283, Santa Cruz Biotechnology USA, 1:500), mouse monoclonal anti-ENT2 IgG_1 (clone D-9, sc-377283, Santa Cruz Biotechnology USA, 1:100), mouse monoclonal anti-Thymidine Kinase 1 IgG_1 (clone C-4, sc-377211, Santa Cruz Biotechnology, 1:100), and rabbit polyclonal anti-β-actin (A5060, Sigma-Aldrich, 1:5000). Prior to the addition of anti-β-actin to blots already stained with anti-hENT2 and anti-TK1, a stripping procedure was performed due to the close kDa proximity of the staining between both antibodies. Stripping buffer (1 L: 15 g glycine, 1 g SDS, 1% Tween20, pH 2.2) was used to wash the membranes twice for 5-10 minutes each, followed by two washes with PBS each for 10 minutes, and two washes with TBST for 5 minutes each. The stripping or regular procedure was followed by incubation for 1 h at 21°C with a peroxidase-conjugated goat anti-mouse IgG secondary antibody (sc-2005, Santa Cruz Biotechnology) in 1:5000 dilution (hENT1, hENT2, TK1) or goat anti-rabbit IgG (A0545, Sigma-Aldrich 1:5000) for anti-β-actin. After incubation with secondary antibodies, membranes were washed in TBST and depending on protein levels, incubated with Supersignal West Pico chemiluminescent substrate (Gibco, ThermoFisher Scientific, Burlington, ON, Canada) or Clarity ECL Western blotting substrate (Bio-Rad Laboratories, Hercules, CA,

USA). Luminescence signals were captured using Fuji Medical X-ray Films (Fujifilm Canada, Mississauga, ON, Canada).

Films were scanned, and analysis was done using the ImageJ program (National Institutes of Health, Bethesda, MD, USA). Density of each band was determined, and individual lane backgrounds were subtracted. Values for hENT1, hENT2, and TK1 were divided by values for the housekeeping protein β-actin. Received values for control cell line MCF10A were set at 100% and compared with the individual value of the cancer cell lines {e.g., (band density hENT1 density lane background)/(band density β-actin 2 density lane background), respectively}. Statistical differences were tested by paired Student's t test and defined accordingly (* $p<0.05$,** $p<0.01$ and *** $p<0.001$.

2.25 In vitro cell uptake studies

MCF10A, MCF7, and MDA-MB231 cells were grown in 12-well plates and treated under normoxic/hypoxic conditions for 24 h prior to the experiment. During radiotracer cell uptake experiments all cells were handled the same, and cells under hypoxia were not under hypoxic conditions during the experimental procedure. Media was removed 1h prior to experiment, cells were washed 2x with phosphate-buffered saline (PBS) and starved of glucose in glucose-free Krebs-Ringer solution (120 mM NaCl, 4 mM KCl, 1.2 mM KH_2PO_4, 2.5 mM $MgSO_4$, 25 mM $NaHCO_3$, 70 μM $CaCl_2$, pH 7.4) for 1 h at 37 °C. Next, 300 μL Krebs-Ringer solution with 0.1-0.5 MBq [^{18}F]FLT or [^{64}Cu]ATSM was added to each well. Plates were incubated at 37°C for specific time points (5, 10, 15, 30, 60 minutes). Radiotracer uptake was stopped with 1 mL ice-cold PBS, cells washed two times with PBS and lysed in 0.4 mL lysis buffer (50 mM Tris, 150 mM NaCl, 0.1% SDS, 0.5% sodium deoxycholate, 0.5% Triton X). Radioactivity in cell lysates was measured using WIZARD2 automatic gamma counter (Perkin Elmer; Waltham, MA, USA). Total protein concentration in the samples was determined using a Pierce BCA based protein

assay (ThermoFisher Scientific). Data were calculated as % of total added radioactivity per mg protein (% radioactivity/mg protein).

2.26 In vitro inhibition of [^{18}F]FLT cellular uptake

Media was removed 1h prior to experiment, cells were washed twice with PBS or sodium free choline buffer (120 mM $C_5H_{14}ClNO$, 4 mM KCl, 1.2 mM KH_2PO_4, 2.5 mM $MgSO_4$, 25 mM $C_5H_{14}NOHCO_3$, 70 μM CaCl2, pH 7.4) and starved of glucose or glucose and sodium in glucose-free Krebs-Ringer solution or glucose and sodium free choline buffer for 1 h at 37 °C. MDA-MB231 cells were incubated with Krebs-Ringer buffer or choline buffer containing [^{18}F]FLT and increasing concentrations (1, 10, 100 nM and 1, 3, 7, 10 μM) of *S*-(4-nitrobenzyl)-6-thioinosine (NBMPR) (Sigma-Aldrich, Oakville, ON, Canada); 1 mM of non-radioactive FLT (Sigma-Aldrich, Oakville, ON, Canada); 100 μM, 300 μM, and 1 mM of gemcitabine hydrochloride (Hospira Healthcare Corporation, Kirkland, QC, Canada); or 1 μM, 10 μM, 100 μM, and 300 μM of dilazep dihydrochloride (Sigma-Aldrich, Oakville, ON, Canada). Control for 100% uptake was determined with Krebs-Ringer buffer only. After 60 min cells were rinsed with ice-cold PBS or ice-cold choline buffer, lysed, and counted for radioactivity as described above.

2.27 Animal models

All animal experiments were carried out in accordance with guidelines of the Canadian Council on Animal Care (CCAC) and approved (AC 15222) by the local Animal Care Committee of the Cross Cancer Institute. Human MCF7 cells were injected subcutaneously ($5x10^6$ cells in 100 μL PBS/Matrigel 50:50) into 8-10 weeks old female NIH-III nude mice (Charles River, Saint-Constant, QC, Canada) plus a 0.72 mg/pellet containing estrogen in a 60-day release preparation (Innovative Research of America, Sarasota, FL, USA) implanted subcutaneously into the upper right flank for the constant estrogen level needed by the ER(+) MCF7 cells. Tumors were grown for 3-4 weeks, reaching sizes of 200-400 mm^3. Human TNBC MDA-MB231 cells ($5x10^6$ cells in

100 µL PBS) were also injected subcutaneously resulting in 300-500 mm^3 sized tumors after 2-3 weeks.

2.28 PET imaging experiments

MCF7 and MDA-MB231 tumor bearing NIH-III nude mice (Charles-River, QC, Canada) were anesthetized with isoflurane (40% O_2, 60% N_2) and their body temperature was kept constant at 37 °C. Mice were positioned and immobilized in prone position into the centre of the field of view of an INVEON® PET scanner (Siemens Preclinical Solutions, Knoxville, TN, USA). A transmission scan for attenuation correction was not acquired. Radioactivity present in the injection solution (0.5 mL syringe) was determined using a dose calibrator (AtomlabTM 300, Biodex Medical Systems, New York, NY, USA). After emission scan was started, radioactivity (4-8 MBq in 100-150 µL saline) was injected with a delay of ~15 s through a tail vein catheter.

Dynamic PET data acquisition was performed in 3D list mode for 60 min. Dynamic list mode data were sorted into sinograms with 54 time frames (10x2 s, 8x5 s, 6x10 s, 6x20 s, 8x60 s, 10x120 s, 5x300 s). Frames were reconstructed using Ordered Subset Expectation Maximization (OSEM) or maximum a posteriori (MAP) reconstruction modes. No correction for partial volume effects were performed. Image files were further processed using the ROVER v2.0.51 software (ABX GmbH, Radeberg, Germany). Masks defining 3D regions of interest (ROI) were set and defined by 50% thresholding.

Mean standardized uptake values [SUV_{mean} = (activity/mL tissue) / (injected activity / body weight), in milliliters per kilogram were calculated for each ROI. Time-activity curves (TAC) were generated from the dynamic scans.

2.29 Confocal microscopy

MCF10A, MCF7, and MDA-MB231 cells were grown in 35 mm glass bottom microwell dishes (MatTek) and treated under normoxic or hypoxic conditions for 24 h. Media was removed prior

to the experiment, and dishes were washed with 200 µL Dulbecco's PBS. Following the wash, 300 µL of a 1 ml Krebs-Ringer Buffer, 0.6 µL pre-diluted CellMask Deep Red (ThermoFisher Scientific, C10046; gift from Cell Imaging Facility, University of Alberta, Edmonton, AB, Canada), 0.75 µL pre-diluted Hoechst 33342 (ThermoFisher Scientific, H1399; gift from Cell Imaging Facility, University of Alberta, Edmonton, AB, Canada) and 10 µL of 10 µM FITC-labeled 5´-S-[2-(6-aminohexanamido)]ethyl-6-*N*-(4-nitrobenzyl)-5´-thio-adenosine (SAHENTA) (28) solution was added to each plate, for both normoxic and previously hypoxic conditions. For the blocking condition using NBMPR, a corresponding 1 mL solution of 10 µM NBMPR in Krebs-Ringer Buffer was made. After the addition of these solutions, the dishes were incubated at 37 °C for 45 min. After incubation, the staining solution was aspirated and 200 µL Dulbecco's PBS was added on top of the cells. The plates were wrapped with a thin piece of parafilm to ensure no spillage. Cells were imaged with a Zeiss 710 Confocal Microscope using the 40x/1.3 Oil DIC M27 magnification setting. Images were analyzed with Zen 2011 SP3 software (Carl Zeiss Microscopy), saved, and optimized using Adobe Photoshop for noise and brightness levels (standardized between all three channels).

2.2a Flow cytometry

For analysis of hENT1 and hENT2; MCF10A, MCF7, and MDA-MB231 cells were subjected to normoxic/hypoxic conditions for 24 h. Following the 24 h treatment time, the media was aspirated, the flask was washed with 5 mL PBS, aspirated, 1.5 mL of trypsin was added to coat the bottom surface of the flask, and then the flask was placed in the sterile 37 °C incubator for 5 minutes. 10 mL of DMEM/F-12 (Gibco, ThermoFisher Scientific, Burlington, ON, Canada) with 10% fetal bovine serum (FBS) (Gibco) and 1% penicillin/streptomycin (Pen/Strep) media was added to inactivate trypsin.

The cell solution was then split equally into 15 mL centrifuge tubes (Corning Science Mexico, Reference # 430791), and centrifuged at 1000 x for 3 min. Following this, two wash steps were performed; the supernatant was aspirated, the pellet was re-suspended in 4 mL PBS, and centrifuged at 1000 x for 3 min, for each subsequent wash. After washing, fixation was performed with 1 mL of 1.5% paraformaldehyde in PBS on ice for 30 min, with occasional mixing of the pellet. After fixation, tubes were centrifuged at 1000 x for 3 min; supernatant was aspirated, washed in 4 mL of PBS, and centrifuged again at 1000 xfor 3 min. The supernatant was aspirated, and the pellet was resuspended in 50 µL of blocking solution (1% bovine serum albumin (A4503-50G, Sigma Aldrich, Oakville, ON, Canada), 0.1% Triton X-100 (93426-100ML, Sigma Aldrich, Oakville, ON, Canada) in PBS), and was incubated on ice for 30 minutes with occasional mixing. After the blocking step, 1 µL of anti-ENT1 Ab (a gift from Dr. Michael Sawyer; Department of Oncology, University of Alberta, Edmonton, AB, Canada) or 1 µL of anti-ENT2 IgG_1 Ab (clone D-9, sc-377283, Santa Cruz Biotechnology) was added directly to this solution, and was incubated for 1.5 h on ice with occasional mixing. Following incubation, the tubes were centrifuged at 1000 x for 3 min, supernatant was aspirated, and pellets were washed 3-times by resuspending cells in 500 µL of blocking solution, centrifuging at 1000 x for 3 min, and then aspirating the supernatant. After the washes and final aspiration of supernatant, 100 µL of blocking solution was added along with 1 µL of donkey anti-mouse IgG Alexa Fluor 488, Secondary Antibody (ThermoFisher Scientific; Rockford, IL, USA; Catalog Number R37114), and incubated in the dark for 30 min on ice. Following incubation, tubes were centrifuged at 1000 x for 3 min, and then washed three times with 500 µL block solution. After three washing steps, pellets were re-suspended in 400 µL 1% paraformaldehyde in PBS, and transferred to a labelled FACS tube (Corning Science Mexico; Reference #352054), wrapped in foil, and then placed on ice until they were analyzed. Quantification was done using a BD

FACSCanto™ II (BD Biosciences; Mississauga, ON, Canada) Flow Cytometer using FACSDiva 8.0 Software. Analysis was then performed using GraphPad Prism 4.0 (GraphPad Software, La Jolla, CA, USA) by determining the mean and SEM from the ratio of Primary+Secondary Ab staining/ Just Secondary Ab staining

2.2b Statistical analysis

All *in vitro* data and semi-quantified PET data are expressed as means ± SEM. Graphs and time-activity curves (TACs) were constructed using GraphPad Prism 4.0 (GraphPad Software, La Jolla, CA, USA). Where applicable, statistical differences were tested by Student's t test (PCR, Western Blot, Flow Cytometry, PET data) or 2-way ANOVA (cell uptakes) and were considered significant for $p<0.05$ (*), $p<0.01$ (**) and $p<0.001$ (***).

2.3 RESULTS

hENT1, hENT2, and TK1 mRNA expression in patient BC samples

Figure 1A presents results of microarray analysis of hENT1, hENT2, and TK1 mRNA in BC tissue biopsy samples from 176 BC patients versus control tissue from 10 normal human breast-tissue samples. In both BC and normal breast-tissue samples, mRNA expression of hENT2 and TK1 was significantly higher, compared to hENT1 which showed no statistical significance. The most pronounced difference was detected for TK1 amounting to a ~9-fold increase in BC ($P < 0.001$). **Figure 1B** shows analysis of 56 TNBC versus 112 ER+ BC samples which revealed no statistically significant differences for hENT1, hENT2, and TK1 mRNA expression in TNBC compared to ER+, indicating no regulation on mRNA level of both transporters and the enzyme responsible for phosphorylation of [^{18}F]FLT.

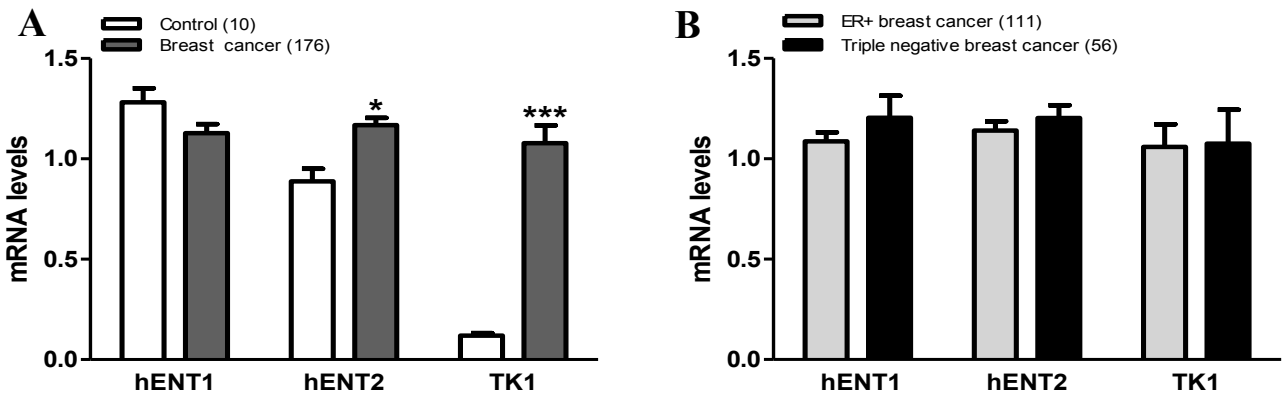

Figure 1. Total mRNA expression of hENT1, hENT2, and TK1 in control breast vs. BC tissue (A) and ER+ vs. TNBC samples (B). Data are shown as mean mRNA levels ± SEM based on log-transformed values of gene-expression microarray signal intensity from analyzed patient samples. $*P < 0.05$ and $***P < 0.001$.

2.31 hENT1, hENT2, and TK1 protein expression levels under normoxia and hypoxia

Figure 2 summarizes data from all Western blot experiments. **Figure 2A** displays original blots and the effects of hypoxia (exposure to 1% O_2 for 24 h) on proteins of interest: hENT1, hENT2, and TK1. A 24 h incubation time under hypoxic conditions was selected based on recent experiments from Hamann *et al.* (22). Maximum HIF-1α protein levels were detected after 24 h leading to a significant increase of the downstream target gene expression of facilitative hexose transporters GLUT1 and GLUT5 in BC cells (22). In the present study, normoxic conditions revealed the following results (**Figure 2B**): Though insignificant, hENT1 protein level was expressed 3.3-times higher ($P < 0.0963$) in MDA-MB231 cells compared to control cell line MCF10A. hENT1 expression in MCF7 cells was not elevated. In contrast to variable hENT1 protein levels amongst the cell lines, hENT2 protein levels were similar in all three cell lines analyzed. TK1 expression levels were also not significantly different in all three analyzed cell lines. Interestingly, hypoxic cell culture conditions did not change protein expression of hENT1, hENT2, and TK1 (Figure 2C-D), except for a somewhat lower observed protein level for TK1 in MCF10A cells (30% decrease; $P < 0.05$).

These results were indicative of no hypoxia regulation of both hENT1 and hENT2 transporters responsible for [^{18}F]FLT uptake into BC cells as well as the TK1 enzyme phosphorylating [^{18}F]FLT which leads to intracellular trapping.

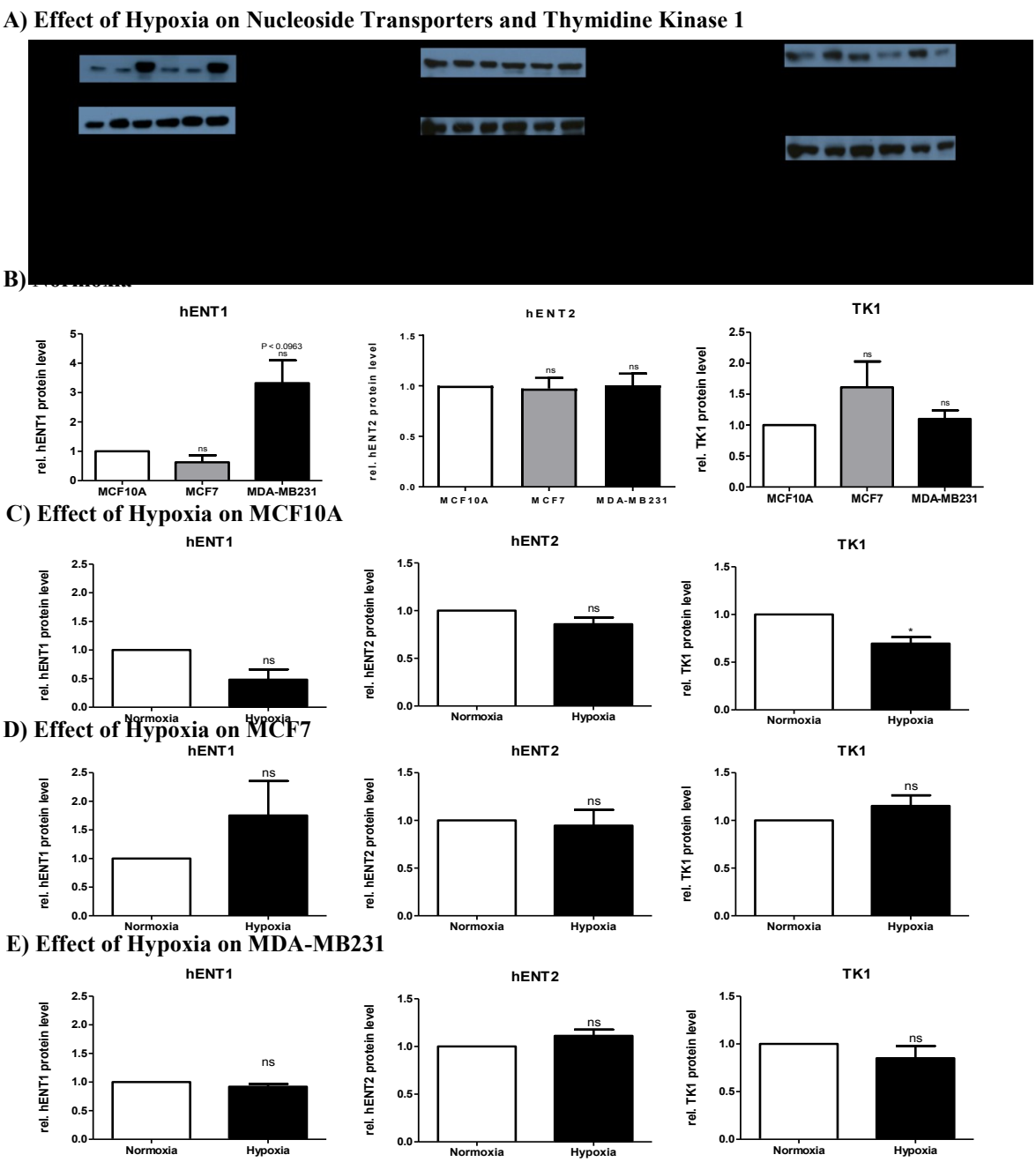

Figure 2. Representative Western blots for hENT1, hENT2, and TK1 expression in MCF10A, MCF7, and MDA-MB231 cells over 24 h of hypoxia (1% O_2) *versus* normoxic conditions (A). Quantitative comparison of hENT1, hENT2, and TK1 protein levels in MCF10A, MCF7, and MDA-MB231 under normoxic conditions (B) and the effects of hypoxia (1% O_2) on hENT1, hENT2, and TK1 protein levels in MCF10A (C), MCF7 (D), and MDA-MB231 (E) cells. Quantitative data are shown as means ± SEM from at least three experiments $^*P < 0.05$.

2.32 Effect of hypoxia on cellular uptake of [^{18}F]FLT

[^{18}F]FLT cellular uptake experiments were performed to test effects of hypoxic conditions on the function of nucleoside transporters in MCF10A, MCF7, and MDA-MB231 cells (**Figure 3A)**. No significant differences were detected between normoxic and hypoxic conditions in all three cell lines over all time points, indicating that [^{18}F]FLT uptake in in MCF10A, MCF7, and MDA-MB231 cells were not affected by hypoxia. Under normoxic conditions, uptake of [^{18}F]FLT was significantly lower in MCF7 BC cells compared to MDA-MB231 BC cells: 147±18 versus 242±9 % radioactivity per milligram protein (n=12/4, $P < 0.001$) after 60 min incubation time. In the control MCF10A cells, [^{18}F]FLT uptake was substantially lower after 60 min incubation: 74±13 % radioactivity per milligram protein (n=12/4, $P < 0.001$) when compared to MCF7 and MDA-MB231. This data indicates that there was particularly increased uptake of [^{18}F]FLT in the MCF7 and MDA-MB231 BC cell lines.

Functional hypoxic conditions for *in vitro* cell uptake studies were confirmed through experiments using hypoxia imaging agent [^{64}Cu]ATSM. Increased uptake of [^{64}Cu]ATSM and subsequent trapping of radioactivity correlates with the reducing cellular environment induced by exposure of cells to hypoxic conditions (1% O_2 for 24 h). Neutral and lipophilic [^{64}Cu]ATSM complex enters the cell through passive diffusion. Inside the cell under oxygen-deficient conditions, ^{64}Cu(II) is reduced to ^{64}Cu(I), which is released from the ATSM complex. ^{64}Cu(I) is then partially re-oxidized and trapped through binding to intracellular proteins (30). Under designated experimental conditions (1% O_2 for 24 h), cell uptake of [^{64}Cu]ATSM was significantly higher (Δ20-30%; $P < 0.001$) in both BC cell lines, MCF7 and MDA-MB231, as well as in the control cell line MCF10A at 15, 30, and 60-min time points (**Figure 3B**).

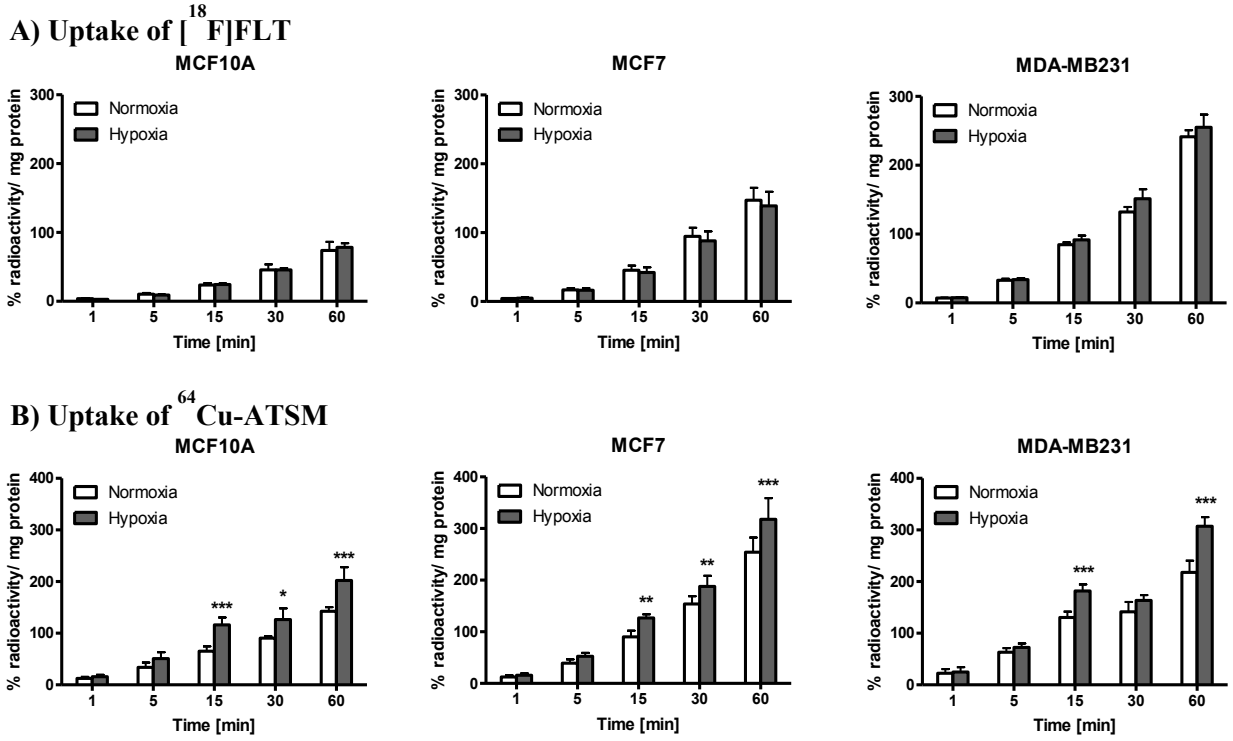

Figure 3. Uptake of (A) [^{18}F]FLT and (B) [^{64}Cu]ATSM in normoxic and hypoxic (1% O_2) MCF10A, MCF7, and MDA-MB231 cells. *In vitro* cell uptake was carried out at 1, 5, 15, 30, and 60 min incubation time using either [^{18}F]FLT (top) or [^{64}Cu]ATSM (bottom). Data are shown as means ± SEM from 3-4 experiments, all performed as triplicates. *$P < 0.05$, **$P < 0.01$, ***$P < 0.001$.

2.33 Competitive cellular inhibition studies with [^{18}F]FLT

To determine potential functional roles of hENT1 and hENT2 on [^{18}F]FLT uptake, competitive inhibition experiments were performed. **Figure 4A** summarizes concentration-dependent effects of the specific hENT1 inhibitor NBMPR (14). Collected data revealed a NBMPR concentration-dependent reduction of [^{18}F]FLT uptake which plateaued at around 100 nM, and was consistent with the known inhibition of hENT1 by NBMPR (IC_{50} 0.4 nM), whereas blocking of hENT2 only occurs at higher concentrations of NBMPR (IC_{50} 2.8 μM) (33,42). The maximum inhibition for this experiment using 100 nM NBMPR across all three cell lines (MCF10A, MCF7 and MDA-MB231) was only ~25-35% (**Figure 4A**). The following IC_{50} values were determined for hENT1 inhibition with NBMPR from Fig. 4A: MCF10A; 6.4 nM, MCF7; 5.9 nM, and MDA-MB231; 3.6 nM. This experiment pointed towards a potential involvement of hENT2 in the remaining uptake of [^{18}F]FLT following inhibition of hENT1 with NBMPR, and the additional possible involvement of concentrative nucleoside transporters (CNT;14,15). Blocking studies with non-radioactive FLT, NBMPR, gemcitabine, and dilazep; a hENT1 inhibitor, were used to further investigate the functional involvement of hENT2 during the [^{18}F]FLT uptake in MDA-MB231 cells. Data are summarized in **Figure 4B**. All inhibitors showed reduced [^{18}F]FLT uptake in MDA-MB231 cells when compared to [^{18}F]FLT uptake data in Krebs-Ringer buffer alone.

Non-radioactive reference compound FLT was used as a positive control and a measure of unspecific uptake, and was able to block all nucleoside transporters involved in uptake of [^{18}F]FLT, which resulted in an almost complete inhibition to 2.7 ± 0.2% (n=3) of control. NBMPR in this experiment at 7 μM reduced [^{18}F]FLT uptake to 54 ± 3% (n=3) of control. High micro-molar concentrations of dilazep, displaying an IC_{50} ~ 18-19 nM for hENT1 and an IC_{50} ~ 9-134 μM for hENT2 (34,39), reduced [^{18}F]FLT uptake to ~6 ± 1% at 100 μM and to ~3 ± 0.3%

at 300 µM (both n=3), of control (100%), respectively. These results suggested a potential involvement of hENT2 in the uptake mechanism of [^{18}F]FLT in BC cells. Additionally, gemcitabine, a chemotherapeutic drug for the treatment of BC, is transported into cancer cells via hENT1 and hCNT1. However, the observed inhibition with gemcitabine was lower than that with NBMPR reaching only 65 ± 3% (n=3) with 300 µM of gemcitabine.

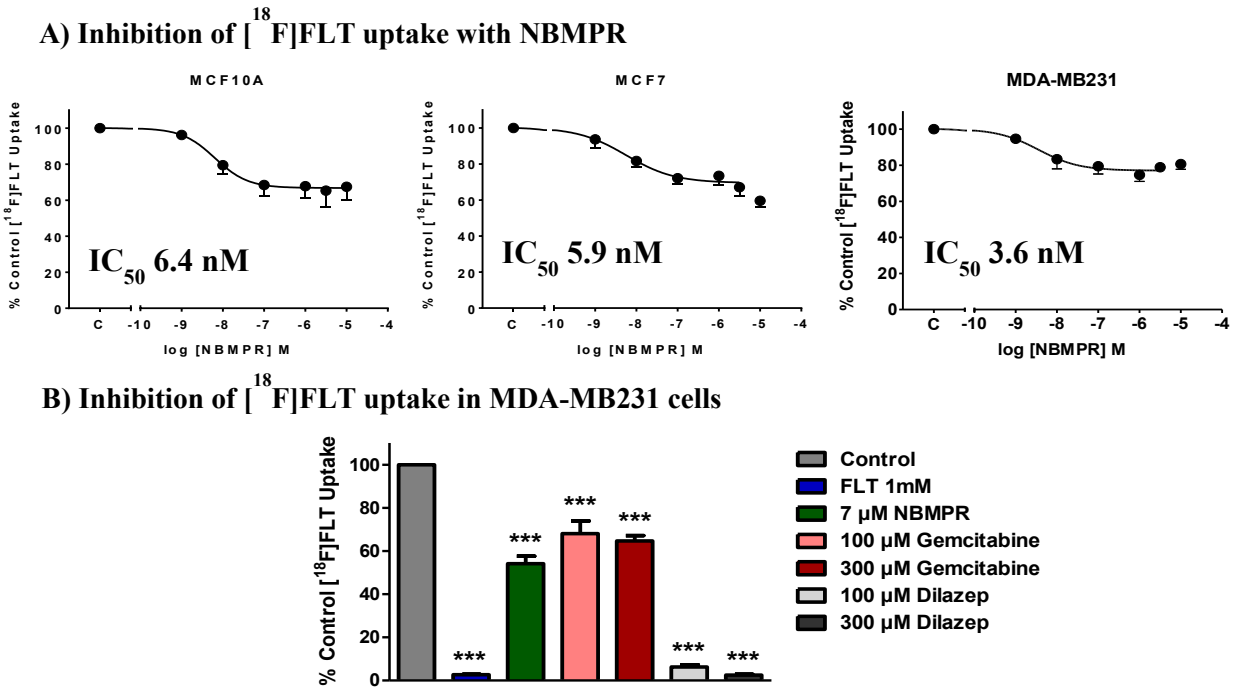

Figure 4. A) Uptake of [^{18}F]FLT into normoxic MCF10A, MCF7, and MDA-MB231 cells at 60 min incubation time in the presence of increasing concentrations of NBMPR (1 nM to 10 µM) compared to 100% control [^{18}F]FLT uptake containing Krebs-Ringer buffer only, with no inhibitor present. Data are shown as means ± SEM from three experiments, all performed as triplicates. **B)** Uptake of [^{18}F]FLT into normoxic MDA-MB231 cells at 60 min incubation time in the presence of 1 mM non-radioactive FLT; 6.7 µM NBMPR; 100-300 µM gemcitabine; or 100-300 µM dilazep compared to control containing Krebs-Ringer buffer only with no blocking compound present.

Next, additional roles of hCNTs were analyzed in more detail in all three cell lines (**Figure 5A**). Cell uptake studies were conducted in sodium-containing Krebs-Ringer buffer as well as choline-containing buffer as transport through hCNT1 and hCNT2 can be blocked in sodium-free buffer (41). Uptake of [^{18}F]FLT was significantly reduced in absence of Na+ in all three cell lines by: 35 ± 1 % in MCF10A, 35 ± 1 % in MDA-MB231, and 52 ± 2 % in MCF7 (all n=6/2, P<0.001). This data point towards the involvement of hCNT1 and hCNT2 in [^{18}F]FLT transport. Unspecific [^{18}F]FLT uptake was shown to be in the range of 6-9% during the experiments as demonstrated through blocking studies with non-radiolabeled FLT. Both, dilazep (1 μM) and NBMPR (1 μM) reduced [^{18}F]FLT uptake in choline buffer significantly in all three cell lines pointing towards the fraction of hENT1 involvement (**Figure 5B**). Interestingly, a statistically significant difference between the blocking effects of 1 μM NBMPR and 1 μM dilazep was only observed in MDA-MB231 cells: 24 ± 2 % (1 μM NBMPR) versus 18 ± 2 % (1 μM dilazep) (both n=6/2; P<0.001). This difference was not observed in the other two cell lines. A high 1 mM concentration of gemcitabine resulted in a small reduction of [^{18}F]FLT uptake in choline buffer only in MDA-MB231 cells. However, the measured 11 ± 3 % inhibitory effect was significant (n=3; P<0.01; **Figure 5B**). This suggests hCNT-mediated inhibitory effects as detected with gemcitabine at 100 μM and 300 μM concentrations during [^{18}F]FLT inhibition studies in MDA-MB231 cells (**Figure 4B**). **Figure 5C** depicts effects of increasing concentrations of dilazep in sodium-containing Krebs-Ringer Buffer. Due to solubility limitations, NBMPR was not tested at concentrations >10 μM. Inhibitory effects at high concentrations of dilazep (100 μM) compared to the effect of 1 μM in choline buffer (blocking of hENT1 and hCNTs) further pointed towards functional involvement of hENT2 in uptake of [^{18}F]FLT in all three investigated cell lines.

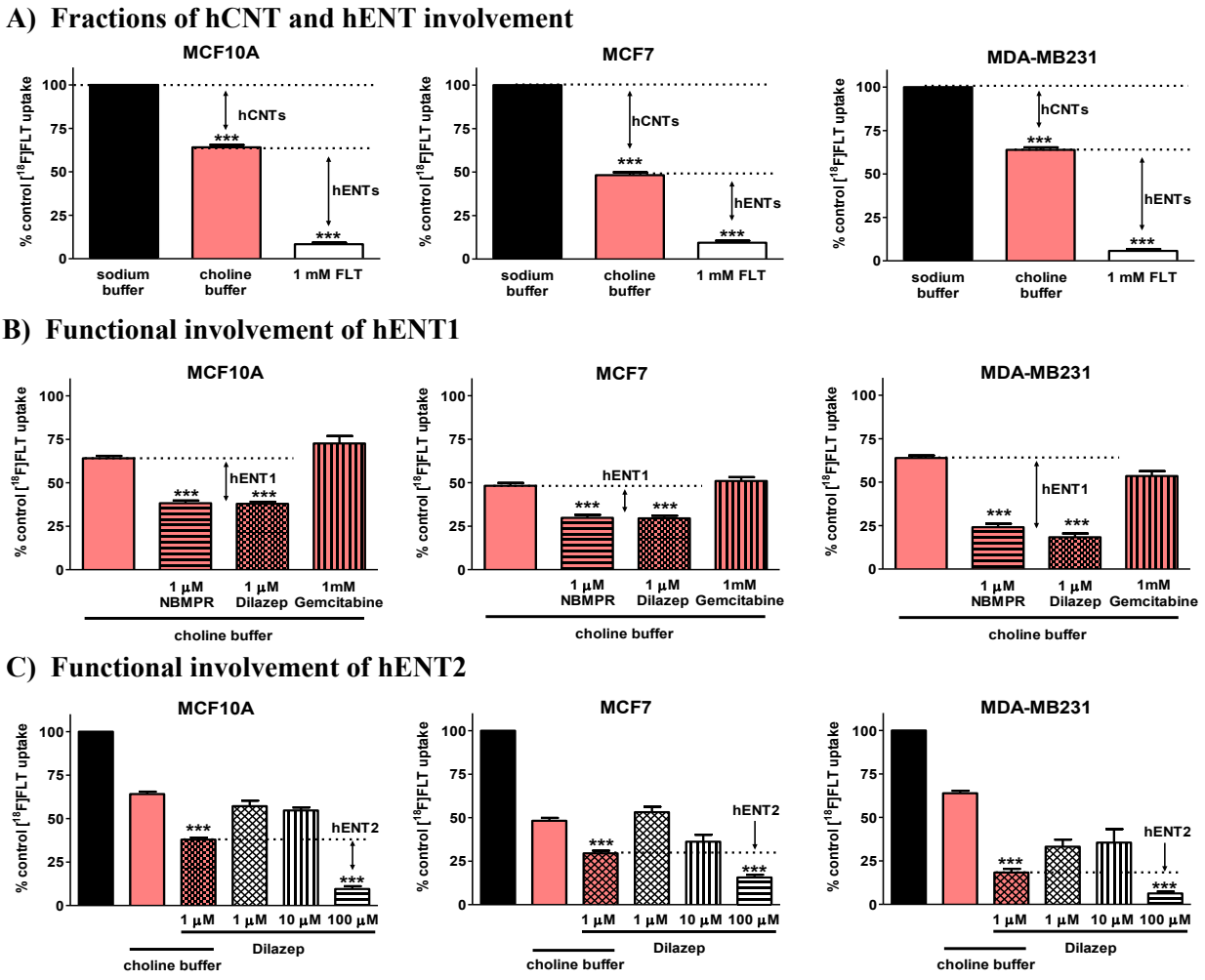

Figure 5. Uptake of [^{18}F]FLT into normoxic MCF10A, MCF7, and MDA-MB231 cells at 60 min incubation time in the presence of **A)** Krebs-Ringer (sodium buffer), choline buffer, or 1 mM cold FLT in sodium buffer; **B)** choline buffer, 1 µM NBMPR in choline buffer, 1 µM dilazep in choline buffer or 1 mM gemcitabine in choline buffer; **C)** Krebs-Ringer (sodium buffer), choline buffer, 1 µM dilazep in choline buffer, and 1 , 10, and 100 µM dilazep in Krebs-Ringer.Data are shown as means ± SEM from three experiments, all performed as triplicates. *** $P< 0.001$.

2.34 hENT1 expression analysis with SAHENTA

Green FITC-labeled fluorescent hENT1 probe, SAHENTA, was used to visualize hENT1 expression on the cell surface of live cells via confocal microscopy (32). Blue staining is noted as Hoechst 33342, a nucleus binding agent. Red staining with CellMask Deep Red targets the membrane, while the green signal represents SAHENTA. Highest binding of SAHENTA was detected visually in MDA-MB231 cells. Comparable binding was observed in MCF7 and MCF10A (**Figure 6A**).

Visually, binding of SAHENTA to membranes of all three cell lines correlated well with hENT1 protein expression results from the Western blot experiments (**Figure 2B**) under normoxic conditions. SAHENTA staining could be blocked almost completely in all three cell lines using 10 μM of the hENT1 inhibitor NBMPR (**Figure 6A**). Blocking by NBMPR was most pronounced in the MDA-MB231 TNBC cells, which is similar to the high hENT1 expression levels in this cell line. In contrast, under hypoxic conditions no differences in SAHENTA binding were detected, indicating no increase of hENT1 expression under hypoxia (**Figure 6B**). This finding also correlated with results of Western blot experiments where no or little effects on hENT1 expression were detected under hypoxia (**Figure 2C-E**).

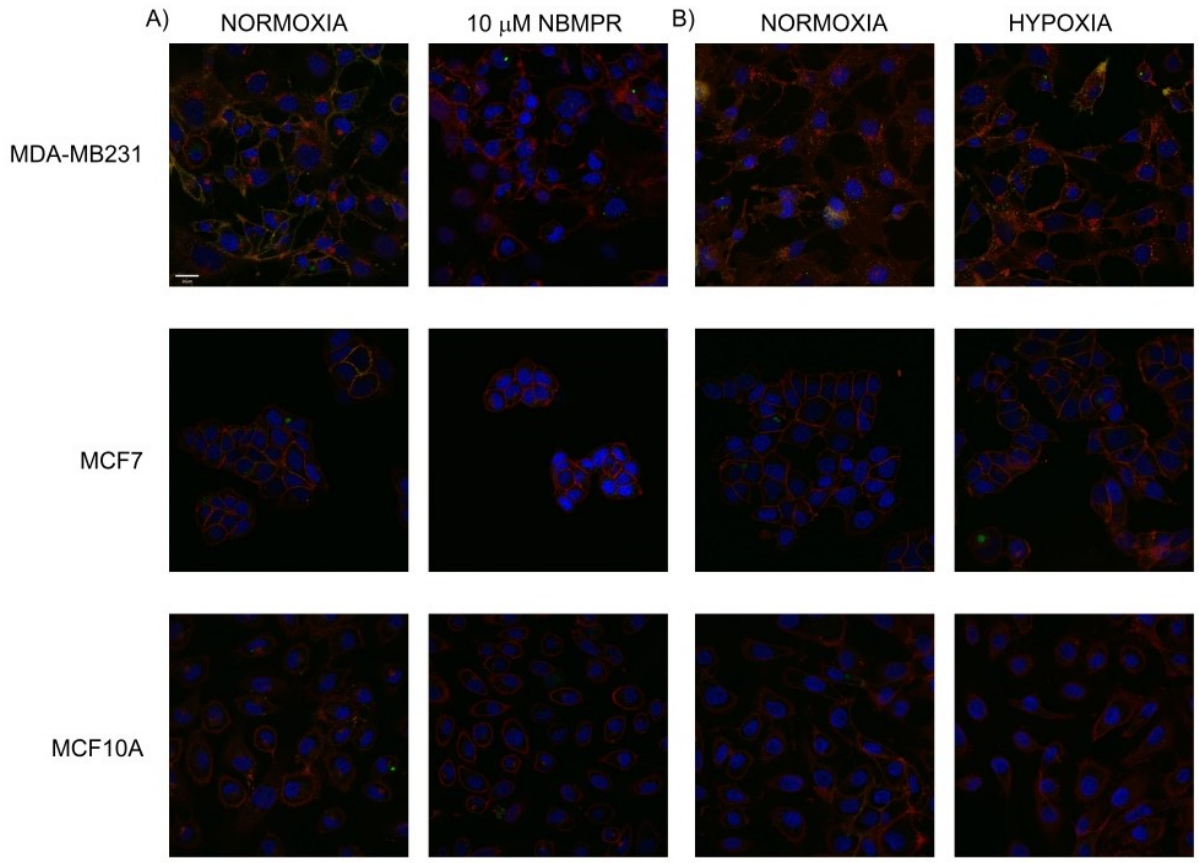

Figure 6. A) Live cell imaging with SAHENTA under normoxic conditions in Krebs-Ringer buffer, or in the presence of 10 μM NBMPR in Krebs-Ringer buffer solution after 45 min of incubation. **B)** Live cell imaging with SAHENTA in Krebs-Ringer buffer solution under normoxic or hypoxic conditions after 45 min of incubation (green – SAHENTA; blue – Hoechst; red – CellMask Deep Red. Scale 1 pixel = 0.1 μM).

2.35 Flow cytometry analysis of hENT1and hENT2 expression

Flow cytometry analysis was performed under normoxic and hypoxic conditions to quantify hENT1 **(Figure 7)** and hENT2 **(Figure 8)** protein expression in MCF10A, MCF7, and MDA-MB231 cells. Under normoxic conditions, specific anti-hENT1 or anti-hENT2 antibody plus Alexa Fluor 488–labeled secondary antibody provided a fluorescent signal confirming expression of hENT1 and hENT2 in all three cell lines. Signal intensity did not change significantly under hypoxic conditions confirming findings of the Western blot analyses for both transporters. However, comparison of flow cytometry data with cellular uptake experiments in triple-negative MDA-MB231 cells (**Figure 3A**) showed a trend for higher expression of hENT1 but not hENT2.

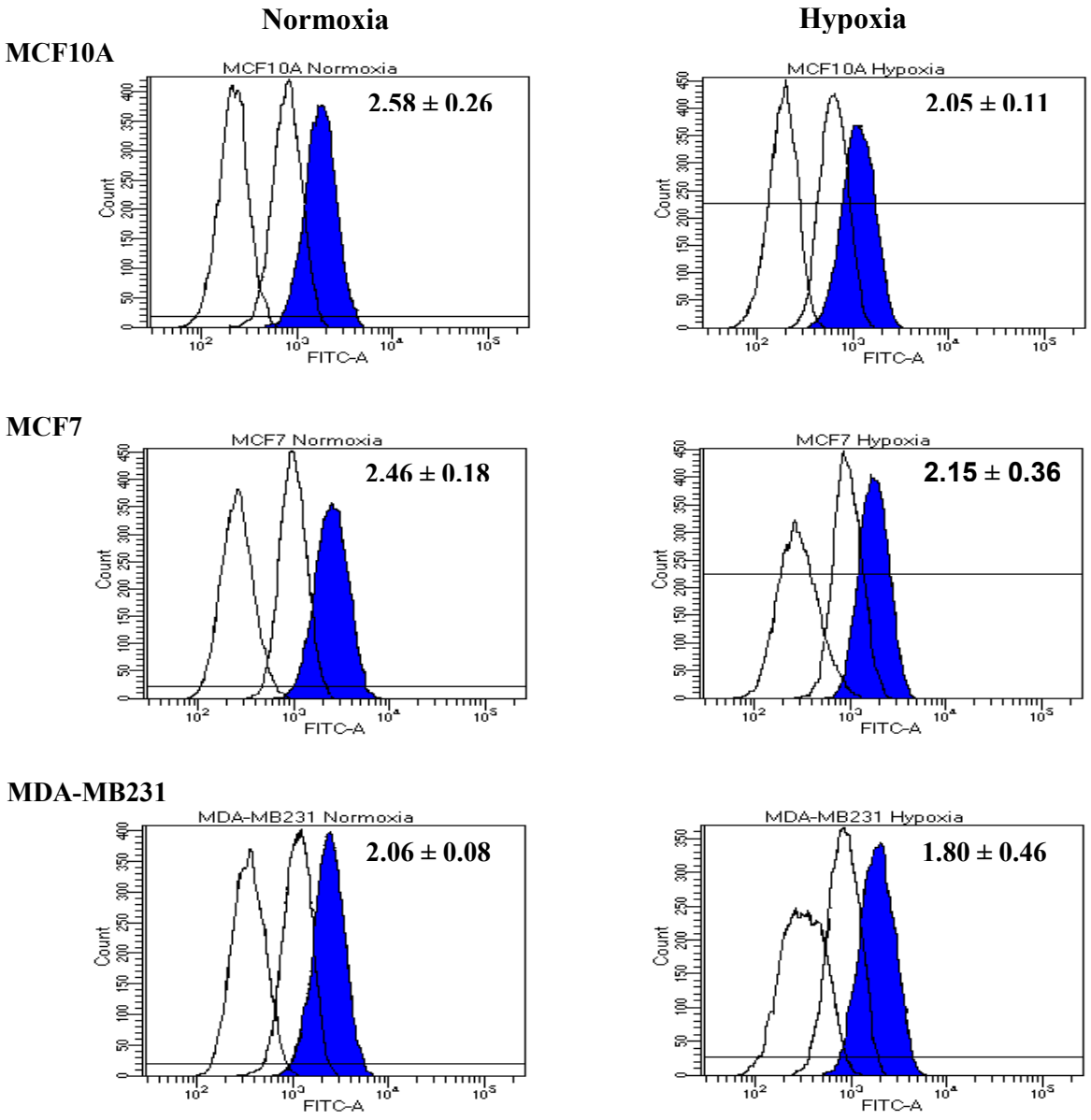

Figure 7. Analysis of hENT1 in MDA-MB231, MCF7, and MCF10A cells cultured under (left) normoxic conditions *vs.* (right) hypoxic conditions. The x- and y-axis of each graph show the fluorescence intensity and the number of cells, respectively. The two left-most histograms depict unstained cells (left) and only-secondary antibody control (middle). Values are ratios of the average of primary and secondary stained cells (calculated by the mean fluorescence intensity of blue-closed which highlights the hENT1 expression) *vs.* the average of only-secondary antibody treated cells (calculated based on the mean fluorescence intensity of black closed which highlights only unspecific binding). Data are shown as means of the calculated ratios of N=3 experiments. Student's t-tests were performed to determine statistical significance.

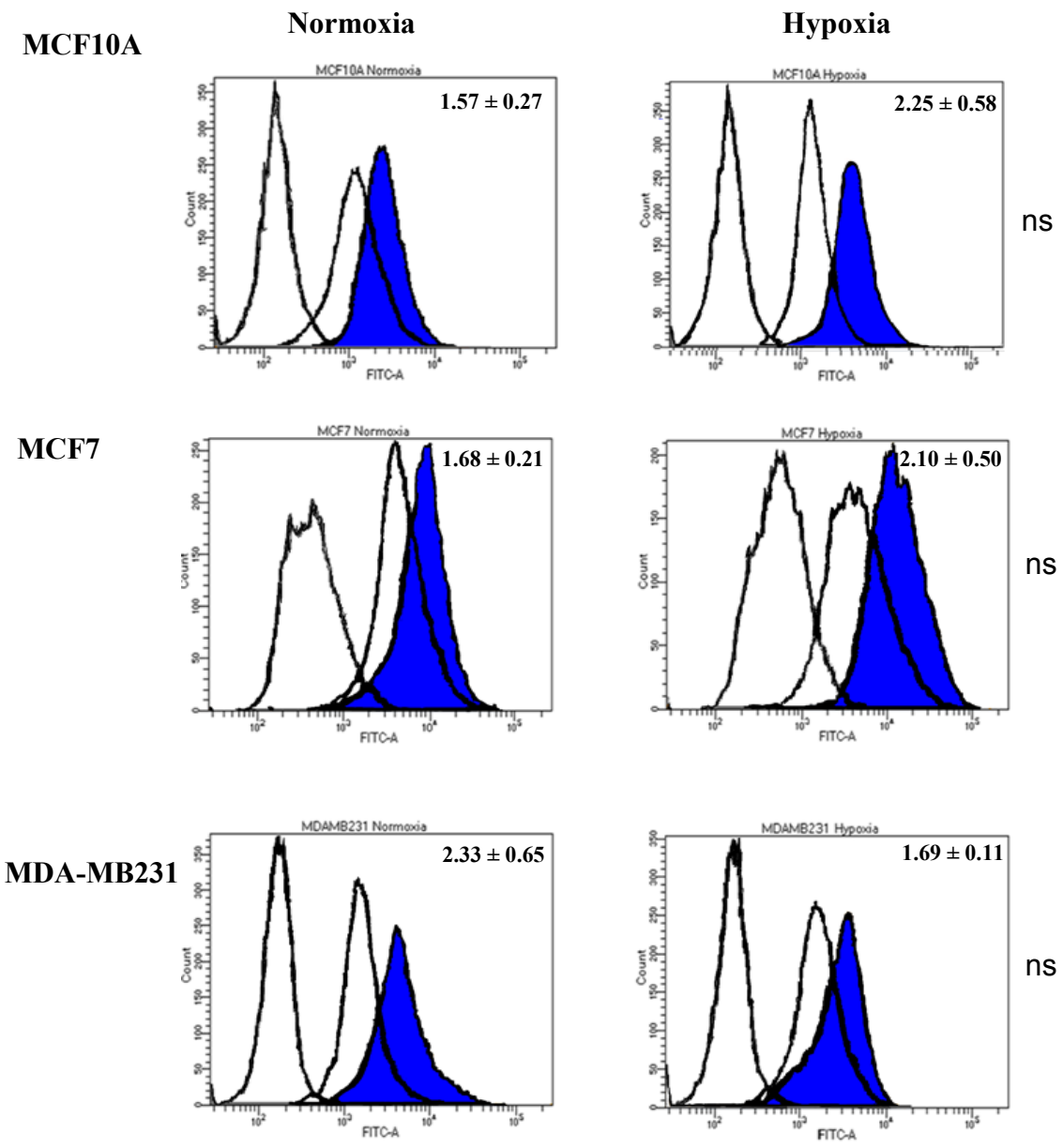

Figure 8. Analysis of hENT2 in MDA-MB231, MCF7, and MCF10A cells cultured under (left) normoxic conditions *vs.* (right) hypoxic conditions. The x- and y-axis of each graph show the fluorescence intensity and the number of cells, respectively. The two left-most histograms depict unstained cells (left) and only-secondary antibody control (middle). Values are ratios of the average of primary and secondary stained cells (calculated by the mean fluorescence intensity of blue-closed which highlights the hENT1 expression) *vs.* the average of only-secondary antibody treated cells (calculated based on the mean fluorescence intensity of black closed which highlights only unspecific binding). Data are shown as means of the calculated ratios of N=3 experiments. Student's t-tests were performed to determine statistical significance.

2.36 In vivo PET imaging experiments

Results of *in vivo* PET imaging experiments with [^{18}F]FLT in MDA-MB231 and MCF7 tumor-bearing mice are summarized in **Figure 9**. Tumor uptake and retention profiles of [^{18}F]FLT over 60 min was comparable in both tumors resulting in similar radioactivity uptake levels: SUV_{60min} 0.96 ± 0.05 (n=3) for MDA-MB231 and 0.89±0.08 (n=3) for MCF7 tumors, respectively. Muscle uptake and clearance of [^{18}F]FLT was also comparable leading to similar tumor-to-muscle ratios (TMR): 1.31 for MDA-MB231 and 1.35 for MCF7 tumors at 60 min post injection (p.i.). The similar results in ER+ MCF7 and TNBC MDA-MB231 tumors indicate that uptake and retention of [^{18}F]FLT seem to be estrogen receptor-independent.

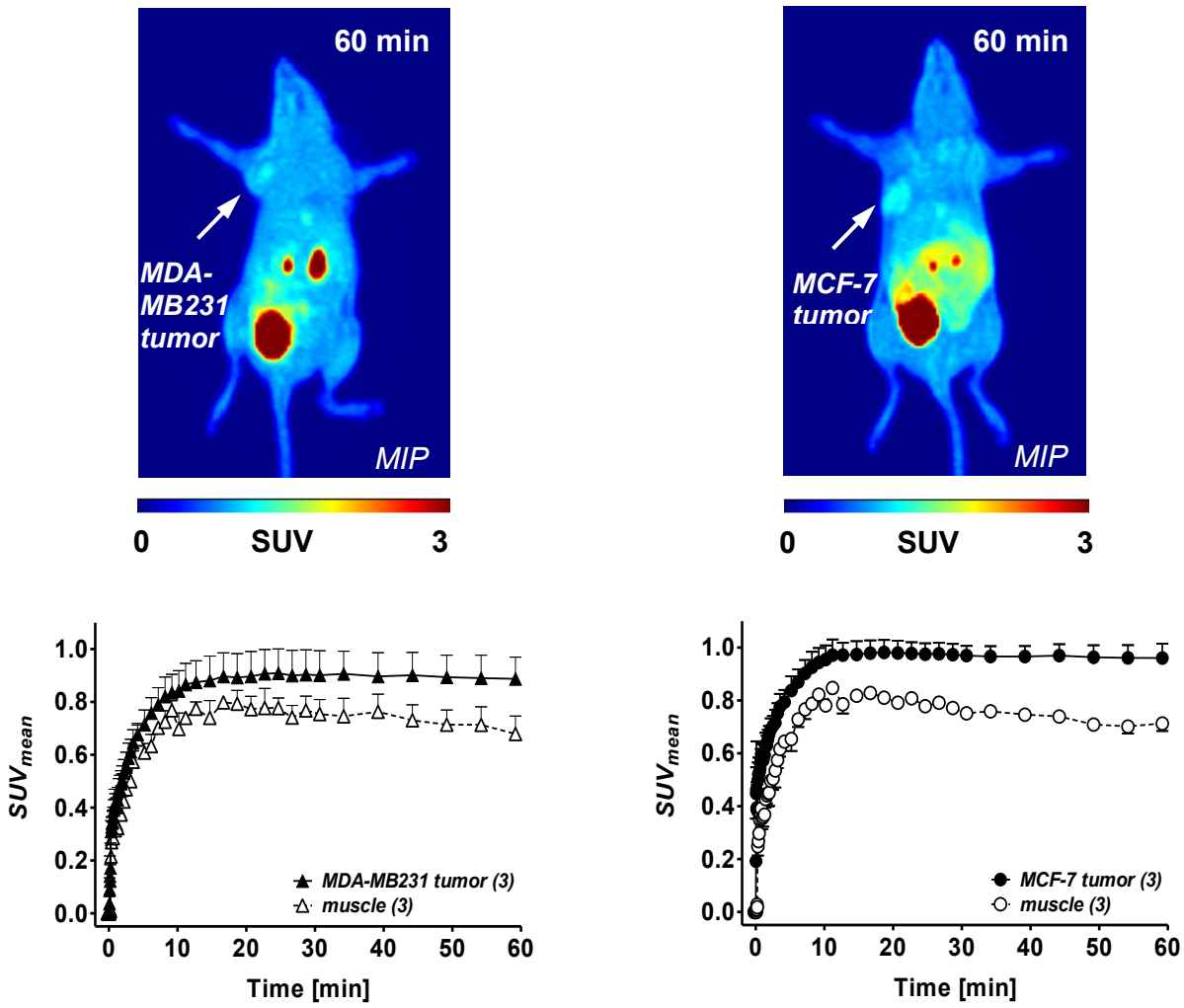

Figure 9. Top: Representative PET images from dynamic scans after injection of [^{18}F]FLT into MDA-MB231 (left) and MCF7 (right) tumour-bearing NIH-III mice at 60 min post-injection. **Bottom:** Corresponding time-activity curves (TACs) for tumor and muscle uptake over the entire time frame of 60 min. Data are shown as means ± SEM from n individual experiments. MIP (maximum intensity projection).

2.4 DISCUSSION

The goals of the current study were to *(1)* analyze the relationship between hypoxia and the expression and function of nucleoside transporters hENT1 and hENT2 in breast cancer, *(2)* determine the effects of additional nucleoside transporters on uptake of [^{18}F]FLT, and *(3)* explore the utility of [^{18}F]FLT-PET in differentiating between ER(+) BC and TNBC.

The following conclusions were made based on the obtained results: *i)* Data from the Canadian Breast Cancer Foundation Tumor Bank showed significantly higher mRNA expression of hENT2 and TK1 in breast cancer, while no differences were observed between ER(+) BC and TNBC *ii)* Triple-negative MDA-MB231 breast cancer cells showed higher levels of [^{18}F]FLT uptake compared to ER(+) MCF7 cells; *iii)* this difference was not observed in MDA-MB231 and MCF7 tumors *in vivo*; *iv)* in contrast to literature which discussed a downregulation of ENT1 during hypoxia in endothelial cells (23, 24), no significant changes of hENT1, hENT2, and TK1 expression under normoxic and hypoxic conditions were found in breast cancer cells; *v)* besides hENT1, hENT2 and hCNT's are also functionally involved in transport and uptake of [^{18}F]FLT into BC cells; *vi)* [^{18}F]FLT-PET imaging results in MDA-MB231 and MCF7 BC tumors and *in vitro* confocal microscopy and flow cytometry experiments targeting hENT1 with FITC-labeled SAHENTA and hENT1 and hENT2 antibody, are similar as no differences were seen.

Triple-negative MDA-MB231 BC cells accumulate and retain more [^{18}F]FLT than ER(+) MCF7 cells *in vitro*. According to literature, [^{18}F]FLT uptake correlates with proliferation index marker Ki-67 (35). Numerous studies have analyzed the role of Ki-67 as a prognostic marker in BC. While ER(+) luminal B BC demonstrated a correlation between elevated proliferative index Ki-67 values and a higher risk of axillary lymph node metastases (36), the prognostic value of Ki-67 was recently challenged based on substantial variations in Ki-67 index between cytology and

histology in samples of different BC subtypes (35). Current literature does not describe detailed analyses on correlation and/or differences between Ki-67 index and [^{18}F]FLT uptake in triple-negative and ER(+) BC samples.

The present [^{18}F]FLT-PET imaging data in MDA-MB231 and MCF7 tumors confirmed this fact, since no differences in tumor uptake and retention were detected. [^{18}F]FLT-PET imaging experiments revealed comparable SUV_{60min} values (~0.9-0.95) and tumor-to-muscle ratios (~1.30-1.35) for MDA-MB231 and MCF7 tumors. To the best of our knowledge, no detailed studies have been reported yet exploring the effects of hypoxia on the regulation of nucleoside transporter expression and function in BC.

The present data indicate no hypoxia-driven regulation on expression and function of hENT1, hENT2, or TK1 in BC. Protein analysis in both BC cell lines did not show significant reduction or elevation of hENT1 and hENT2 expression under hypoxic conditions. Cellular uptake experiments with [^{18}F]FLT also revealed no significant differences between normoxic and hypoxic conditions in BC and control cell lines.

Hypoxic induction in all cell lines was functionally verified with [^{64}Cu]ATSM, a radiotracer for imaging hypoxia (37). Uptake of [^{64}Cu]ATSM was significantly increased in all three cell lines starting at the 15 min time point, confirming that all cells were functionally hypoxic, for the [^{18}F]FLT uptake experiments. Recently, we also have confirmed the presence of hypoxic conditions and related elevated HIF-1α protein expression through cellular uptake experiments with [^{18}F]FAZA, an alternative PET radiotracer for hypoxia imaging (22).

The observed comparable [^{18}F]FLT uptake profile in MCF7 and MDA-MB231, despite the higher, though insignificant, hENT1 expression levels ($P < 0.0936$) in MDA-MB231 cells, could

be explained by a basal level of hENT2 and CNTs expression and uptake of [^{18}F]FLT, as well as the overall expression of TK1 which leads to phosphorylation and therefore cellular retention of [^{18}F]FLT.

Protein expression levels of hENT2 are similar in both BC cell lines. Uptake and retention of ^{18}F-labeled thymidine analogue [^{18}F]FLT is mediated through nucleoside transporters hENT1 and hENT2, followed by phosphorylation with TK1. Both processes may contribute with complementary compensation effects to the overall comparable uptake and retention of [^{18}F]FLT in MCF7 and MDA-MB231 tumors *in vivo*. The observed comparable uptake and retention profile of [^{18}F]FLT in TNBC or ER(+) BC tumors is also in alignment with the reported discrepancies in Ki-67 index and [^{18}F]FLT uptake in BC patient samples (35). In addition to these reports, the present data showed no significant changes in expression or function of nucleoside transporters hENT1 and hENT2 under hypoxic conditions. Flow cytometry experiments further confirmed that no changes in hENT1 and hENT2 expression were induced through hypoxic conditions in both BC cell lines MCF7 and MDA-MB231. Present data on human mRNA expression also supported this data. All three genes (hENT1, hENT2, and TK1) showed no significant differences in ER(+) and triple-negative BC samples. Samples from triple-negative patient cohorts contained significantly higher levels of HIF1α (22) making triple-negative breast tumors presumably more hypoxic compared to ER(+) BC. Facilitative hexose transporters GLUT1 and GLUT5 as HIF1α downstream target genes showed also elevated mRNA levels in triple-negative BC (22). However, present hENT1, hENT2, and TK1 mRNA data showed no elevated levels in triple-negative versus ER(+) BC. This further supports the assumption that hypoxia and therefore HIF1α do not regulate equilibrative nucleoside transporters in BC.

However, previous studies have demonstrated that the majority of [^{18}F]FLT uptake into different types of cancer cells is mediated through hENT1 transporters (14). Functional involvement of hENT1 for [^{18}F]FLT uptake was confirmed in a hENT1 knockdown tumor model *in vivo* (28).

The essential role of hENT1 as a drug target for therapy was explored with nucleoside analogue 5′-deoxy-5-fluorouridine (5'DFUR) (38). This study confirmed the essential role of hENT1 for full transcriptional response of nucleoside-based chemotherapeutic drug treatments in an MCF7 BC tumor model (38).

In the present study high hENT2 expression levels were also detected in both BC cell lines. To elucidate the role of hENT2 for [^{18}F]FLT uptake in both BC cell lines, selective *in vitro* inhibition studies were performed.

Nucleoside transporters hENT1 and hENT2 differ in their affinity for nucleoside substrates and in their sensitivity to inhibitors. In a first set of experiments NBMPR was used as a specific inhibitor for hENT1 with only minimal hENT2 inhibition at low nM concentrations. Inhibition of hENT2 by NBMPR only occurs at higher concentrations above 10 μM range. Equilibrative nucleoside transporter hENT1 is functionally present in both studied BC cell lines as well as in the MCF10A control cell line. The comparable low nanomolar IC_{50} values (3.6-6.4 nM) in the [^{18}F]FLT inhibition studies with NBMPR show conclusive evidence that there are no significant functional differences of hENT1 in all three cell lines. Additional inhibition experiments confirmed potential functional involvement of hENT2 during the [^{18}F]FLT transport studies. Moreover, presence of hCNTs was also elucidated as hCNTs are known to be involved in nucleoside transport (15). Interestingly, about 30% of [^{18}F]FLT uptake is mediated by hCNTs in MDA-MB231 and MCF10A cells. A 50% hCNTs-mediated [^{18}F]FLT uptake was observed in MCF7 cells. Experiments were performed in sodium-free choline-containing buffer to block

hCNTs as their function depends on the presence of free sodium ions (41). Blocking experiments with 1 μM of NBMPR or 1 μM of dilazep in choline buffer revealed the fraction of hENT2-mediated [^{18}F]FLT uptake. NBMPR and dilazep specifically inhibit hENT1 at low μM concentrations, and hCNTs are blocked through their sodium-dependent transport mechanism in sodium-free choline-containing buffer.

A comparison of IC_{50} values from binding studies with [^{3}H]uridine revealed that NBMPR is slightly more potent for both transporters than dilazep: hENT1 0.4 nM versus 17.5 nM; hENT2 2.8 μM versus 8.8 μM (39, 42). Data in Figure 5B showed the direct comparison of 1 μM of dilazep to 1 μM of NBMPR in sodium-free choline buffer on [^{18}F]FLT uptake. A small but significant difference of Δ 6% was detected in MDA-MB231 cells only. However, the total fraction of hENT1-mediated [^{18}F]FLT transport could be higher in triple-negative cells versus ER(+) MCF7 cells, in which the hCNTs-mediated fraction was found to be higher (51% versus 31%). This difference could explain the overall higher [^{18}F]FLT uptake in triple-negative MDA-MB231 breast cancer cells.

After subtracting the unspecific transport portion as measured with cold FLT, hENT2 mediates [^{18}F]FLT transport in MCF10A cells by ~30%, in MCF7 cells by ~20%, and in MDA-MB231 cells by~17%. Comprehensive functional *in vitro* analysis suggests that [^{18}F]FLT uptake is mediated by ~36% hCNT, ~30% hENT2, ~26% hENT1, and ~8% unspecific in MCF10A cells; ~52% hCNT, ~20% hENT2, ~19% hENT1, and ~9% unspecific in MCF7 cells; ~37% hCNT, ~17% hENT2, ~40% hENT1, and ~6% unspecific in MDA-MB231 cells.

Therefore, it can be concluded that both equilibrative nucleoside transporters hENT1 and hENT2, as well as concentrative nucleoside transporters are functionally involved into the cellular uptake of [^{18}F]FLT in all tested cell lines. This finding may have implications for the

therapy of BC patients using nucleoside derivatives like gemcitabine as chemotherapeutic drugs as it has been demonstrated that gemcitabine treatment has low or no activity when the BC phenotype is hENT1 deficient (27).

As dilazep and some of its derivatives displayed hENT1 and hENT2 inhibition potential, there are currently no selective hENT2 inhibitors around for the treatment of BC (39). It remains to be elucidated in more detail as to how hENT2 functional expression is regulated in BC and if the development of selective hENT2 inhibitors as potential new anticancer drugs would have effects on BC therapy (40).

2.5 CONCLUSIONS

In contrast to previously reported downregulation of hENT1 expression in vascular endothelial cells during hypoxic events such as ischemia, the present data demonstrate that the treatment of cells for 24 h with 1 % O_2 had no effect on downstream expression and function of hENT1 and hENT2 in BC. Noteworthy, we did not measure mRNA levels after 24 h, thus it cannot be excluded that there is no upregulation of hENT1 and hENT2 mRNA. However, hENT2 and TK1, but not hENT1 mRNA, are upregulated in samples from breast cancer patients. Expression levels of all three genes do not show significant differences in ER(+) and triple-negative BC samples. As a result of similar levels of TK1 expression in ER(+) and triple-negative BC, complementary effects on nucleoside transport and nucleoside phosphorylation must result in comparable [^{18}F]FLT uptake and retention profiles in both BC tumors despite their different phenotypes. Clinically, this could pose a challenge in differentiating between different cancer subtypes. Additionally, this study also provides primary evidence that the nucleoside transporter hENT2 plays an important role in [^{18}F]FLT uptake by BC cells. This finding should stimulate interest in exploring the role of hENT2 as a biomarker in BC management and furthermore

stimulate research in finding hENT2 specific inhibitors as novel drugs for targeted therapy of BC.

ACKNOWLEDGEMENTS

The authors thank Dr. John Wilson, David Clendening, and Blake Lazurko from the Edmonton Radiopharmaceutical Center for ^{18}F production. The authors thank Ali Akbari and Cody Bergman for preparation of [^{18}F]FLT. The authors are also grateful to Dan McGinn (Vivarium of the Cross Cancer Institute, Edmonton, AB, Canada) for supporting the animal work and Dr. Hans-Soenke Jans (University of Alberta) for technical help and support of the PET imaging experiments. We also thank Dr. Xuejun Sun and Geraldine Barron of the Cell Imaging Facility of Department of Oncology for their help with the cell imaging experiments. D.K. thanks the Alberta Cancer Foundation for a Graduate Student Scholarship and the Cancer Research Institute of Northern Alberta (CRINA) for la Vie en Rose Scholarship for Breast Cancer Research. The authors also gratefully acknowledge the Dianne and Irving Kipnes Foundation for supporting this work.

AUTHOR CONTRIBUTIONS

D. Krys was responsible for cell culture, Western blot experiments, cell imaging, *in vitro* cell-uptake experiments, flow cytometry, analysis, contributed to the animal experiments, and wrote the manuscript; I. Hamann contributed to cell culture, Western blot experiments, and flow cytometry; M. Wuest performed all *in vivo* PET experiments and analysis, and wrote portions of and revised the manuscript; F. Wuest was responsible for the design of the study and critically reviewed the manuscript; and all authors read and approved the final manuscript and agreed to be accountable for the integrity of the work.

2.6 REFERENCES

1. DeSantis, C. E., Ma, J., Goding Sauer, A., Newman, L. A., and Jemal, A. (2017) Breast cancer statistics, 2017, racial disparity in mortality by state. *CA. Cancer J. Clin.* **67**, 439–448

2. Kabat, G. C., Ginsberg, M., Sparano, J. A., and Rohan, T. E. (2017) Risk of Recurrence and Mortality in a Multi-Ethnic Breast Cancer Population. *J. Racial Ethn. Health Disparities.* **4**, 1181–1188

3. Tevaarwerk, A. J., Gray, R. J., Schneider, B. P., Smith, M. L., Wagner, L. I., Fetting, J. H., Davidson, N., Goldstein, L. J., Miller, K. D., and Sparano, J. A. (2013) Survival in Patients With Metastatic Recurrent Breast Cancer After Adjuvant Chemotherapy Little Evidence of Improvement Over the Past 30 Years Characteristics of Included Trials. *Cancer* **119**, 1140–1148

4. Bychkovsky, B. L. and Lin, N. U. (2019) Imaging in the evaluation and follow-up of early and advanced breast cancer : When , why , and how often? *The Breast* **31**, 318–324

5. Sun, Y., Yang, Z., Zhang, Y., Xue, J., Wang, M., Shi, W., Zhu, B., Hu, S., Yao, Z., Pan, H., and Zhang, Y. (2015) The preliminary study of 16 α-[^{18}F] fluoroestradiol PET/CT in assisting the individualized treatment decisions of breast cancer patients. *PLoS One* **10**, 1–9

6. Liao, G. J., Clark, A. S., Schubert, E. K., and Mankoff, D. A. (2016) ^{18}F-Fluoroestradiol PET: Current Status and Potential Future Clinical Applications. *J. Nucl. Med.* **57**, 1269–1275

7. Mcguire, A. H., Dehdashti, F., Siegel, B. A., Lyss, A. P., Brodack, J. W., Mathias, C. J., Mintun, M. A., Katzenellenbogen, J. A., and Welch, M. J. (1991) Positron Tomographic Assessment of 16a-[^{18}F] Fluoro-17/3-Estradiol Uptake in Metastatic Breast Carcinoma. *J. Nucl. Med.* **32**, 1526–1531

8. Groheux, D., Cochet, A., Humbert, O., Alberini, J.L., Hindie, E., and Mankoff, D. (2016) ^{18}F-FDG PET/CT for Staging and Restaging of Breast Cancer. *J. Nucl. Med.* **57**, 17S–26S

9. Shen, B., Huang, T., Sun, Y., Jin, Z., and Li, X.F. (2017) Revisit ^{18}F-fluorodeoxyglucose oncology positron emission tomography: 'systems molecular imaging' of glucose metabolism. *Oncotarget* **8**, 43536–43542

10. Alvarez, J. V., Belka, G. K., Pan, T. C., Chen, C. C., Blankemeyer, E., Alavi, A., Karp, J. S., and Chodosh, L. A. (2014) Oncogene pathway activation in mammary tumors dictates FDG-PET uptake. *Cancer Res.* **74**, 7583–7598

11. Kubota, K., Yamashita, H., and Mimori, A. (2017) Clinical Value of FDG-PET/CT for the Evaluation of Rheumatic Diseases: Rheumatoid Arthritis, Polymyalgia Rheumatica, and Relapsing Polychondritis. *Semin. Nucl. Med.* **47**, 408–424

12. Adejolu, M., Huo, L., Rohren, E., Santiago, L., and Yang, W. T. (2012) False-positive lesions mimicking breast cancer on FDG PET and PET/CT. *AJR. Am. J. Roentgenol.* **198**, W304-W314

13. Toyohara, J., Waki, A., Takamatsu, S., Yonekura, Y., Magata, Y., and Fujibayashi, Y. (2002) Basis of FLT as a cell proliferation marker: Comparative uptake studies with [^{3}H]thymidine and [^{3}H]arabinothymidine, and cell-analysis in 22 asynchronously growing tumor cell lines. *Nucl. Med. Biol.* **29**, 281–287

14. Paproski, R. J., Ng, A. M. L., Yao, S. Y. M., Graham, K., Young, J. D., and Cass, C. E. (2008) The Role of Human Nucleoside Transporters in Uptake of 3'-Deoxy-3'-fluorothymidine. *Mol. Pharmacol.* **74**, 1372–1380

15. Young, J.D., Yao, S.Y., Baldwin, J.M., Cass, C.E., and Baldwin, S.A. (2013) The human concentrative and equilibrative nucleoside transporter families, SLC28 and SLC29. *Mol. Aspects Med.* **34**, 529–547

16. Pastor-Anglada, M., Cano-Soldado, P., Errasti-Murugarren, E. & Casado, F. J. SLC28 genes and concentrative nucleoside transporter (CNT) proteins. *Xenobiotica* **38,** 972–994 (2008).

17. Barthel, H., Perumal, M., Latigo, J., He, Q., Brady, F., Luthra, S. K., Price, P. M., and Aboagye E. O., (2005) The uptake of 3′-deoxy-3′-[^{18}F]fluorothymidine into L5178Y tumours in vivo is dependent on thymidine kinase 1 protein levels. *Eur. J. Nucl. Med. Mol. Imaging* **32**, 257–263

18. Semenza, G. L. (2016) The hypoxic tumor microenvironment: A driving force for breast cancer progression. *Biochim. Biophys. Acta - Mol. Cell Res.* **1863**, 382–391

19. Kumar, H. and Choi, D.K. (2015) Hypoxia Inducible Factor Pathway and Physiological Adaptation : A Cell Survival Pathway? **2015**, 1-11

20. Lee, K. E. and Simon, M. C. (2015) SnapShot: Hypoxia-Inducible Factors. *Cell* **163**, 1288

21. Masoud, G. N. and Li, W. (2015) HIF-1α pathway: Role, regulation and intervention for cancer therapy. *Acta Pharm. Sin. B* **5**, 378–389

22. Hamann, I., Krys, D., Glubrecht, D., Bouvet, V., Marshall, A., Vos, L., Mackey, J. R., Wuest, M., and Wuest, F. (2018) Expression and function of hexose transporters GLUT1, GLUT2, and GLUT5 in breast cancer—effects of hypoxia. *FASEB J.* **32**, 5104–5118

23. Eltzschig, H. K., Abdulla, P., Hoffman, E., Hamilton, K. E., Daniels, D., Schönfeld, C., Löffler, M., Reyes, G., Duszenko, M., Karhausen, J., Robinson, A., Westerman, K. A., Coe, I. R., and Colgan, S. P. (2005) HIF-1–dependent repression of equilibrative nucleoside transporter (ENT) in hypoxia *J. Exp. Med.* **202**, 1493–1505

24. Casanello, P., Torres, A., Sanhueza, F., González, M., Farías, M., Gallardo, V., Pastor-Anglada, M., San Martín, R., and Sobrevia, L. (2005) Equilibrative nucleoside transporter 1 expression is downregulated by hypoxia in human umbilical vein endothelium. *Circ. Res.* **97**, 16–24

25. Salman, S. and Nurse, C.A. (2018) Molecular Characterization of Equilibrative Nucleoside Transporters in the Rat Carotid Body and Their Regulation by Chronic Hypoxia. *Adv. Exp. Med. Biol.* **1071**, 43-50

26. Santini, D., Vincenzi, B., Fratto, M. E., Perrone, G., Raymond, L. A. I., Catalano, V., Cass, C., Ruffini, P. A., Spoto, C., Muretto, P., Rizzo, S., Muda, A. O., Mackey, J. R., Russo, A., Tonini, G., and Graziano, F. (2010) Prognostic role of human equilibrative transporter 1 (hENT1) in patients with resected gastric cancer. *J. Cell. Physiol.* **223**, 384–388

27. Mackey, J. R., Jennings, L. L., Clarke, M. L., Santos, C. L., Dabbagh, L., Vsianska, M., Koski, S. L., Coupland, R. W., Baldwin, S. A., Young, J. D., and Cass, C. E. (2002) Immunohistochemical variation of human equilibrative nucleoside transporter 1 protein in primary breast cancers *Clin. Cancer Res.* **8**, 110–116

28. Paproski, R. J., Wuest, M., Jans, H.S., Graham, K., Gati, W. P., McQuarrie, S., McEwan, A., Mercer, J., Young, J. D., and Cass, C. E. (2010) Biodistribution and Uptake of 3'-Deoxy-3'-Fluorothymidine in ENT1-Knockout Mice and in an ENT1-Knockdown Tumor Model *J. Nucl. Med.* **51**, 1447–1455,.

29. Machulla, H.J., Blocher, A., Kuntzsch, M., Piert, M., Wei, R., and Grierson, J.R. (2000) Simplified labeling approach for synthesizing 3'-deoxy-3'-[^{18}F]fluorothymidine ([^{18}F]FLT). *J. Rad. Nuc. Chem.* **243**, 843-846

30. Dehdashti, F. D., Rigsby, P. W. G., Mintun, M. A. M., Lewis, J. S., Siegel, B. A., and Welch, M. J. (2003) Assessing tumor hypoxia in cervical cancer by positron emission tomography with ^{60}Cu-ATSM: Relationship to therapeutic response—a preliminary report. *Int. J. Radiat. Onco.l Biol. Phys.* **55**, 1233–1238

31. Wuest, M., Kuchar, M., Sharma, S.K., Richter, S., Hamann, I., Wang, M., Vos. L., Mackey, J.R., Wuest, F., and Löser, R. (2015) Targeting lysyl oxidase for molecular imaging in breast cancer. *Breast Cancer Res.* **17,** 1–15

32. Robins, M. J., Peng, Y., Damaraju, V. L., Mowles, D., Barron, G., Tackaberry, T., Young, J. D., and Cass, C. E., (2010) Improved syntheses of 5′- S -(2-Aminoethyl)-6- N -(4-nitrobenzyl)- 5′-thioadenosine (SAENTA), analogues, and fluorescent probe conjugates: Analysis of cell-surface human equilibrative nucleoside transporter 1 (hENT1) levels for prediction of the antitumor efficacy of gemcitabine. *J. Med. Chem.* **53**, 6040–6053

33. Griffiths, M., Yao, S. Y. M., Abidi, F., Phillips, S. E. V., Cass, C. E., Young, J. D., and Baldwin, S. A. (1997) Molecular cloning and characterization of a nitrobenzylthioinosine-insensitive (ei) equilibrative nucleoside transporter from human placenta. *Biochem. J.* **328**, 739–743

34. Visser, F., Vickers, M. F., Ng, A. M. L., Baldwin, S. A., Young, J. D., and Cass, C. E. (2002) Mutation of residue 33 of human equilibrative nucleoside transporters 1 and 2 alters sensitivity to inhibition of transport by dilazep and dipyridamole. *J. Biol. Chem.* **277**, 395–401

35. Inic, Z., Zegarac, M., Inic, M., Markovic, I., Kozomara, Z., Djurisic, I., Inic, I., Pupic, G., and Jancic, S. (2014) Difference between Luminal A and Luminal B Subtypes According to Ki-67, Tumor Size, and Progesterone Receptor Negativity Providing Prognostic Information. *Clin. Med. Insights. Oncol.* **8**, 107–111

36. Robertson, S., Stålhammar, G., Darai-ramqvist, E., Rantalainen, M., Tobin, N. P., Bergh, J., and Hartman, J. (2018) Prognostic value of Ki67 analysed by cytology or histology in primary breast cancer. *J. Clin. Pathol.* **71**, 787–794

37. Lewis, J. S. (2007) Cu – ATSM : A radiopharmaceutical for the PET imaging of hypoxia. *Dalton. Trans*. **43**, 4893–4902

38. Moreno-bueno, G., Cano-soldado, P., and Casado, F. J. (2006) Human equilibrative nucleoside transporter-1 (hENT1) is required for the transcriptomic response of the nucleoside-derived drug 50-DFUR in breast cancer MCF7 cells. *Biochem. Pharmacol.* **72**, 1646–1656

39. Playa, H., Lewis, T. A., Ting, A., Suh, B., Muñoz, B., Matuza, R., Passer, B. J., Schreiber, S. L., and Buolamwini, J. K. (2014) Dilazep analogues for the study of equilibrative nucleoside transporters 1 and 2 (ENT1 and ENT2). *Bioorg. Med. Chem. Lett.* **24**, 5801–5804

40. Pastor-Anglada, M. and Pérez-Torras, S. (2015) Nucleoside transporter proteins as biomarkers of drug responsiveness and drug targets. *Front. Pharmacol.* **6**, 1–14

41. Plotnik, D.A., McLaughlin, L.J., Chan, J., Redmayne-Titley, J.N., Schwartz, J.L. (2011) The role of nucleoside/nucleotide transport and metabolism in the uptake and retention of 3'-fluoro-3'-deoxythymidine in human B-lymphoblast cells. *Nucl Med Biol.* **38,** 979-986

42. Ward, J.L., Sherali, A., Mo, Z.P., Tse, C.M. (2000) Kinetic and pharmacological properties of cloned human equilibrative nucleoside transporters, ENT1 and ENT2, stably expressed in nucleoside transporter-deficient PK15 cells. Ent2 exhibits a low affinity for guanosine and cytidine but a high affinity for inosine. *J. Biol. Chem.* **275**, 8375-8381

CHAPTER 3

Effect of hypoxia on amino acid transporters; ASCT1, ASCT2, LAT1, and x_c- in breast cancer, analyzed with [^{18}F]FDOPA and [^{18}F]FSPG

Effect of hypoxia on LAT1 and x_c- in breast cancer; analyzed with [^{18}F]FDOPA and [^{18}F]FSPG

Daniel Krys, Stephanie Mattingly, Darryl Glubrecht, Melinda Wuest[1], Frank Wuest[*]

Department of Oncology, University of Alberta, Edmonton, Alberta, Canada

In preparation for submission…

Abstract:

Introduction: Elevated amino acid metabolism and accumulation in cancer cells can be visualized with [^{18}F]FDOPA-PET and [^{18}F]FSPG-PET. This study investigates whether transport proteins; LAT1, x_c-, ASCT1, and ASCT2, are regulated by hypoxia.

Methods: Expression and function of these transporters were studied under hypoxia and normoxia, assessed with [^{18}F]FDOPA and [^{18}F]FSPG in estrogen receptor positive (ER(+)) MCF7, triple-negative MDA-MB231 breast cancer (BC) cells, and MCF10A cells; human mammary epithelial cells. Experimental analyses were conducted using Western blot, immunohistochemistry, radiotracer cellular uptake assays, and small animal PET experiments.

Results: ASCT1 and ASCT2 was not differentially expressed at the protein level in BC cell lines. LAT1 had high protein expression and high uptake *in vitro* and *in vivo* with [^{18}F]FDOPA in MCF7. System x_c- displayed high protein expression in MDA-MB231 and high uptake *in vitro* and *in vivo* with [^{18}F]FSPG. Hypoxia significantly increased [^{18}F]FDOPA uptake in MCF7 cells at 15 and 30 mins, and in MDA-MB231 cells at 30 and 60 mins. [^{18}F]FSPG uptake was increased in MDA-MB231 cells under hypoxia at 30 and 60 mins: 95±34% vs. 40±9.8 % and 164±37% vs. 127±33 %. *In vivo* PET imaging revealed greater tumor uptake of [^{18}F]FDOPA in MCF7 tumor models and [^{18}F]FSPG in MDA-MB231 tumor models.

Conclusions: Our study demonstrates hypoxia has significant effects on amino acid transport as tested with [^{18}F]FDOPA and [^{18}F]FSPG in BC.

Advances in Knowledge and Implications for Patient Care: This study demonstrates the first *in vivo* use of [^{18}F]FDOPA in breast cancer tumor models and its utility in differentiating between ER(+) and triple negative breast cancer.

3.1 INTRODUCTION

Worldwide, breast cancer (BC) is the most commonly diagnosed cancer and the second leading cause of cancer death in women. With the increase in diagnostic procedures, imaging modalities, and treatment options, the 5 year overall survival rate for women diagnosed with BC has increased (1). Though there has been a substantial decrease in mortality, much work still has to be done in diagnosing, determining appropriate treatment methods, and treating patients to further decrease BC mortality. In almost all BC patients, it is not the primary tumor, but metastasis that is the main cause of death (2). Therefore, metastatic breast cancer still remains incurable, which means that quicker diagnoses must be made or different treatment approaches must be explored.

Clinically, there are multiple imaging modalities that are used to diagnose and monitor BC. The main ones used are ultrasound, computed tomography (CT), mammography, and magnetic resonance imaging (MRI) (3). One major issue with these methodologies is that they image tumor morphology, rather than the tumor metabolic, functional, and receptor profile as pioneered by positron emission tomography (PET). Although there have been radiotracers developed that target estrogen receptors of ER (+) BC cells, the gold standard for BC PET imaging still remains as 2-deoxy-2-[^{18}F]fluoro-D-glucose ([^{18}F]FDG) (4). [^{18}F]FDG is a fluorinated glucose analog whose primary mode of entry into cancer cells is through the glucose transporter, GLUT1. The reason for its preferential entry into cancer cells is due to the "Warburg Effect", which describes the pathophysiological situation experienced by most cancer cells, wherein there is an increase in metabolic demand for glucose (5). [^{18}F]FDG does not enter anaerobic oxidative phosphorylation but is rather trapped intracellularly by hexokinase II, which allows physicians to image cancer for diagnostic, treatment monitoring, and treatment decision purposes (5). Though [^{18}F]FDG remains the gold standard, there are significant drawbacks with its use in breast cancer. The

primary limitation with [^{18}F]FDG is that if high levels of GLUT1 are not expressed, as is seen in many forms of BC, there are situations where false negatives are seen clinically (6). In addition to this, inflammatory lesions within the breast are also prone to false positives, as the body facilitates increased entry of glucose to help heal such injuries (7,8). Consequently, PET is still not considered a primary tool for initial diagnosis and treatment monitoring of BC, which spurs the search for other alternatives to [^{18}F]FDG-PET imaging.

Amino acids, taken into cells via amino acid transporters, are key components in fueling the rapid progression and proliferation of different types of cancers. As with glucose, glutamine is a major fuel source needed for the Warburg effect to occur (9). Certain amino acid membrane transporters such as ASCT2, LAT1, and x_c- have been extensively described in a recent review article published by Cha *et al.* (10) as altered in their expression and functionality in BC.

Aside from general transporter expression in normoxic BC, it is also important to look at dysregulated expression of these transporters in hypoxia. As tumor proliferation increases, internal regions of tumors become too distant from blood vessels to receive normal oxygenation which induces chronic and transient hypoxia. Induction of hypoxia promotes dissociation of hypoxia inducible factor-1α (HIF-1α) from HIF-1β and translocation of HIF-1α to the nucleus, thereby stimulating the transcription of different HIF1 responsive genes (20). In a past study we have determined that the facilitative hexose transporter GLUT5, the main transporter for fructose, is regulated by HIF-1α in BC, while the hexose transporter for both glucose and fructose, GLUT2, is not (21).

To date, there have been few studies exploring effects of hypoxia and HIF-1α on amino acid transporters in BC. Other studies however have focused on the effects of hypoxia on LAT1 in other forms of cancer, and have found that LAT1 regulated by HIF-2α induced mTORC1 activity and excitatory amino acid homeostasis, which is essential for tumor growth in hypoxic and

normoxic conditions (22). Specifically, [^{18}F]FDOPA has been traditionally used to assess terminal dopa decarboxylase activity and dopamine turnover in brains of Parkinson's patients (23). It has also shown to have a progressive decrease in uptake as the Parkinson's disease worsens (23). In more recent times, [^{18}F]FDOPA has been used to diagnose neuroendocrine tumors (24) and insulinoma in infants and adults (25,26). For system x_c-, extracellular glutamate inhibits xCT and influx of cystine, thereby depleting intracellular cysteine levels which leads to activation of HIF-1α (10).

In this study we aimed to better characterize expression of ASCT1, ASCT2, LAT1, and x_c-, and functionality of LAT1 and x_c- in BC, in both normoxic and hypoxic conditions. We aim to further explore the use of [^{18}F]FSPG in BC, which has been described previously, but in a more extensive fashion. In addition to this, we will determine the unexplored potential use of [^{18}F]FDOPA PET in imaging LAT1 functionality in BC. The three main amino acid (AA) transporters, ASCT2, LAT1, and xCT, which have been described as altered in BC, have all been reported to be poor prognostic indicators in various cancers. Having a minimally invasive technique to image transporter expression of these AA transporters, will allow physicians to determine the best treatment, for the right patient, at the right time.

3.2 METHODS

3.21 Radiosynthesis of (2S,4S)-4-(3-[^{18}F]fluoropropyl)-glutamic acid ([^{18}F]FSPG)

[^{18}F]FSPG was synthesized similarly to published methods (27). Full synthetic details and characterization data are supplied in the supporting information. Cyclotron produced [^{18}F]fluoride was captured from [^{18}O]H_2O target solution onto a Chromafix PS-HCO_3 cartridge and eluted with 0.6 mL of 1:1 Bu_4NHCO_3 (0.075 M)/MeCN. Eluted [^{18}F]fluoride was dried by sequential azeotrope with acetonitrile (3x1 mL) under a N_2 stream at 90 °C. To the residue was

added 4-6 mg of an esterified, tosylated glutamate derivative (see SI compound **5**) in 0.3 mL anhydr. MeCN. The mixture was heated at 100 °C for 20 minutes. Following dilution with water (5 mL), the ^{18}F-labeled ester intermediate was captured on a Waters Sep-Pak tC18 Plus short cartridge, washed with additional 10 mL water, and eluted in 3 mL MeCN. The solvent was evaporated under a N_2 stream at 90 °C. The labeling intermediate was deprotected by addition of 1 mL 2N aq. HCl and heating at 100 °C for 15 min. Following dilution with water [^{18}F]FSPG was purified by HPLC (Phenomenex Luna C18, gradient 1:0-1:4 H_2O+0.2% TFA/MeCN) and confirmed by chromatographic comparison against cold standard [^{19}F]FSPG prepared according to Koglin *et al.* (18). Decay corrected radiochemical yield: 13%±3.6 (SEM, n=5); synthesis time: ~2 h 30; radiochemical purity: >98% by radioTLC. Solvents were removed by rotary evaporation and the purified [^{18}F]FSPG was dissolved in PBS for cell and animal experiments.

3.22 Radiosynthesis of 3,4-dihydroxy-6-[^{18}F]-fluoro-l-phenylalanine ([^{18}F]FDOPA)

Radiosynthesis of 3,4-dihydroxy-6-[^{18}F]-fluoro-l-phenylalanine ([^{18}F]FDOPA) followed a previously described procedure by Fuchtner *et al.*, and prepared at the cyclotron facility of the Cross Cancer Institute (28).

3.23 Patient samples

Gene-expression microarray analysis was performed on primary samples from 176 treatment-naive patients with BC and on 10 healthy breast-tissue samples collected from reduction mammoplasties through the Canadian Breast Cancer Foundation Tumor Bank (Northern Alberta Study Center, Cross Cancer Institute, Edmonton, AB, Canada), as previously described (29). Patient information was collected under Research Ethics Board Protocol ETH-02-86-17. All necessary consents from all patients involved in this study were obtained according to each aforementioned ethics protocol. Tumor samples, collected at surgery, were frozen in liquid nitrogen within 20 min after collection. Histologic analysis of the frozen samples allowed the

differentiation of neoplastic and benign tissue and indicated that at least 70% of the cells present were invasive tumor cells. Total RNA was isolated from frozen samples using Trizol (Thermo Fisher Scientific, Waltham, MA, USA) and RNeasy columns (Qiagen, Toronto, ON, Canada). The RNA was quantified using a NanoDrop 1000 Spectrophotometer (Thermo Fisher Scientific) and its integrity evaluated using a Bioanalyzer 2100 (Agilent Technologies, Santa Clara, CA, USA). RNA samples with RNA Integrity Numbers >7.0 were used. RNA was subjected to linear amplification and Cyanine 3 (Cy3) labeling and then hybridized to Agilent Whole Human Genome Arrays using One Color Low RNA Input Linear Amplification Kit Plus, One Color RNA Spike-In Kit, and Gene Expression Hybridization Kit (Agilent Technologies). Arrays were scanned using an Agilent scanner. Data were extracted and quality evaluated using Feature Extraction Software 9.5 and normalized and analyzed using GeneSpring GX 7.3 (Agilent Technologies).

3.24 Cell cultures

The following cell lines were used in the study: MCF10A (American Type Culture Collection (ATCC) CRL-10317; ATTC, Manassas, VA, USA) is a human non-carcinogenic basal B cell line, derived from fibrocystic breast disease and obtained during a reduction mammoplasty. MCF7 (ATCC HBT-22) is an estrogen receptor (ER) and progesterone receptor (PR) positive breast cancer cell line, derived from luminal invasive ductal carcinoma, while MDA-MB231 (ATCC HTB-26) is a triple negative basal B breast cancer (TNBC) cell line. MCF7 and MDA-MB231 cells were grown in DMEM/F-12 (Gibco, ThermoFisher Scientific, Burlington, ON, Canada) with 10% fetal bovine serum (FBS) (Gibco) and 1% penicillin/streptomycin (Pen/Strep), while MCF10A cells were grown in DMEM/F-12 containing Clonetics® MEGM SingleQuots® (Lonza, Walkersville, MD, USA). For experiments, cells were seeded in their medium and grown for 24 h. Medium was conditioned for 2-3 h in a hypoxia chamber

(Department of Pharmacy and Pharmaceutical Sciences, University of Alberta, Edmonton, AB, Canada) used at 1% O_2 and 5% CO_2 at 37°C and was used to exchange growth medium for hypoxia experiments and compared to cells under normoxic conditions (19).

3.25 Western blotting

For analysis of ASCT1, ASCT2, LAT1, x_c-, and β-actin, MCF10A, MCF7, and MDA-MB231 cells were subjected to normoxic/hypoxic conditions for 24 h, then removed from the incubation chambers and suspended in lysis buffer (50 mM Tris, 150 mM NaCl, 0.1% SDS, 0.5% sodium deoxycholate, 0.5% Triton X) on ice for 30 min. Extracts were sonicated (10% amplitude, 10 s) on ice and centrifuged at 14,500 g for 10 min at 4°C to remove debris. Protein determination in supernatants was conducted using a BCA based protein assay (Pierce/Thermo Scientific, Rockford, IL, USA). Aliquots of supernatants were mixed with 1/4 volume of 4x Laemmli buffer (250 mM Tris/HCl, 8% (w/v) SDS, 40% glycerol, 200 mM dithiothreitol and 0.04% (w/v) bromophenol blue, pH 6.8) and heated for 5 min at 95°C. Protein extracts were loaded onto SDS-polyacrylamide gels and separated by electrophoresis. Proteins were transferred to nitrocellulose membranes by electroblotting and blocked for 1 h at room temperature in 5% (w/v) non-fat dry milk in Tris-buffered saline containing 0.05% (v/v) of Tween-20 (TBST). Membranes were incubated overnight at 4°C with the following primary antibodies: mouse monoclonal anti-ASCT1 IgG_1 (clone H-60, sc-134846, Santa Cruz Biotechnology, 1:500), mouse monoclonal anti-ASCT2 IgG_1 (clone J-25, sc-130963, Santa Cruz Biotechnology, 1:500), mouse monoclonal anti-LAT1 IgG_1 (clone D-10, sc-374232, Santa Cruz Biotechnology, 1:500), mouse monoclonal anti-xCT IgG_{2a} (NB300-318, Novus Biologicals, Oakville, ON, Canada, 1:500) and rabbit polyclonal anti-β-actin (A5060, Sigma-Aldrich, 1:5000) followed by incubation for 1 h at 21°C with a peroxidase-conjugated goat anti-mouse IgG1 secondary antibody (sc-2060, Santa Cruz Biotechnology), goat anti-mouse IgG secondary antibody (sc-2005, Santa Cruz Biotechnology)

in 1:5000 dilution (ASCT1, ASCT2, LAT1, x_c-) or 1:10000 dilution (β-actin). After incubation with secondary antibodies, membranes were washed in TBST and depending on protein levels, incubated with Supersignal West Pico chemiluminescent substrate (Thermo Fisher Scientific) or Clarity ECL Western blotting substrate (Bio-Rad Laboratories, Hercules, CA, USA). Luminescence signals were captured using Fuji Medical X-ray Films (Fujifilm Canada, Mississauga, ON, Canada). Films were scanned, and analysis was done using the ImageJ program (National Institutes of Health, Bethesda, MD, USA). Density of each band was determined, and individual lane backgrounds were subtracted. Values for ASCT1, ASCT2, LAT1, and x_c- were divided by values for the housekeeping protein β-actin. Values determined for control cell line MCF10A were set at 100% and compared with the individual value of the cancer cell lines {e.g., (band density LAT1 density lane background)/(band density β-actin 2 density lane background), respectively}.

3.26 Immunohistochemistry for ASCT1, ASCT2, LAT1, and x_c-

Excised murine tumor tissues were fixed in neutral-buffered 10% formalin overnight and embedded into paraffin. Slides with 5-µm sections were dried at 60°C for 1 h and rehydrated by 3 changes of xylene for 10 min each and then graded ethanol from 100 to 50%, followed by water and TBS. Slides were microwaved in a pressure cooker for 6 min in citraconic anhydride (0.05% in water, pH 7.4) for antigen retrieval; blocked with 0.5% fish gelatin in TBST for 30 min; rabbit polyclonal non-conjugated anti-ASCT1 IgG (orb136309, Biorbyt, 1:300), rabbit polyclonal non-conjugated anti-ASCT2 IgG (HPA035240, Prestige Antibodies, MilliSpore Sigma, Sigma Aldrich, 1:150), rabbit monoclonal non-conjugated anti-LAT1 IgG (EPR17573, product# AB208776, Abcam, 1:500), mouse monoclonal anti-xCT IgG_{2a} (NB300-318, Novus Biologicals, 1:300) in a humidity chamber overnight at 4°C. After incubation in 3% H_2O_2 in water for 15 min, slides were incubated with EnVision+ anti-mouse- or anti-rabbit-labeled

polymer horseradish peroxidase (Dakocytomation, Glostrup, Denmark) for 1 h, developed using the Dako Liquid DAB+ Substrate Chromagen System and 1% copper sulfate, and counterstained with hematoxylin. Slides were dehydrated by reversing rehydration and then cover-slipped.

3.27 In vitro cell uptake studies

MCF10A, MCF7, and MDA-MB231 cells were grown in 12-well plates and treated under normoxic/hypoxic conditions for 24 h. Media was removed 1 h prior to experiment, cells were washed twice with PBS and starved of glucose in glucose-free Krebs-Ringer solution (120 mM NaCl, 4 mM KCl, 1.2 mM KH_2PO_4, 2.5 mM $MgSO_4$, 25 mM $NaHCO_3$, 70 μM $CaCl_2$, pH 7.4) for 1 h at 37 °C. Next, 300 μL Krebs-Ringer solution with 0.1-0.5 MBq [^{18}F]FDOPA or [^{18}F]FSPG were added to each well. Plates were incubated at 37°C for specific time points (1, 5, 15, 30, 60 minutes). Radiotracer uptake was stopped with 1 mL ice-cold PBS, cells washed 2x with PBS and lysed in 0.4 mL lysis buffer (50 mM Tris, 150 mM NaCl, 0.1% SDS, 0.5% sodium deoxycholate, 0.5% Triton X). Radioactivity in cell lysates was measured using WIZARD2 automatic gamma counter (Perkin Elmer; Waltham, MA, USA). Total protein concentration in the samples was determined using a Pierce BCA based protein assay (ThermoFisher Scientific). Data were calculated as % of total added radioactivity per mg protein (% radioactivity/mg protein).

3.28 Animal models

All animal experiments were carried out in accordance with guidelines of the Canadian Council on Animal Care (CCAC) and approved by the local animal care committee of the Cross Cancer Institute. Human MCF7 cells were injected subcutaneously (5 x 10^6 cells in 100 μL PBS/Matrigel 50:50) into 8-10 weeks old female NIH-III nude mice (Charles River, Saint-Constant, QC, Canada) plus a 0.72 mg/pellet containing estrogen in a 60-day release preparation (Innovative Research of America, Sarasota, FL, USA) implanted subcutaneously into the upper

right flank for the constant estrogen level needed by the ER(+) MCF7 cells. Tumors were grown for 3-4 weeks, reaching sizes of 200-400 mm^3. Human TNBC MDA-MB231 cells (5 x 10^6 cells in 100 µL PBS) were also injected subcutaneously resulting in 300-500 mm^3 sized tumors after 2-3 weeks.

3.29 PET imaging experiments

MCF7 and MDA-MB231 tumor bearing NIH-III nude mice (Charles-River, QC, Canada) were anesthetized with isoflurane (40% O_2 60% N_2) and their body temperature was kept constant at 37°C. Mice were positioned and immobilized in prone position into the centre of the field of view of an INVEON® PET scanner (Siemens Preclinical Solutions, Knoxville, TN, USA). A transmission scan for attenuation correction was not acquired. Radioactivity present in the injection solution (0.5 mL syringe) was determined using a dose calibrator (AtomlabTM 300, Biodex Medical Systems, New York, NY, USA). After emission scan was started, radioactivity (4-8 MBq in 100-150 µL saline) was injected with a delay of ~15 s through a tail vein catheter.

Dynamic PET data acquisition was performed in 3D list mode for 60 min. Dynamic list mode data were sorted into sinograms with 54 time frames (10x2 s, 8x5 s, 6x10 s, 6x20 s, 8x60 s, 10x120 s, 5x300 s). Frames were reconstructed using ordered subset expectation maximization (OSEM) or maximum a posteriori (MAP) reconstruction modes. No correction for partial volume effects were performed. Image files were further processed using the ROVER v2.0.51 software (ABX GmbH, Radeberg, Germany). Masks defining 3D regions of interest (ROI) were set and defined by 50% thresholding.

Mean standardized uptake values [SUV_{mean} = (activity/mL tissue) / (injected activity / body weight), in milliliters per kilogram were calculated for each ROI. Time-activity curves (TAC) were generated from the dynamic scans.

3.30 Statistical analysis

All *in vitro* data and semi-quantified PET data are expressed as means ± SEM. Graphs and time-activity curves (TACs) were constructed using GraphPad Prism 4.0 (GraphPad Software, La Jolla, CA, USA).

Where applicable, statistical differences were tested by Student's t test (PCR, Western Blot, PET data) or 2-way ANOVA (cell uptakes) and were considered significant for $p<0.05$ (*), $p<0.01$ (**) and $p<0.001$ (***).

3.3 RESULTS

3.31 ASCT1, ASCT2, LAT1, and x_c- mRNA expression in patient BC samples

Figure 10 presents results of a microarray analysis of ASCT1, ASCT2, LAT1, and x_c- mRNA in different tissue-biopsy samples. **Figure 10A** displays results from 176 BC patients vs. control tissue from 10 normal human breast-tissue samples. All membrane transporters, excluding ASCT2, showed significantly higher mRNA expression in the BC patients compared to normal breast-tissue samples. The highest mRNA expression in general was seen in the second monomer of LAT1. **Figure 10B** demonstrates analysis of 56 TNBC vs. 112 ER+ BC samples. These results showed significantly higher mRNA expression of LAT1 (monomer 2) in TNBC samples vs. ER+ BC samples. ASCT1 however revealed an opposite effect, where ER+ BC samples had significantly higher mRNA expression than their TNBC counterparts. ASCT2, LAT1 (monomer 1), and x_c- mRNA expression in TNBC was found to be quite comparable with ER+ BC samples, as no significant differences were seen.

A) Total mRNA expression in normal and breast cancer tissue

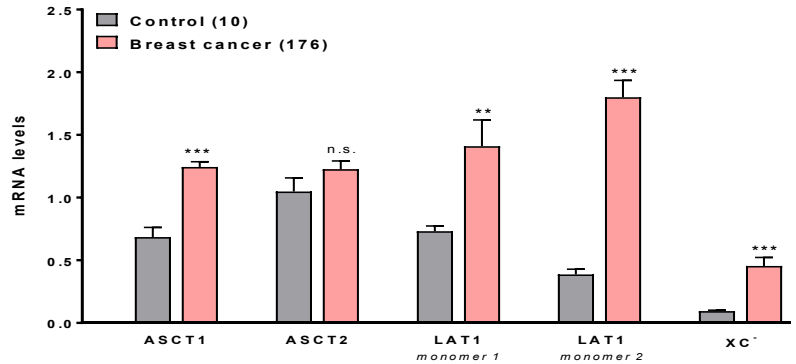

B) Total mRNA expression in ER+ and triple-negative breast cancer tissue

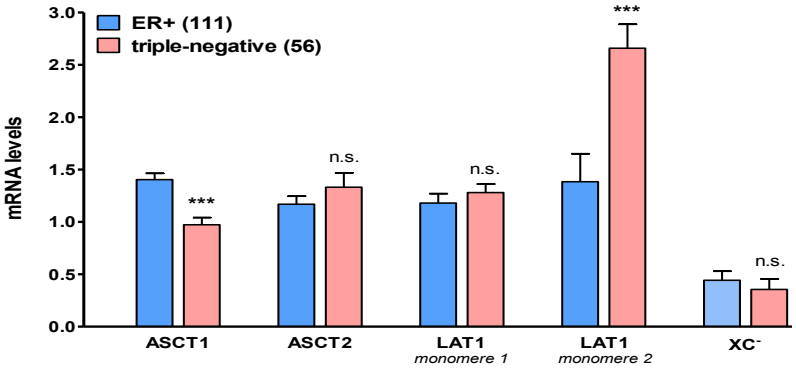

Figure 10. Total mRNA expression of ASCT1, ASCT2, LAT1 (monomer 1), LAT1 (monomer 2), and x_c- in control breast versus breast cancer tissue (top) and estrogen receptor (ER)-positive versus triple-negative breast cancer samples (bottom). Data are shown as mean ± standard error of the mean of mRNA levels based on log-transformed values of the gene expression microarray signal intensity from analyzed patient samples. n.s. not significant, *p<0.05, **p<0.01, ***p<0.001.

3.32 ASCT1, ASCT2, LAT1, and x_c- protein levels in MCF10A, MCF7, and MDA-MB231 cells under normoxia and hypoxia

Figure 11 summarizes data from all Western blot experiments. **Figure 11A** displays original representative blots and effects of hypoxia (exposure to 1% O_2 for 24 h) on proteins of interest: ASCT1, ASCT2, LAT1, and x_c-. Hypoxia was implemented over 24 h of incubation based on recent experiments conducted by Hamann *et al.* (21) where maximum HIF-1α protein expression levels were found, which would subsequently effect the downstream target gene expression of GLUT1. The following results were seen under normoxic conditions (**Figure 11B**): ASCT1 protein was expressed fairly equally amongst all three cell lines explored, showing no significant differences. Surprisingly, MCF7 and MDA-MB231 cells had very little basal normoxic ASCT2 protein compared to MCF10A. Furthermore, LAT1 normoxic protein levels were highest in MCF10A, with MCF7 (0.74-times) and MDA-MB231 (0.33-times) displaying lower levels. On the other hand, x_c- protein levels were the highest in the TNBC cell line MDA-MB231 (152-times), when compared to the control cell line MCF10A.

No significant differences in ASCT1, ASCT2, LAT1, and x_c- protein levels under normoxic and hypoxic conditions were observed for all three cell lines. MCF10A showed similar levels of expression of all four AA membrane transporters (**Figure 11B**). In the BC cell lines however, the only banding in Western blots was seen in ASCT1 for both MCF7 and MDA-MB231; for LAT1 in MCF7; and for x_c- in MDA-MB231. Hypoxia had no effect on ASCT1 in MCF7 and MDA-MB231 cells (**Figure 11C and 11D**). Hypoxia had no effect on LAT1 expression in MCF7 cells (**Figure 11C)**. Expression levels of x_c- under hypoxia showed an insignificant 0.36-fold decrease in MDA-MB231 cells (**Figure 11D)**. Since ASCT1 showed no difference in expression level between both BC cell lines and the control, and ASCT2 displayed no expression in both MCF7 and MDA-MB231, further research into their functionality was not undertaken.

A) Effect of Hypoxia on Amino Acid

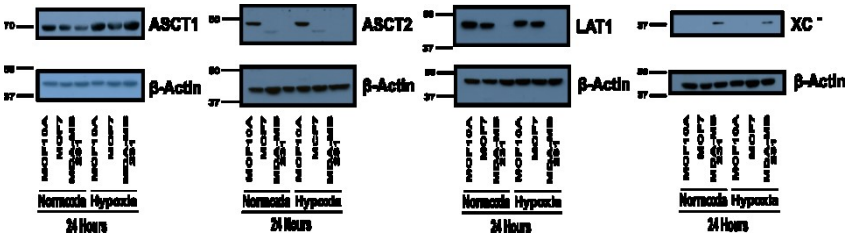

B) Normoxia

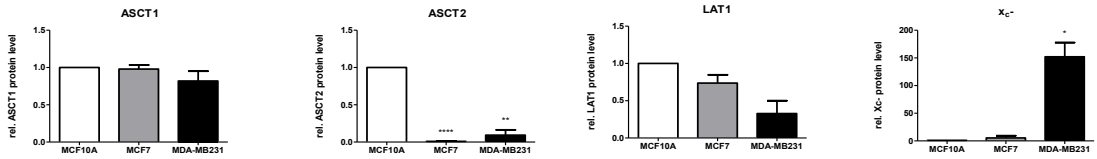

C) MCF10A

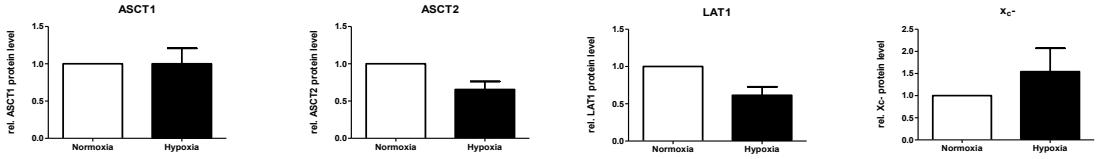

D) MCF7

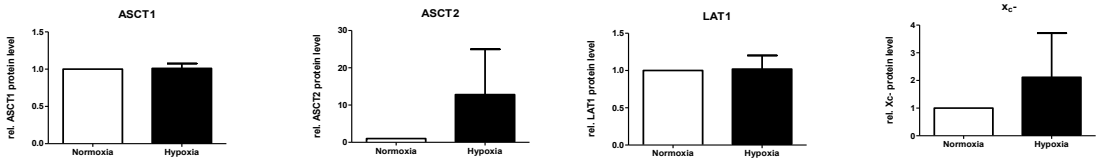

E) MDA-MB231

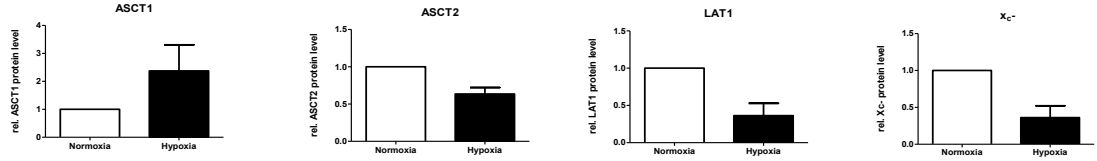

Figure 11. Representative Western blots for ASCT1, ASCT2, LAT1, and x_c- expression in MCF10A, MCF7, and MDA-MB231 cells after 24 h of hypoxia (1% O_2) vs. normoxic conditions (A). Quantitative comparison of ASCT1, ASCT2, LAT1, and x_c- protein levels in MCF10A, MCF7, and MDA-MB231 under normoxic conditions (B) and the effects of hypoxia (1% O_2) on ASCT1, ASCT2, LAT1, and x_c- protein levels in MCF10A (C), MCF7 (D), and MDA-MB231 (E). Quantitative data are shown as means ± SEM from at least three experiments.

3.33 Effect of hypoxia on cellular uptake of [^{18}F]FDOPA and [^{18}F]FSPG

[^{18}F]FDOPA and [^{18}F]FSPG cellular uptake experiments were performed under both normoxic and hypoxic conditions to test the functionality of LAT1 and x_c- respectively, in MCF10A, MCF7, and MDA-MB231 cells (**Figure 12)**. Under normoxic conditions, uptake of [^{18}F]FDOPA was significantly higher in MCF7 BC cells compared to MDA-MB231 BC cells and MCF10A cells: 467±51 % versus 105±27 % and 217±38 %, radioactivity per milligram protein (n=12/4), respectively, after a 30-min incubation (**Figure 12A)**. These data indicate that there was increased uptake of [^{18}F]FDOPA in the MCF7 ER+ BC cell line, with an uptake lower than MCF10A in the MDA-MB231 cell line. In addition to normoxic results, significant differences were detected between normoxic and hypoxic conditions in MCF7 cells at 15 ($p<0.001$) and 30 ($p<0.001$) minutes, and for MDA-MB231 cells at 30 ($p<0.01$) and 60 ($p<0.05$) minutes, indicating that [^{18}F]FDOPA uptake in BC was increased in these cell lines by hypoxia. [^{18}F]FDOPA uptake seemed to reach a maximum and then began to decrease after the 30 minute time point. To confirm that [^{18}F]FDOPA was a substrate for the LAT1 AA membrane transporter, transport was almost entirely blocked at 60 minutes with 1 μM tyrosine. When comparing to the 60-min time point of the MCF7 cell line, 1 μM tyrosine inhibited only 83% of the [^{18}F]FDOPA uptake.

[^{18}F]FSPG was used to determine the functionality of x_c- glutamate/cystine anti-port (**Figure 12B**). The only substantial transport of [^{18}F]FSPG was seen in MDA-MB231 cells. Under normoxic conditions at 60 minutes, we saw 127 ± 33 % radioactivity/mg protein in MDA-MB231 cells, compared to 9.8 ± 0.8 % radioactivity/mg protein in MCF7 and 21 ± 4.7 % radioactivity/mg protein in MCF10A. In contrast to uptake with [^{18}F]FDOPA, no washout effect was seen with [^{18}F]FSPG after 30 minutes, as uptake levels only increased after this time point in all three cell lines. When looking at hypoxic effects on [^{18}F]FSPG transport, we can see higher

uptake under hypoxic conditions in MDA-MB231 cells at 30 and 60 minutes: 95 ± 34 % vs. 40 ± 9.8 % radioactivity/mg protein ($p<0.001$) and 164 ± 37 % vs. 127 ± 33 % radioactivity/mg protein ($p<0.05$), respectively. An interesting effect was seen in MCF10A cells at 60 minutes, where it was determined that under normoxic conditions at 60 minutes, higher uptake was seen: 21 ± 5 % vs. 15 ± 3 % radioactivity/mg protein ($p<0.001$). To confirm that our radiotracer was being transported by the x_c- transporter, blocking was performed with 25 μM cystine. In all three cell lines, an average blocking effect of 97 ± 0.5 % radioactivity/mg protein at 60-min was observed in normoxic conditions.

Induction of hypoxia was confirmed via past experiments by Hamann *et al.* (21) with [^{18}F]FAZA and in work by Krys, D., Hamann, I., Wuest, M., and Wuest, F. (unpublished observations) with [^{64}Cu]ATSM, in experiments performed with the same procedure.

A) Uptake of [^{18}F]FDOPA

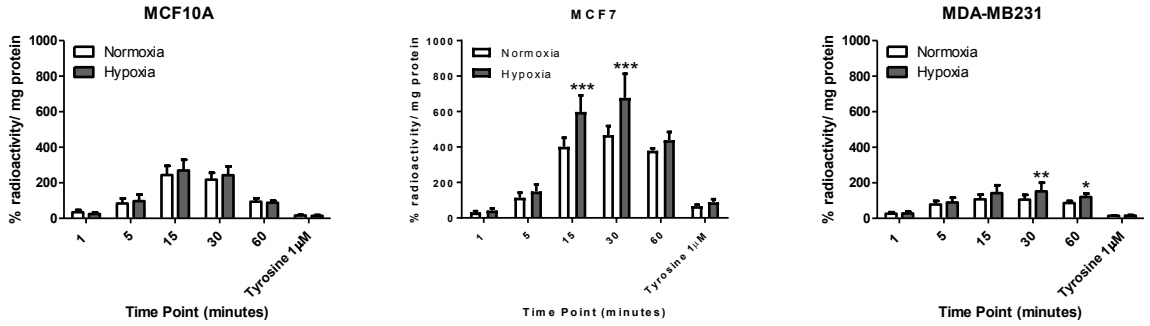

B) Uptake of [^{18}F]FSPG

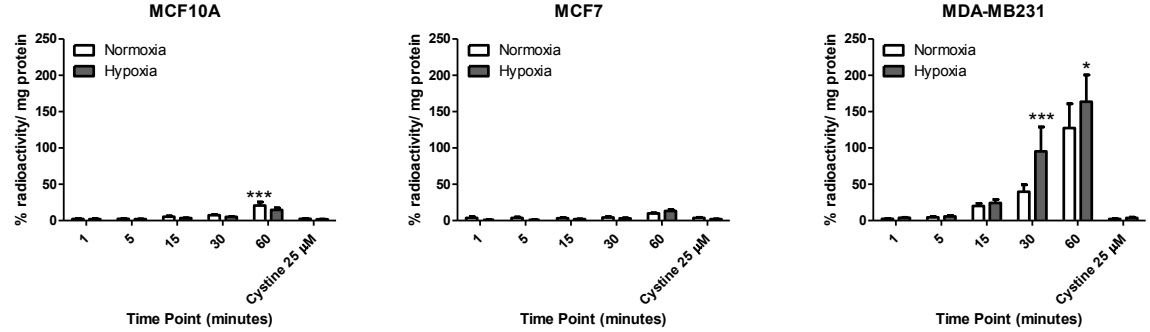

Figure 12. Uptake of [^{18}F]FDOPA (A) and [^{18}F]FSPG (B) into normoxic and hypoxic (1% O_2) MCF10A, MCF7, and MDA-MB231 cells. In vitro cell uptake was carried out at 1, 5, 15, 30, and 60 minute incubation time points for [^{18}F]FSPG. Data are shown as means ± SEM from 3 experiments, all performed as triplicates.

3.34 Immunohistochemical determination of ASCT1, ASCT2, LAT1, and x_c- in MCF7 and MDA-MB231 tumors

In the case of ASCT1 and ASCT2, we see that the MCF7 tumor types showed less staining than the strong, positive staining of the MDA-MB231 tumor (**Figure 13)**. In x_c-, we also saw that tumor staining was considerably higher in MDA-MB231 *vs.* MCF7 tumors. In comparison to these three membrane transporters, LAT1 showed minimal staining in both tumor types, with only a small noticeable region of staining seen in MCF7 as demonstrated by the red arrow **(Fig. 13A).**

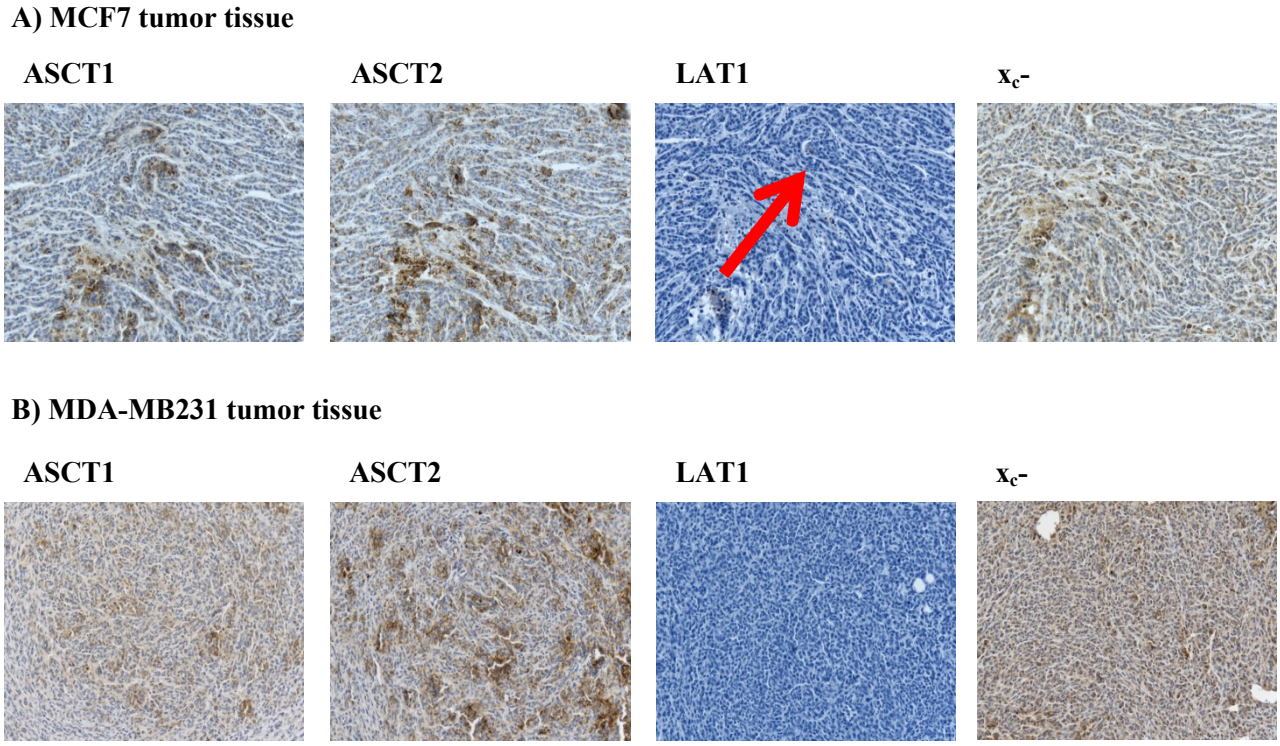

Figure 13. A, B) Immunohistochemical staining of ASCT1, ASCT2, LAT1, and x_c- in MCF7 (A) and MDA-MB231 (B) tumor-tissue slices, taken from MDA-MB231 and MCF7 tumour bearing mice. Original magnification, ×20.

3.35 In vivo PET imaging in MCF7 and MDA-MB231 tumor-bearing mice with [^{18}F]FDOPA and [^{18}F]FSPG

Results of *in vivo* PET imaging experiments with [^{18}F]FDOPA and [^{18}F]FSPG in MDA-MB231 and MCF7 tumor-bearing mice are summarized in **Figure 14 and Figure 15**. Tumor uptake and retention profiles of [^{18}F]FDOPA over 60 min were significantly higher in the MCF7 tumor model: SUV_{60min} 0.51±0.03 (n=3) for MCF7 and 0.27±0.02 (n=3) for MDA-MB231 tumors, respectively (**Figure 14)**. Muscle uptake and clearance of [^{18}F]FDOPA was also higher in the MCF7 tumor model, which resulted in similar tumor-to-muscle ratios (TMR): 1.72 for MDA-MB231 and 1.98 for MCF7 tumors at 60 min post injection (p.i.). Results in MCF7 and MDA-MB231 tumors indicate that uptake and retention of [^{18}F]FDOPA seems to show estrogen receptor-dependency.

Initial tumor uptake [^{18}F]FSPG, in the primary tumor was comparable between both *in vivo* models, but retention profiles of [^{18}F]FSPG over 60 min were higher in MDA-MB231 tumors, in contrast to MCF7 tumors: SUV_{60min} 0.43±0.04 (n=3) for MDA-MB231 and 0.21±0.01 (n=3) for MCF7 tumors, respectively (**Figure 15)**. Muscle uptake and clearance of [^{18}F]FSPG was higher in the MCF7 tumor model, with SUV_{60min} 0.05±0.01 (n=3) vs. 0.11±0.01 (n=3) in the MDA-MB231 model at 60 min post injection (p.i.), which resulted in comparable tumor-to-muscle ratios (TMR) for MDA-MB231, 4.07, paralleled to 4.24 for MCF7 tumors at 60 min p.i. Aside from the results seen in the primary tumors for MCF7 and MDA-MB231, additional uptake of [^{18}F]FSPG was seen in possible metastatic lesions, seemingly in mouse lymph nodes of the MDA-MB231 tumor model.

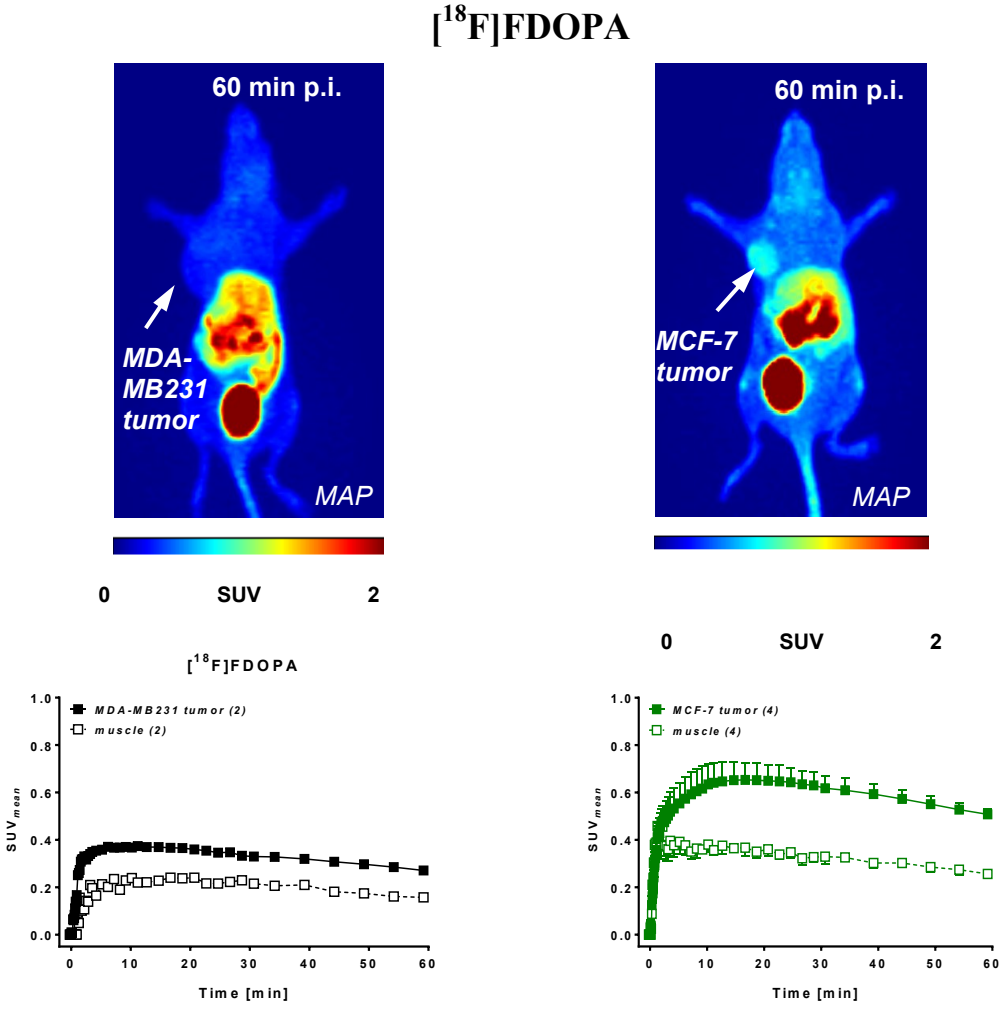

Figure 14. Representative PET images from dynamic scans after injection of L-DOPA derivative [^{18}F]FDOPA into MDA-MB231 and MCF7 tumour bearing mice at 60 minutes post-injection. All semiquantitative data are shown as means ± SEM from individual experiments. MAP, maximum activity projection.

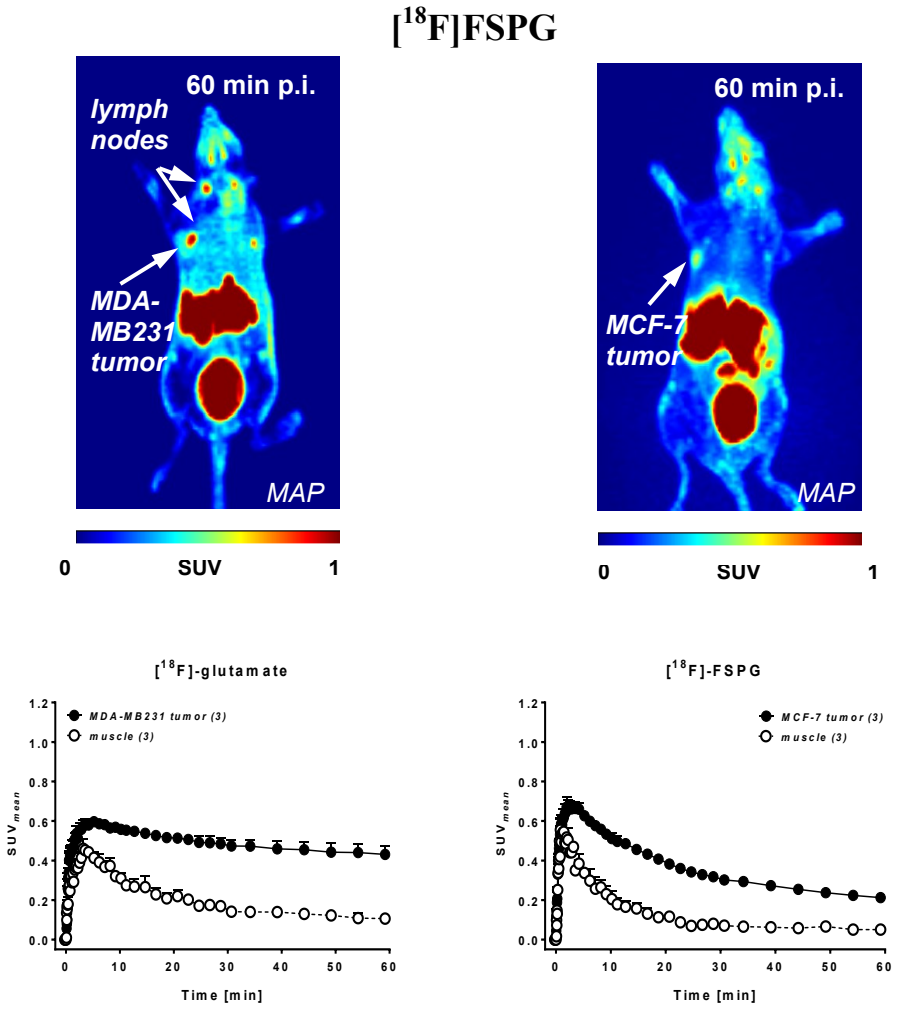

Figure 15. Representative PET images from dynamic scans after injection of glutamate derivative [^{18}F]FSPG into MDA-MB231 and MCF7 tumour bearing mice at 60 minutes post-injection. All semiquantitative data are shown as means ± SEM from individual experiments. MAP, maximum activity projection.

3.4 DISCUSSION

The goal of the current study was to determine the relationship between hypoxia and the protein expression of ASCT1, ASCT2, LAT1, and x_c-, as well as the relationship of hypoxia with the functionality of LAT1 and x_c- using [^{18}F]FDOPA and [^{18}F]FSPG, respectively. Based on the results gathered, the following conclusions were made: *1)* mRNA data did not correlate with the protein expression seen in Western blot or immunohistochemistry, nor the functionality of the amino acid transporters studied; *2)* From ASCT1 and ASCT2 protein expression profiles, we determined that these transporters had minimal effects in providing differentiating characteristics in MCF7 and MDA-MB231 BC cell lines; *3)* Elevated protein expression and *in vitro* and *in vivo* functionality of LAT1 was seen only in ER(+) MCF7 BC cells when compared to MDA-MB231; *4)* Substantial expression and functionality of system x_c- transporter was exhibited by MDA-MB231 TNBC cells; *5)* Hypoxia does not upregulate total protein levels of LAT1 and x_c- but has effects on functionality as seen with increased transport of [^{18}F]FDOPA and [^{18}F]FSPG under hypoxic conditions.

Systematically, literature was reviewed, and our experimental process began with the determination of mRNA expression in specific amino acid transporters that were determined to have altered regulation in BC. With data collected and analyzed by the Canadian Breast Cancer Foundation Tumor Bank, we saw little correlation between these results and our Western blot protein expression analyses. ASCT1 mRNA levels, showing higher expression in BC and higher mRNA expression in ER+ BC, were not similar to the overall uniform protein expression of ASCT1 amongst our three studied cell lines. ASCT2 mRNA levels showed similar levels between control and BC as well as similar levels between ER+ and TN BC, which was in stark contrast to an overall nil expression of ASCT2 protein in our BC cell lines in the western blot studies. Due to results seen from our western blot experiments, it was decided to not further

pursue functional analysis of these transporters, as it did not seem that they played a pivotal role in BC metabolism, or at least metabolism in MCF7 and MDA-MB231 cells. Nevertheless, we did perform immunohistochemistry with these antibodies following our uptake experiments, and found that the results did not correlate with our western blot experiments and that staining was more pronounced in MDA-MB231 tumors in both cases.

Even for the two other AA membrane transporters, LAT1 and x_c-, mRNA data did not correlate with protein data. Whereas we see greater mRNA expression in BC and then in TNBC compared to ER+ BC, LAT1 protein is expressed at most, the same as MCF10A in MCF7 and not at all in MDA-MB231. For the system x_c- transporter, greater expression is seen in BC, but from western blots, x_c- is only expressed in the MDA-MB231 TNBC cell line which diverges from the similar expression of mRNA in ER+ and TN BC. Though there are not many similarities seen between mRNA and protein expression from our results, this phenomenon has also been reported by other research groups globally. The best explanations at this stage are that the points in time that analysis has been conducted are not similar, and our current technologies are not able to correctly assess in small space and time scales (30), or that protein translation may have not occurred.

Though results did not correlate between mRNA and protein expression, the data collected from western blots spurred interest into the *in vitro* and *in vivo* functionality of LAT1 and x_c-. The uptake of [^{18}F]FDOPA correlated somewhat well with the western blot results, as the highest protein expression and uptakes were seen in the MCF7 cell line. This correlation further continued on with our *in vivo* tumor models, which showed high uptake in the MCF7 tumor, and little to no uptake in the MDA-MB231 tumor, pointing to this radiotracer's ability to discriminate biomarker expression in these tumor models. This is the first documented use of [^{18}F]FDOPA for the imaging of LAT1 membrane transporters in BC tumor models. However,

when comparing to the immunohistochemistry results obtained after these experiments were performed, we see no correlation between [^{18}F]FDOPA uptake and LAT1 staining, as LAT1 staining was minimal.

These results do however confirm that [^{18}F]FDOPA can be used as an alternative to [^{18}F]FET, a radiotracer whose uptake is also mediated by LAT1 (31). [^{18}F]FDOPA-PET would provide an alternative to immunohistochemistry for determining LAT1 expression, and would allow physicians to better guide therapy in BC patients for specifically targeting LAT1 transport. 2-amino-2-norbornane-carboxylic acid (BCH) is potent inhibitor of LAT membrane transporters, and has shown the ability to suppress growth and induce apoptosis in different cancer models, including MCF7 and MDA-MB231 (32,33). JPH203 blocks LAT1 transport and has lethal effects on cancer cells with minimal toxic effects on non-tumor tissue (34,35). With these two drugs being more general for the entire family of LATs, there is ongoing work in developing potent inhibitors of LAT1 by mapping the binding pocket of the transporter and screening potential ligands (36). The use of [^{18}F]FDOPA-PET would allow for a more patient-specific approach to treating BC based on each individual's LAT1 expression profile, which would allow for the greater utilization of these drugs.

In parallel to the results of [^{18}F]FDOPA-PET in BC, [^{18}F]FSPG was used to assess the functional involvement of system x_c- in BC. Results of the *in vitro* radiotracer uptake experiments correlated well with results of Western blot experiments, where both substantial protein expression and [^{18}F]FSPG uptake were only seen in the TNBC MDA-MB231 cell line. These results are in line with Yang *et al.* where they "confirmed that the basal expression and function of x_c- were significantly higher in MDA-MB231 cells than in MCF-7 cells" (37). Analysis of *in vivo* [^{18}F]FSPG-PET in MDA-MB231 and MCF7 tumor models revealed further correlations

with the western blots and *in vitro* uptakes, though a slight difference was seen as the MCF7 tumor model did show uptake of [^{18}F]FSPG. This finding can be attributed to possible upregulation of system x_c- in MCF7, due to possible *in vivo* induction by NRF2 and IGF-1 which have been reported in literature (37,38). *In vivo* [^{18}F]FSPG uptake in the MDA-MB231 tumor model displayed additional areas of uptake that point to possible metastases, in the lymph nodes of the mice (n=3). This assumption is likely to be true since previous models have demonstrated that MDA-MB231 cells are used for modelling BC metastasis and MCF7 are not (39), and additionally x_c- has been seen as a metastatic marker of BC (40).

From these results, [^{18}F]FSPG-PET seems to be able to determine x_c- biomarker expression in BC. A previous study has used [^{18}F]FSPG for imaging of BC and non-small cell lung carcinoma (NSCLC), and have found that in 5 BC patients, immunohistochemical staining for x_c- did not correlate with [^{18}F]FSPG uptake levels, except for in the one case where staining was high (41). In relation to our results obtained from immunohistochemistry, the high staining levels in MDA-MB231 seems to correlate with our levels of [^{18}F]FSPG uptake. With the results of these experiments, and the relatively small patient cohort used by Baek *et al.* (41), more work must be done to determine the value of [^{18}F]FSPG in BC. Larger patient cohorts have shown that [^{18}F]FSPG is a useful imaging agent, as was seen with Cheng *et al.* and their imaging of pancreatic ductal adenocarcinoma (42). The potential use of [^{18}F]FSPG as a determinant of x_c-transporter function would allow physicians to use chemotherapeutics which target system x_c-transport. Inhibitors such as sulfasalazine target x_c-, and work by blocking cellular entry of cystine, thereby depleting GSH levels and increasing ROS, which target cells for death via ferroptosis, a form programmed cell death dependent on iron (43,44).

This study has also determined that hypoxia had minimal effects on LAT1 and x_c- transporter protein expression, but under hypoxic conditions the uptake of [^{18}F]FDOPA and [^{18}F]FSPG was increased. This points to a functional regulation by hypoxia on LAT1 and x_c- in MCF7 and MDA-MB231 BC cells, through the increased uptake of these radiotracers as seen in *in vitro* assays. LAT1 and x_c- are both involved in transport of amino acids that are needed for tumor promoting effects. LAT1 facilitates entry of excitatory AAs (EAA) which stimulate $mTORC_1$ activity. It has been confirmed that *SLC7A5*, the gene which encodes LAT1, is repressed by HIF-1α but sufficiently upregulated by HIF-2α to usurp this repression, thereby promoting EAA entry, increased $mTORC_1$ activity, and the tumorigenic effects seen under hypoxic conditions (22,45). The related elevated *in vitro* [^{18}F]FDOPA uptake but absent increased LAT1 expression under hypoxic conditions, may point to a functional effect that HIF-2α has on LAT1 in ER+ MCF7 BC cells. In addition to this, increased phosphorylation of the transporter as well as increased membrane trafficking could play roles in the elevated functionality of the transporter.

System x_c- is needed for inward transport of cystine, subsequent conversion to cysteine and then GSH, which is needed to regulate reactive oxygen species (ROS) and protect cancer cells from oxidative damage. In hypoxic conditions, there is an increased need for cystine entry by xCT to facilitate the degradation of ROS to maintain growth and anti-apoptotic effects, as was previously seen in glioma cells (46). The increased transport conducted by x_c- in MDA-MB231 in hypoxic conditions is evident here for [^{18}F]FSPG. [^{18}F]FSPG, even though a glutamate derivative, is useful in measuring x_c- cystine import as x_c- does not have the capability to distinguish between cystine and glutamate for inward directed transport (13). The decreased transport of [^{18}F]FSPG under hypoxic conditions seen in MCF10A, our control breast cell line, is

paralleled by previous data collected in mouse fibroblasts and macrophages, where hypoxia reduced x_c- protein expression and cystine uptake (47).

3.5 CONCLUSIONS

In accordance to previously reported increased functionality of LAT1 and x_c- in hypoxia, our data demonstrates that the induction of hypoxia and upregulation of HIF-1α have major effects on [^{18}F]FDOPA and [^{18}F]FSPG uptake, respectively. As for the protein expression of amino acid transporters, in opposition to previously reported upregulation under hypoxia in other forms of cancer, there was no increased expression of ASCT2, LAT1, or x_c-. Additionally, this study provides evidence that [^{18}F]FDOPA and [^{18}F]FSPG could be used as imaging agents in BC. This finding should stimulate interest in using these radiotracers to find biomarkers needed to better manage BC and allow a better guided therapy, for the right patient, at the right time.

ACKNOWLEDGEMENTS

The authors thank Dr. John Wilson, David Clendening, and Blake Lazurko from the Edmonton Radiopharmaceutical Center for ^{18}F production. The authors thank David Clendening and Blake Lazurko for preparation of [^{18}F]FDOPA. The authors are also grateful to Dan McGinn (Vivarium of the Cross Cancer Institute, Edmonton, AB, Canada) for supporting the animal work and Dr. Hans-Soenke Jans (University of Alberta) for technical help and support of the PET imaging experiments. D.K. thanks the Alberta Cancer Foundation for a Graduate Student Scholarship and the Cancer Research Institute of Northern Alberta (CRINA) for la Vie en Rose Scholarship for Breast Cancer Research. The authors also gratefully acknowledge the Dianne and Irving Kipnes Foundation for supporting this work.

AUTHOR CONTRIBUTIONS

D. Krys was responsible for cell culture, Western blot experiments, *in vitro* cell-uptake experiments , analysis, contributed to the animal experiments, and wrote the manuscript; S. Mattingly for the preparation of [^{18}F]FSPG and for the writing of [^{18}F]FSPG radiosynthesis protocol and supplemental information; D. Glubrecht for the entirety of the immunohistochemistry work; M. Wuest performed all *in vivo* PET experiments and analysis, and wrote portions of and revised the manuscript; F. Wuest was responsible for the design of the study and critically reviewed the manuscript; and all authors read and approved the final manuscript and agreed to be accountable for the integrity of the work.

3.6 SUPPLEMENTAL INFORMATION

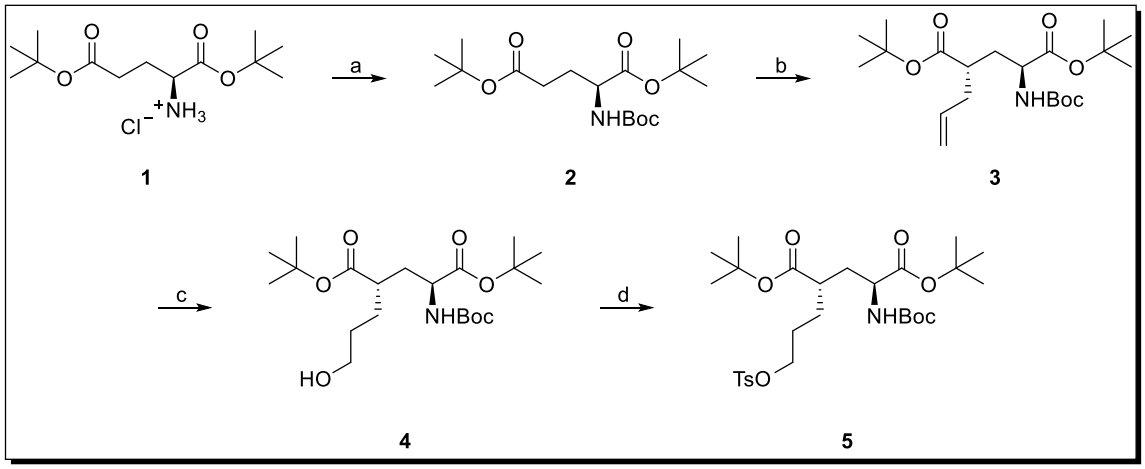

Scheme S1. Preparation of radiolabeling precursor **5.** Reagents and conditions: (a) Boc_2O, THF/ $NaHCO_3$ aq., rt, ON, quant.; (b) LiHMDS, allyl bromide THF, -78 °C, 5h, 54%; (c) 9-BBN, THF, rt, 19h, NaOH, H_2O_2, 0 °C-rt 30 min, 74%; (d) TsCl, TEA, DCM, 0 °C-rt ON, 69%.

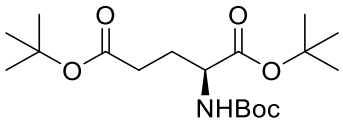

3.61 Synthesis of 1,5-di-tert-butyl (2S)-2-{[(tert-butoxy)carbonyl]amino}pentanedioate (2)

Following a procedure by Hartmann et al., (48) to a solution of L-glutamic acid di-*tert*-butyl ester hydrochloride **1** (1.00 g, 3.38 mmol, 1.0 eq.) in THF/saturated aqueous $NaHCO_3$ (1:4, 10 mL total vol.) was added di-*tert*-butyl dicarbonate (0.922 g, 4.23 mmol, 1.25 eq.). The reaction mixture was stirred at rt overnight. After dilution with 15 mL water, the aqueous mixture was extracted with EtOAc (3 x 10 mL). The combined organic layers were washed with brine (5 mL) and dried over Na_2SO_4. The solvents were removed *in vacuo* to yield an off white solid (1.22 g, quant.). Spectral properties were in agreement with literature (49). Rf = 0.55 (hexanes/EtOAc 4:1, $KMnO_4$ stain). ^{1}H NMR (600 MHz, $CDCl_3$)δppm 1.41-1.45 (m, 18H); 1.46 (s, 9H); 1.81-1.90 (m, 1H); 2.04-2.12 (m, 1H); 2.21-2.36 (m, 2H); 4.14-4.20 (m, 1H); 5.04 (d, J = 7.8 Hz, 1H).

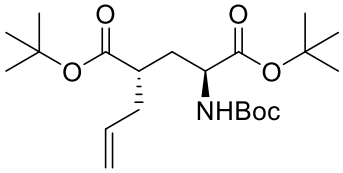

3.62 Synthesis of 1,5-di-tert-butyl (2S,4S)-2-{[(tert-butoxy)carbonyl]amino}-4-(prop-2-en-1-yl)pentanedioate (3)

Following a procedure modified from a patent protocol, (1) Boc-protected glutamic acid diester **2** (1.25 g, 3.47 mmol) was dissolved in THF (25 mL) and chilled in a dry ice/acetone bath for 30 minutes. 7.62 mL (7.62 mmols, 2.2 eq.) of 1 M lithium bis(trimethylsilyl)amide in THF was added dropwise over 2h and was stirred for 0.5 h at this temperature. (Note: rapid addition of the amine base produced undesired side products). Allyl bromide (1.26 g, 10.4 mmol, 3 eq.) was added dropwise and the reaction mixture was stirred for 2h at -78 °C. The reaction mixture was poured into 40 mL of 2N aqueous HCl. 50 mL EtOAc was added to the mixture. After

separation of the organic phase, the aqueous phase was further extracted with EtOAc (2 x 15 mL). The combined organic phases were washed with water (3 x 15 mL) until the pH was neutral, dried over Na_2SO_4 and concentrated *in vacuo*. The crude product was purified by silica column chromatography (1:9 EtOAc/hexanes, isocratic) and isolated as a clear, colorless oil (0.748 g, 54 %). Rf = 0.51 (hexanes/EtOAc 4:1, $KMnO_4$ stain). ^{1}H NMR (600 MHz, $CDCl_3$)δppm 1.37-1.52 (m, 27H); 1.83-1.90 (m, 2H); 2.27-2.36 (m, 2H); 2.39-2.45 (m, 1H); 4.10-4.17 (m, 1H); 4.87 (d, *J* = 8.4 Hz, 1H); 5.01-5.10 (m, 2H); 5.67-5.76 (m, 1H). ^{13}C NMR (150 MHz, $CDCl_3$) 28.12; 28.24; 28.45; 33.58; 36.79; 43.10; 53.27; 79.79; 80.91; 81.96; 117.49; 134.84; 155.67; 172.01; 174.52.

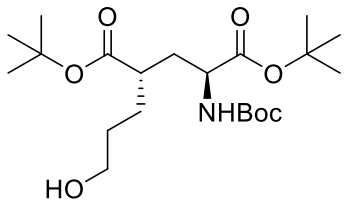

3.63 Synthesis of 1,5-di-tert-butyl (2S,4S)-2-{[(tert-butoxy)carbonyl]amino}-4-(3-hydroxypropyl)pentanedioate (4)

To a solution of alkene **3** (0.826 g, 2.07 mmol, 1.0 eq) in 5 mL THF was added 9-borabicyclo[3.3.1]nonane as a 0.5 M solution in THF (20.6 mL, 10.3 mmol, 5 eq.). The reaction was stirred at RT for 19 h. The mixture was cooled to 0 °C and stirred for 5 minutes after addition of aqueous NaOH (3.1 mL of 1N, 3.1 mmol, 1.5 eq.). H_2O_2 (3.1 mL of 30%, 27.3 mmol, 13.2 eq) was then added and the mixture was stirred for 5 min at 0 °C and a further 30 min at RT. Water (25 mL) was added and the THF was evaporated *in vacuo*. The remaining aqueous solution was extracted with EtOAc (3x 20 mL), washed with brine (2x 10 ml), dried

over Na_2SO_4 and concentrated *in vacuo.* The crude product was purified by silica column chromatography (gradient elution, 1:0 to 1:1 hexanes/EtOAc) and isolated as clear, colorless oil (0.638 g, 74%). Rf = 0.36 (hexanes/EtOAc 1:1, $KMnO_4$ stain). This product is not stable to long term storage at -20 °C. Spectral properties were in agreement with literature (27). For a similar procedure, see also Koglin *et al.* (18). ^{1}H NMR (600 MHz, $CDCl_3$)δppm 1.42-1.58 (m, 27H); 1.58-1.70 (m, 2H); 1.70-1.89 (m, 4H); 2.19 (br s, 1H); 2.33-2.40 (m, 1H); 3.57-3.68 (m, 2H); 4.15-4.23 (m, 1H); 5.00 (d, *J* = 9.0 Hz, 1H). ^{13}C NMR (150 MHz, $CDCl_3$) 27.7; 28.1; 28.2; 28.4; 29.9; 35.3; 42.4; 52.8; 61.5; 80.0; 80.8; 82.1; 155.9; 171.9; 175.1.

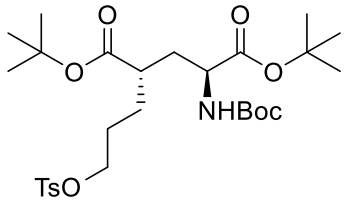

3.64 Synthesis of 1,5-di-tert-butyl (2S,4S)-2-{[(tert-butoxy)carbonyl]amino}-4-{3-[(4-methylbenzenesulfonyl)oxy]propyl}pentanedioate (5)

Following a slight modification to the reported procedure (27) alcohol **4** (0.634 g, 1.52 mmol, 1.0 eq.) was dissolved in CH_2Cl_2 (30 mL) and the solution chilled to 0 °C. Triethylamine (0.922 g, 9.11 mmol, 6.0 eq) was added, followed by *p*-toluenesulfonyl chloride (0.833 g, 4.37 mmol, 2.9 eq.) The reaction mixture was stirred at 0 °C for 2h and was allowed to come to rt overnight. The solvent was evaporated *in vacuo* and the crude product was purified by silica column chromatography (gradient elution, 1:0 to 1:1 hexanes/EtOAc) and isolated as a clear, colorless oil (0.601 g, 69%). Rf = 0.51 (hexanes/EtOAc 3:2). Spectral properties were in agreement with literature (23). ^{1}H NMR (600 MHz, $CDCl_3$)δppm 1.38-1.48 (m, 27H); 1.51-1.59 (m, 2H); 1.59-1.71 (m, 2H); 1.71-1.80 (m, 1H); 1.81-1.90 (m, 1H); 2.22-2.31 (m, 1H); 2.44 (s, 3H); 4.00 (t, *J* =

6.6 Hz, 2H); 4.03-4.10 (m, 1H); 4.84 (d, *J* = 9.0 Hz, 1H); 7.34 (d, *J* = 7.8 Hz, 2H); 7.78 (d, *J* = 8.4 Hz, 2H). ^{13}C NMR (150 MHz, $CDCl_3$) 21.6; 26.3; 27.9; 28.0; 28.2; 28.3; 34.3; 42.8; 53.1; 70.0; 79.7; 81.0; 81.9; 127.8; 129.8; 133.0; 144.7; 155.5; 171.6; 174.3.

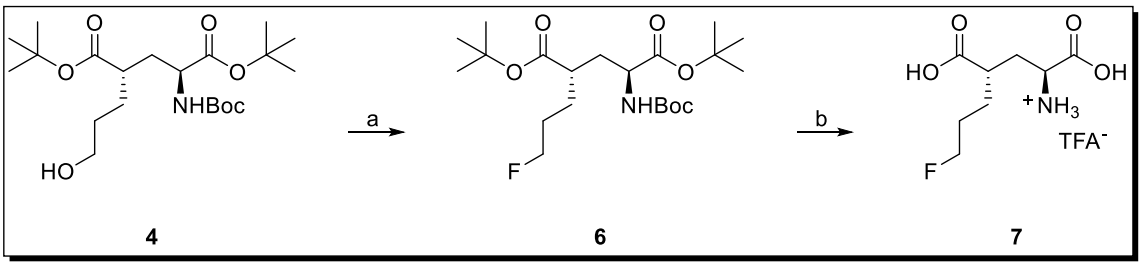

Scheme S2. Synthetic scheme for the preparation of cold standard **7.** Reagents and conditions: (a) NtF, TEA, PPHF, THF, rt, 4d, 39%; (b) 1:1 DCM/TFA, rt, 17h, 94%.

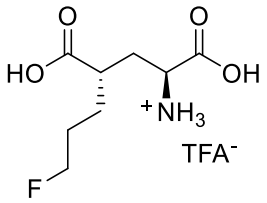

3.65 Synthesis of [19F]FSPG: (2S,4S)-4-(3-fluoropropyl)-glutamic acid (7)

Following a procedure described by Koglin *et al.* (18), alcohol **4** was dissolved in THF (2.5 mL) and triethylamine was added (0.147 g, 1.46 mmol, 6 eq.). Perfluoro-1-butansulfonyl fluoride (0.147 g, 0.486 mmol) was added followed by hydrogen fluoride pyridine (pyridine ~30 %, hydrogen fluoride ~70%, 0.042 g, ~6 eq) and the reaction was stirred at rt for 4 days. The solvent was removed *in vacuo.* The crude product **6** was purified by silica column chromatography (eluting in 9:1 hexanes:EtOAc) and isolated as a clear, colorless viscous liquid (0.040 g, 39%). ^{1}H NMR (600 MHz, $CDCl_3$)δppm 1.40-1.50 (m, 27H); 1.56-1.61 (m, 1H); 1.64-1.79 (m, 3H); 1.80-1.87 (m, 1H); 1.88-1.96 (m, 1H); 2.34-2.41 (m, 1H); 4.11-4.18 (m, 1H); 4.44 (dt, *J* = 48.0,

6.0 Hz, 2H); 4.88 (d, *J* = 9.0 Hz, 1H). ^{19}F NMR (470 MHz, CDCl3)δppm -218.7 (tt, *J* = 47.0, 24.2 Hz).

Intermediate **6** (0.030g, 0.071 mmol) was dissolved in DCM (1 mL) and TFA (1 mL) was added. The mixture was stirred at rt for 17h. The solvent was removed *in vacuo.* The crude product was purified by HPLC (Phenomenex Luna C18, gradient 1:0-1:4 H_2O+0.2% TFA/MeCN) and isolated as a white solid TFA salt (0.014g, 94%). ^{1}H NMR (600 MHz, CD_3OD)δppm 1.65-1.83 (m, 4H); 1.96-2.05 (m, 1H); 2.11-2.19 (m, 1H); 2.74-2.82 (m, 1H); 3.96 (dd, *J* = 8.7, 5.6 Hz, 1H); 4.44 (dt, *J* = 47.4, 5.4 Hz, 2H). ^{13}C NMR (150 MHz, CD_3OD) 28.9 (d, *J* = 21.0 Hz); 29.5 (d, *J* = 4.4 Hz); 33.7; 42.5; 52.5; 84.5 (d, *J* = 164.8 Hz); 171.7; 177.8. ^{19}F NMR (470 MHz, CD_3OD)δppm -220.9 (tt, *J* = 48.3, 25.4 Hz). For spectral properties of the free amine, which differ slightly from those reported here for the ammonium salt, refer to Koglin et al. (18).

3.7 REFERENCES

1. DeSantis, C. E., Ma, J., Goding Sauer, A., Newman, L. A., and Jemal, A. (2017) Breast cancer statistics, 2017, racial disparity in mortality by state. *CA. Cancer J. Clin.* **67**, 439–448

2. Tevaarwerk, A. J., Gray, R. J., Schneider, B. P., Smith, M. L., Wagner, L. I., Fetting, J. H., Davidson, N., Goldstein, L. J., Miller, K. D., and Sparano, J. A. (2013) Survival in Patients With Metastatic Recurrent Breast Cancer After Adjuvant Chemotherapy Little Evidence of Improvement Over the Past 30 Years Characteristics of Included Trials. *Cancer* **119**, 1140–1148

3. Bychkovsky, B. L. and Lin, N. U. (2019) Imaging in the evaluation and follow-up of early and advanced breast cancer : When , why , and how often? *The Breast* **31**, 318–324

4. Groheux, D., Cochet, A., Humbert, O., Alberini, J.L., Hindie, E., and Mankoff, D. (2016) ^{18}F-FDG PET/CT for Staging and Restaging of Breast Cancer. *J. Nucl. Med.* **57**, 17S–26S

5. Shen, B., Huang, T., Sun, Y., Jin, Z., and Li, X.F. (2017) Revisit ^{18}F-fluorodeoxyglucose oncology positron emission tomography: 'systems molecular imaging' of glucose metabolism. *Oncotarget* **8**, 43536–43542

6. A Alvarez, J. V., Belka, G. K., Pan, T. C., Chen, C. C., Blankemeyer, E., Alavi, A., Karp, J. S., and Chodosh, L. A. (2014) Oncogene pathway activation in mammary tumors dictates FDG-PET uptake. *Cancer Res.* **74**, 7583–7598

7. Kubota, K., Yamashita, H., and Mimori, A. (2017) Clinical Value of FDG-PET/CT for the Evaluation of Rheumatic Diseases: Rheumatoid Arthritis, Polymyalgia Rheumatica, and Relapsing Polychondritis. *Semin. Nucl. Med.* **47**, 408–424

8. Adejolu, M., Huo, L., Rohren, E., Santiago, L., and Yang, W. T. (2012) False-positive lesions mimicking breast cancer on FDG PET and PET/CT. *AJR. Am. J. Roentgenol.* **198**, W304-W314

9. Smith, B,. Schafer, X.L., Ambeskovic, A., Spencer, C.M., Land, H., and Munger, J. (2016) Addiction to Coupling of the Warburg Effect with Glutamine Catabolism in Cancer Cells. *Cell Rep.* **17**, 821–36.

10. Cha, Y.J., Kim, E.-S., and Koo, J.S. (2018) Amino Acid Transporters and Glutamine Metabolism in Breast Cancer. *Int. J. Mol. Sci.* **19**, 907

11. Jin, L., Alesi, G.N., and Kang, S. (2016) Glutaminolysis as a target for cancer therapy. *Oncogene*. **35**, 3619-3625

12. Schulte, M.L., Fu, A., Zhao, P., Li, J., Geng, L., Smith, S.T., Kondo, J., Coffey, R.J., Johnson, M.O., Rathmell, J.C., Sharick, J.T., Skala, M.C., Smith, J.A., Berlin, J., Washington, M.K., Nickels, M.L., and Manning, H.C. (2018) Pharmacological blockade of ASCT2-dependent glutamine transport leads to antitumor efficacy in preclinical models. *Nat. Med.* **24**, 194-202

13. Patel, S.A., Warren, B.A., Rhoderick, J.F., and Bridges, R.J. (2004) Differentiation of substrate and non-substrate inhibitors of transport system xc(-): an obligate exchanger of L-glutamate and L-cystine. *Neuropharmacology*. **46**, 273-284.

14. Wang, Q., and Holst, J. (2015) L-type amino acid transport and cancer : targeting the mTORC1 pathway to inhibit neoplasia. *Am. J. Cancer Res.* **5,** 1281-1294

15. Bartlett, J.M., Thomas, J., Ross, D.T., Seitz, R.S., Ring, B.Z., Beck, R.A., Pedersen, H.C., Munro, A., Kunkler, I.H., Campbell, F.M., Jack, W., Kerr, G.R., Johnstone, L., Cameron, D.A., and Chetty, U. (2010) Mammostrat ® as a tool to stratify breast cancer patients at risk of recurrence during endocrine therapy. *Breast Cancer Res.* **12**, R47-R58

16. Oka, S., Okudaira, H., Yoshida, Y., Schuster, D.M., Goodman, M.M., and Shirakami, Y. (2012) Transport mechanisms of trans-1-amino-3-fluoro[1-(14)C]cyclobutanecarboxylic acid in prostate cancer cells. *Nucl. Med. Biol.*; **39**, 109–119

17. Way, J.D., Wang, M., Hamann, I., Wuest, M., and Wuest, F. (2014) Synthesis and evaluation of 2-amino-5-(4-[(18)F]fluorophenyl)pent-4-ynoic acid ([(18)F]FPhPA): a novel (18)F-labeled amino acid for oncologic PET imaging. *Nucl. Med. Biol.* **41,** 660–669

18. Koglin, N., Mueller, A., Berndt, M., Schmitt-Willich, H., Toschi, L., Stephens, A.W., Gekeler, V., Friebe, M., and Dinkelborg, L.M. (2011) Specific PET imaging of xC- transporter activity using a ^{18}F-labeled glutamate derivative reveals a dominant pathway in tumor metabolism. *Clin. Cancer Res.* **17**, 6000-6011

19. Youland, R.S., Kitange, G.J., Peterson, T.E., Pafundi, D.H., Ramiscal, J.A., Pokorny, J.L., Giannini, C., Laack, N.N., Parney, I.F., Lowe, V.J., Brinkmann, D.H., and Sarkaria, J.N. (2013) The role of LAT1 in (18)F-DOPA uptake in malignant gliomas. *J. Neurooncol.* **111**, 11-18.

20. Semenza, G. L. (2016) The hypoxic tumor microenvironment: A driving force for breast cancer progression. *Biochim. Biophys. Acta - Mol. Cell Res.* **1863**, 382–391

21. Hamann, I., Krys, D., Glubrecht, D., Bouvet, V., Marshall, A., Vos, L., Mackey, J. R., Wuest, M., and Wuest, F. (2018) Expression and function of hexose transporters GLUT1, GLUT2, and GLUT5 in breast cancer—effects of hypoxia. *FASEB J.* **32**, 5104–5118

22. Elorza, A., Soro-Arnáiz, I., Meléndez-Rodríguez, F., Rodríguez-Vaello, V., Marsboom, G., de Cárcer, G., Acosta-Iborra, B., Albacete-Albacete, L., Ordóñez, A., Serrano-Oviedo, L., Giménez-Bachs, J.M., Vara-Vega, A., Salinas, A., Sánchez-Prieto, R., Martín del Río, R., Sánchez-Madrid, F., Malumbres, M., Landázuri, M.O., and Aragonés, J. (2012) HIF2α acts as an mTORC1 activator through the amino acid carrier SLC7A5. *Mol. Cell* **48**, 681-691.

23. Sarikaya, I. (2015) PET imaging in neurology: Alzheimer's and Parkinson's diseases. *Nucl. Med. Commun.* **36,** 775-781.

24. Minn, H., Kemppainen, J., Kauhanen, S., Forsback, S., Seppänen, M. (2014) 18F-fluorodihydroxyphenylalanine in the diagnosis of neuroendocrine tumors. **9**, 27-36.

25. Zhang, J.S., Li, L., Cheng, W. (2016) Single incision laparoscopic 90 % pancreatectomy for the treatment of persistent hyperinsulinemic hypoglycemia of infancy. *Pediatr. Surg. Int.* **32**, 1003-1007.

26. Imperiale, A., Sebag, F., Vix, M., Castinetti, F., Kessler, L., Moreau, F., Bachellier, P., Guillet, B., Namer, I.J., Mundler, O., Taïeb, D. (2015) F-FDOPA PET / CT imaging of insulinoma revisited. *Eur. J. Nucl. Med. Mol. Imaging*. **42,** 409-418.

27. Berndt, M., Schmitt-Willich, H., Friebe, M., Graham, K., Brumby, T., Hultsch, C., Wester, H.-J., Wagner, F. (2013) Method for production of F-18 labeled glutamic acid derivatives. US20130149243A1.

28. Füchtner, F., Angelberger, P., Kvaternik, H., Hammerschmidt, F., Simovc, B.P., Steinbach, J. (2002) Aspects of 6-[18F]fluoro-L-DOPA preparation: precursor synthesis, preparative HPLC purification and determination of radiochemical purity. *Nucl. Med. Biol.* **29**, 477-481.

29. Wuest, M., Kuchar, M., Sharma, S., Richter, S., Hamann, I., Wang, M., Vos, L., Mackey, J.R., Wuest, F., and Löser, R. (2015) Targeting lysyl oxidase for molecular imaging in breast cancer. *Breast Cancer Res.* **13**, 107-132

30. Liu, Y., Beyer, A., and Aebersold, R. (2016) On the Dependency of Cellular Protein Levels on mRNA Abundance. *Cell* **165**, 535–550.

31. Habermeier, A., Graf, J., Sandhöfer, B.F., Boissel, J.P., Roesch, F., and Closs, E.I. (2015) System L amino acid transporter LAT1 accumulates O-(2-fluoroethyl)-L-tyrosine (FET). *Amino Acids* **47**, 335-344.

32. Shennan, D.B., and Thomson, J. (2008) Inhibition of system L (LAT1 / CD98hc) reduces the growth of cultured human breast cancer cells. *Oncol, Rep*. **20**, 885-889

33. Kim, C.S., Cho, S.H., Chun, H.S., Lee, S.Y., Endou, H., Kanai, Y., and Kim, D.K. (2008) BCH, an inhibitor of system L amino acid transporters, induces apoptosis in cancer cells. *Biol. Pharm. Bull.* **31**, 1096–1100

34. Rosilio, C., Nebout, M., Imbert, V., Griessinger, E., Neffati, Z., Benadiba, J., Hagenbeek, T., Spits, H., Reverso, J., Ambrosetti, D., Michiels, J.F., Bailly-Maitre, B., Endou, H., Wempe, M.F., and Peyron, J.F. (2015) L-type amino-acid transporter 1 (LAT1): a therapeutic target supporting growth and survival of T-cell lymphoblastic lymphoma/T-cell acute lymphoblastic leukemia. *Leukemia* **29**, 1253-1266

35. Häfliger, P., Graff, J., Rubin, M., Stooss, A., Dettmer, M.S., Altmann, K.H., Gertsch, J., and Charles, R.P. (2018) The LAT1 inhibitor JPH203 reduces growth of thyroid carcinoma in a fully immunocompetent mouse model. *J. Exp. Clin. Cancer Res.* **37**, 234-249

36. Singh, N., Scalise, M., Galluccio, M., Wieder, M., Seidel, T., Langer, T., Indiveri, C., and Ecker, G.F. (2018) Discovery of Potent Inhibitors for the Large Neutral Amino Acid Transporter 1 (LAT1) by Structure-Based Methods. *Int. J. Mol. Sci.* **20**, 27-53

37. Yang, Y., and Yee, D. (2014) IGF-I regulates redox status in breast cancer cells by activating the amino acid transport molecule xC-. *Cancer Res.* **74,** 2295-2305

38. Habib, E., Linher-Melville, K., Lin, H.X., and Singh, G. (2015) Expression of xCT and activity of system xc(-) are regulated by NRF2 in human breast cancer cells in response to oxidative stress. *Redox. Biol.* **5,** 33-42

39. Iorns, E., Drews-Elger, K., Ward, T.M., Dean, S., Clarke, J., Berry, D., El Ashry, D., and Lippman, M. (2012) A New Mouse Model for the Study of Human Breast Cancer Metastasis. *PLoS One*. **7**, e47995

40. Sato, R., Nakano, T., Hosonaga, M., Sampetrean, O., Harigai, R., Sasaki, T., Koya, I., Okano, H., Kudoh, J., Saya, H., and Arim, Y. (2017) RNA Sequencing Analysis Reveals Interactions between Breast Cancer or Melanoma Cells and the Tissue Microenvironment during Brain Metastasis. *Biomed. Res. Int.* **2017,** 10

41. Baek, S., Choi, C.M., Ahn, S.H., Lee, J.W., Gong, G., Ryu, J.S., Oh, S.J., Bacher-Stier, C., Fels, L., Koglin, N., Hultsch, C., Schatz, C.A., Dinkelborg, L.M., Mittra, E.S., Gambhir, S.S., and Moon, D.H. (2012) Exploratory clinical trial of (4S)-4-(3-[18F]fluoropropyl)-L-glutamate for imaging xC- transporter using positron emission tomography in patients with non-small cell lung or breast cancer. *Clin. Cancer Res.* **18,** 427-437

42. Cheng, M.F., Huang, Y.Y., Ho, B.Y., Kuo, T.C., Hsin, L.W., Shiue, C.Y., Kuo, H.C., Jeng, Y.M., Yen, R.F., and Tien, Y.W. (2019) Prospective comparison of (4S)-4-(3-^{18}F-fluoropropyl)-L-glutamate versus ^{18}F-fluorodeoxyglucose PET/CT for detecting metastases from pancreatic ductal adenocarcinoma: a proof-of-concept study. *Eur. J. Nucl. Med. Mol. Imaging.* **46**, 810-820

43. Stockwell, B.R., Friedmann Angeli, J.P., Bayir, H., Bush, A.I., Conrad, M., Dixon, S.J., Fulda, S., Gascón, S., Hatzios, S.K., Kagan, V.E., Noel, K., Jiang, X., Linkermann, A., Murphy M.E., Overholtzer, M., Oyagi, A., Pagnussat, G.C., Park, J., Ran, Q., Rosenfeld, C.S., Salnikow, K., Tang, D., Torti, F.M., Torti, S.V., Toyokuni, S., Woerpel, K.A., and Zhang, D.D. (2017) Ferroptosis: A Regulated Cell Death Nexus Linking Metabolism, Redox Biology, and Disease. *Cell* **171**, 273-285

44. Sehm, T., Fan, Z., Ghoochani, A., Rauh, M., Engelhorn, T., Minakaki, G., Dörfler, A., Klucken, J., Buchfelder, M., Eyüpoglu, I.Y., and Savaskan, N. (2016) Sulfasalazine impacts on ferroptotic cell death and alleviates the tumor microenvironment and glioma-induced brain edema. *Oncotarget* **7**, 36021-36033.

45. Onishi, Y., Hiraiwa, M., Kamada, H., Iezaki, T., Yamada, T., Kaneda, K., and Hinoi, E. (2019) Hypoxia affects Slc7a5 expression through HIF-2α in differentiated neuronal cells. *FEBS Open Bio.* **9**, 241-247

46. Ogunrinu, T.A., and Sontheimer, H. (2010) Hypoxia increases the dependence of glioma cells on glutathione. *J. Biol. Chem.* **285**, 37716-37724

47. Sato, H., Kuriyama-Matsumura, K., Hashimoto, T., Sasaki, H., Wang, H., Ishii, T., Mann, G.E., and Bannai S. (2001) Effect of Oxygen on Induction of the Cystine Transporter by Bacterial Lipopolysaccharide in Mouse Peritoneal Macrophages. *J. Biol. Chem.* **276**, 10407-10412.

48. Hartmann, O., Kalesse, M. (2014) The structure elucidation and total synthesis of β-lipomycin. *Angew. Chem. Int. Ed. Engl.* **53**, 7335-7338.

49. Horikawa, R., Fujimoto, C., Yazaki, R., and Ohshima, T. (2016) μ-Oxo-Dinuclear-Iron(III)-Catalyzed O-Selective Acylation of Aliphatic and Aromatic Amino Alcohols and Transesterification of Tertiary Alcohols. *Chemistry.* **22**, 12278-12281.

CHAPTER 4

Discussion and Future Directions

4.1 Discussion

The completed project can be generalized as a probe into expression and function of SLC membrane transporters in two breast cancer cell lines and in a control breast cell line. The SLC transport family is one that is comprised of more than 300 membrane proteins, which contribute to the transport of a variety of compounds across biological membranes. In a recent review article published by Lin *et al.*, SLC transporters were highlighted as novel and potential targets for therapy, specifically in cancer (1). Nutrient transporters, such as the nucleoside and amino acid transporters investigated in my project, have come into particular interest for drug discovery, as their inhibition might have the ability to starve extremely metabolically sensitive cancer cells and induce cancer cell death (1). In the context of this research potential, my project has shown that amino acid transporters and nucleoside transporters are important in breast cancer.

In addition to roles of these specific SLC transporters in breast cancer, we also explored effects of hypoxia on these nutrient transporters. Hypoxia, which is well characterized in solid tumors, also has major consequences on cancer cell metabolic activities. By exploring effects of hypoxia on expression and function of these transporters, we are able to definitively state how they respond to hypoxic conditions. Clinically, this becomes relevant when tumors are found to be extremely hypoxic, say with a PET imaging agent such as ^{64}Cu-ATSM, and would help guide physicians based on the expected response of these transporters and whether a treatment can be determined based on this response. Minimal to no research has been done exploring effects of hypoxia on the membrane transporters studied in this project, in breast cancers.

In terms of the context outlined in the previous two paragraphs, with completion of the nucleoside and amino acid membrane transporter projects, we have addressed these shortcomings in the literature. Specifically, in relation to our hypotheses, we were able to

determine that the phenotypes, expression and function, of breast cancer cells are related to the specific PET radiotracers for that membrane transporter. Additionally, we were able to determine that hypoxia has minimal effects on nucleoside transporters in BC but has significant effects on amino acid transporter functionality. Aside from these hypotheses we were able to deduce additional conclusions from our experiments as well, such as with the transport profiles of additional nucleoside transporters in relation to [^{18}F]FLT.

Goals of the nucleoside membrane transporter study were to (1) analyze relationships between hypoxia and expression and function of nucleoside transporters hENT1 and hENT2 in breast cancer, (2) determine the effects of additional nucleoside transporters on uptake of [^{18}F]FLT, and (3) explore the utility of [^{18}F]FLT-PET in differentiating between ER(+) BC and TNBC. From those goals, the following conclusions were made based on the obtained results: i) data from the Canadian Breast Cancer Foundation Tumor Bank showed significantly higher mRNA expression of hENT2 and TK1 in breast cancer, while no differences were observed between ER(+) BC and TNBC; ii) triple-negative MDA-MB231 breast cancer cells showed higher levels of [^{18}F]FLT uptake compared to ER(+) MCF7 cells; iii) this difference was not observed in MDA-MB231 and MCF7 tumors *in vivo*; iv) in contrast to the literature which discussed a downregulation of ENT1 during hypoxia in endothelial cells (2, 3), no significant changes of hENT1, hENT2, and TK1 expression under normoxic and hypoxic conditions were found in breast cancer cells; v) besides hENT1 and hENT2, hCNT's are also important for the transport of [^{18}F]FLT into BC cells; vi) [^{18}F]FLT-PET imaging results in MDA-MB231 and MCF7 BC tumors are consistent with *in vitro* data obtained with confocal microscopy and flow cytometry experiments targeting hENT1 with FITC-labeled SAHENTA and hENT1 and hENT2 antibody, respectively.

The nucleoside membrane transporter project's main finding demonstrated that in contrast to previously reported downregulation of hENT1 expression in vascular endothelial cells during

hypoxic events such as ischemia, our data showed that the induction of hypoxia and upregulation of HIF-1α had no effect on hENT1, hENT2, TK1 expression and function in our tested breast cancer cell lines. In addition to expression based assays, with western blot, immunohistochemistry, and confocal microscopy as mentioned in the thesis objectives, we were also able to determine the functional role that the nucleoside transporters have in uptake of [^{18}F]FLT in BC. Specifically, we found primary evidence that the nucleoside transporter hENT2 and the hCNT family plays large roles in the uptake of [^{18}F]FLT in BC cells, using multiple blocking studies. This finding should stimulate interest in exploring the role of hENT2 as a biomarker in BC management and additionally spur research in finding hENT2 specific inhibitors as novel drugs for targeted therapy of BC. *In vivo* work showed that [^{18}F]FLT was poor in differentiating between MCF7 and MDA-MB231, or ER(+) and TNBC. Theoretically, the interplay of all nucleoside transporters and thymidine kinase, which is responsible for [^{18}F]FLT phosphorylation, must work together in mediating its uptake. Our findings also support that [^{18}F]FLT is not entirely representative of the uptake profile of hENT1, as was mentioned in previous studies (4, 5).

The amino acid project provided us with interesting and highly impactful results as well. The goal of the current study was to determine relationships between hypoxia and protein expression of ASCT1, ASCT2, LAT1, and x_c-, as well as relationships of hypoxia with the functionality of LAT1 and x_c- using [^{18}F]FDOPA and [^{18}F]FSPG, respectively. Based on results gathered, the following conclusions were made: 1) mRNA data did not correlate with the protein expression seen in western blot or immunohistochemistry, nor functionality of the amino acid transporters studied; 2) From ASCT1 and ASCT2 protein expression profiles, we determined that these transporters had minimal effects in providing differentiating characteristics in MCF7 and MDA-MB231 BC cell lines; 3) BC protein expression of LAT1 and *in vitro* and *in vivo* functionality of

LAT1 was seen only in ER(+) MCF7 BC cells; 4) Substantially increased protein levels and functionality of system x_c- transporter was exhibited by MDA-MB231 TNBC cells; 5) Hypoxia does not upregulate protein expression of LAT1 and x_c- but has effects on functionality as seen with increased transport of [^{18}F]FDOPA and [^{18}F]FSPG under hypoxic conditions. Though it was not my portion of the project, Dr. Mattingly was able to create an optimized method for the synthesis of [^{18}F]FSPG, which is highly useful for centres that may use this radiotracer in the future. In addition to chemistry, the main finding of the study showed that LAT1 and x_c-, in accordance with previous literature, in hypoxia via induction from HIF-1α upregulates uptake of [^{18}F]FDOPA and [^{18}F]FSPG into MCF7 and MDA-MB231 cells, respectively. Additionally, this study provides primary evidence that [^{18}F]FDOPA whose current primary use is in brain imaging and neuroendocrine tumor detection (6), can be used successfully for the imaging of ER+ BC. [^{18}F]FSPG, though previously discounted as unsuccessful for imaging of BC in a small clinical study (7), should be reconsidered as a useful imaging agent in BC, as uptake in TNBC was high and small metastatic lesions were imaged. These findings should stimulate interest in using these radiotracers to determine biomarker expression profiles in BC patients so that currently available amino acid transporter inhibitors, such as BCH (8), sulfasalazine (9), and JPH203 (10), as well as novel inhibitors could be used for better treatment of BC.

4.2 Future Directions

Through the course of this Masters research project, many possible future directions have come to the forefront. It is in my hopes that this research can progress further, with new researchers.

With the success of cancer therapies that target certain upregulated transport mechanisms in breast cancer, it only makes sense to image these transport pathways and determine whether BC patients are suitable for these treatments. Seeing that [^{18}F]FDG is the current "gold" standard for PET imaging of BC, [^{18}F]FLT, [^{18}F]FDOPA, and [^{18}F]FSPG should be used more prevalently clinically. This research should provide support for this notion, so that BC patients have a wider scope of radiotracers available to them which will provide them with a more specialized treatment plan and could potentially provide great value to the health care system.

This research has also provided evidence for the significance of amino acid and nucleoside transporters in BC. With this in mind, this should spur greater interest in exploring the determination of new potent inhibitors. Specifically, hENT2 would be a very appealing target as there are currently no specific hENT2 inhibitors. Additionally, it was determined that LAT1 plays a significant role in BC amino acid entry, therefore making it an attractive target for inhibition as well as there are also currently no specific inhibitors for this transporter. By creating potent inhibitors, it also opens up the potential to tag these molecules with radioisotopes, such as ^{18}F, which could be used for more specific PET imaging.

Finally, a broader area of research could come from access to the tumor bank and the clinical partnership with the Cross Cancer Institute at the University of Alberta. One limitation of this project are the cell lines which we use, as they are common and have been altered significantly since the beginning of their global laboratory use. Through the acquisition of tumor samples and ethical consent, a project could be created centering on culturing BC tumor cells. By doing so, a more unique library of BC cells could be created, which would allow us to more realistically

assess the connection between membrane transporter expression profiles and functionality, as it would mimic patient tumors seen clinically. With this, we could also compare the biomarker expression profiles, and evaluate the treatment plans these patients received. Any significant oversights of high transporter expression which could be treated with current therapeutics would provide further evidence as to why multiple radiotracers, such as the ones described in this thesis, should be used other than just [^{18}F]FDG to determine the metabolic profile of BC patients.

Bibliography

1. Lin, L., Yee, S.W., Kim, R.B., and Giacomini, K.M. (2015) SLC transporters as therapeutic targets : emerging opportunities. *Nat. Rev. Drug Discov.* **14**, 543-560

2. Eltzschig, H. K., Abdulla, P., Hoffman, E., Hamilton, K. E., Daniels, D., Schönfeld, C., Löffler, M., Reyes, G., Duszenko, M., Karhausen, J., Robinson, A., Westerman, K. A., Coe, I. R., and Colgan, S. P. (2005) HIF-1–dependent repression of equilibrative nucleoside transporter (ENT) in hypoxia J. Exp. Med. 202, 1493–1505

3 Casanello, P., Torres, A., Sanhueza, F., González, M., Farías, M., Gallardo, V., Pastor-Anglada, M., San Martín, R., and Sobrevia, L. (2005) Equilibrative nucleoside transporter 1 expression is downregulated by hypoxia in human umbilical vein endothelium. *Circ. Res.* **97**, 16–24

4 Paproski, R. J., Ng, A. M. L., Yao, S. Y. M., Graham, K., Young, J. D., and Cass, C. E. (2008) The Role of Human Nucleoside Transporters in Uptake of 3'-Deoxy-3'-fluorothymidine. Mol. Pharmacol. 74, 1372–1380

5 Paproski, R. J., Wuest, M., Jans, H.S., Graham, K., Gati, W. P., McQuarrie, S., McEwan, A., Mercer, J., Young, J. D., and Cass, C. E. (2010) Biodistribution and Uptake of 3'-Deoxy-3'-Fluorothymidine in ENT1-Knockout Mice and in an ENT1-Knockdown Tumor Model J. Nucl. Med. 51, 1447–1455,.

6. Youland, R.S., Kitange, G.J., Peterson, T.E., Pafundi, D.H., Ramiscal, J.A., Pokorny, J.L., Giannini, C., Laack, N.N., Parney, I.F., Lowe, V.J., Brinkmann, D.H., and Sarkaria, J.N. (2013) The role of LAT1 in (18)F-DOPA uptake in malignant gliomas. *J. Neurooncol.* **111**, 11-18.

7. Baek, S., Choi, C.M., Ahn, S.H., Lee, J.W., Gong, G., Ryu, J.S., Oh, S.J., Bacher-Stier, C., Fels, L., Koglin, N., Hultsch, C., Schatz, C.A., Dinkelborg, L.M., Mittra, E.S., Gambhir, S.S., and Moon, D.H. (2012) Exploratory clinical trial of (4S)-4-(3-[18F]fluoropropyl)-L-glutamate for imaging xC- transporter using positron emission tomography in patients with non-small cell lung or breast cancer. *Clin. Cancer Res.* **18,** 427-437

8. Kim, C.S., Cho, S.H., Chun, H.S., Lee, S.Y., Endou, H., Kanai, Y., and Kim, D.K. (2008) BCH, an inhibitor of system L amino acid transporters, induces apoptosis in cancer cells. *Biol. Pharm. Bull.* **31**, 1096–1100

9 Sehm, T., Fan, Z., Ghoochani, A., Rauh, M., Engelhorn, T., Minakaki, G., Dörfler, A., Klucken, J., Buchfelder, M., Eyüpoglu, I.Y., and Savaskan, N. (2016) Sulfasalazine impacts on ferroptotic cell death and alleviates the tumor microenvironment and glioma-induced brain edema. *Oncotarget* **7**, 36021-36033.

10. Häfliger, P., Graff, J., Rubin, M., Stooss, A., Dettmer, M.S., Altmann, K.H., Gertsch, J., and Charles, R.P. (2018) The LAT1 inhibitor JPH203 reduces growth of thyroid carcinoma in a fully immunocompetent mouse model. *J. Exp. Clin. Cancer Res.* **37**, 234-249.

Bibliography

Chapter 1

1. Ruan, K., Song, G., and Ouyang, G. (2009) Role of Hypoxia in the Hallmarks of Human Cancer. *J. Cell Biochem.* **107**, 1053-62.

2. Kakkad, S., Krishnamachary, B., Jacob, D., Pacheco-Torres, J., Goggins, E., Bharti, S.K., Penet, M.F., and Bhujwalla, Z.M. (2019) Molecular and functional imaging insights into the role of hypoxia in cancer aggression. *Cancer Metastasis Rev.* doi: 10.1007/s10555-019-09788-3.

3. Dehdashti, F. D., Rigsby, P. W. G., Mintun, M. A. M., Lewis, J. S., Siegel, B. A., and Welch, M. J. (2003) Assessing tumor hypoxia in cervical cancer by positron emission tomography with ^{60}Cu-ATSM: Relationship to therapeutic response—a preliminary report. *Int. J. Radiat. Onco.l Biol. Phys.* **55**, 1233–1238

4. Bollineni, V.R., Kerner, G.S., Pruim, J., Steenbakkers, R.J., Wiegman, E.M., Koole, M.J., de Groot, E.H., Willemsen, A.T., Luurtsema, G., Widder, J., Groen, H.J., and Langendijk, J.A. (2019) PET Imaging of Tumor Hypoxia Using 18F-Fluoroazomycin Arabinoside in Stage III – IV Non – Small Cell Lung Cancer Patients. *J. Nucl. Med.* **54**, 1175-1180

5. Lin, L., Yee, S.W., Kim, R.B., and Giacomini, K.M. (2015) SLC transporters as therapeutic targets : emerging opportunities. *Nat. Rev. Drug Discov.* **14**, 543-560

6. Rives, M., Javitch, J.A., and Wickenden, A.D. (2017) Potentiating SLC transporter activity : Emerging drug discovery opportunities. *Biochem. Pharmacol.* **135**, 1-11

7. Courtnay, R., Ngo, D.C., Malik, N., Ververis, K., Tortorella, S.M., and Karagiannis, T.C. (2015) Cancer metabolism and the Warburg effect: the role of HIF-1 and PI3K. *Mol. Biol. Rep.* **42**, 841-51

8. Liberti, M.V., and Locasale, J.W. (2016) The Warburg Effect: How Does it Benefit Cancer Cells? *Trends Biochem. Sci.* **41**, 11-218.

9. Hamann, I., Krys, D., Glubrecht, D., Bouvet, V., Marshall, A., Vos, L., Mackey, J. R., Wuest, M., and Wuest, F. (2018) Expression and function of hexose transporters GLUT1, GLUT2, and GLUT5 in breast cancer—effects of hypoxia. *FASEB J.* **32**, 5104–5118

10. Semenza, G.L. (2010) HIF-1 : upstream and downstream of cancer metabolism. *Curr. Opin. Genet. Dev.* **20**, 51-56

11. Semenza, G. L. (2016) The hypoxic tumor microenvironment: A driving force for breast cancer progression. *Biochim. Biophys. Acta - Mol. Cell Res.* **1863**, 382–391

12. Groheux, D., Cochet, A., Humbert, O., Alberini, J.L., Hindie, E., and Mankoff, D. (2016) ^{18}F-FDG PET/CT for Staging and Restaging of Breast Cancer. *J. Nucl. Med.* **57**, 17S–26S

13. Alvarez, J. V., Belka, G. K., Pan, T. C., Chen, C. C., Blankemeyer, E., Alavi, A., Karp, J. S., and Chodosh, L. A. (2014) Oncogene pathway activation in mammary tumors dictates FDG-PET uptake. *Cancer Res.* **74**, 7583–7598

14. Kubota, K., Yamashita, H., and Mimori, A. (2017) Clinical Value of FDG-PET/CT for the Evaluation of Rheumatic Diseases: Rheumatoid Arthritis, Polymyalgia Rheumatica, and Relapsing Polychondritis. *Semin. Nucl. Med.* **47**, 408–424

15. Adejolu, M., Huo, L., Rohren, E., Santiago, L., and Yang, W. T. (2012) False-positive lesions mimicking breast cancer on FDG PET and PET/CT. *AJR. Am. J. Roentgenol.* **198**, W304-W314

16. Wuest, M., Hamann, I., Bouvet, V., Glubrecht, D., Marshall, A., Trayner, B., Soueidan, O.M., Krys, D., Wagner, M., Cheeseman, C., West, F., and Wuest, F. (2018) Molecular Imaging of GLUT1 and GLUT5 in Breast Cancer : A Multitracer Positron Emission Tomography Imaging Study in Mice *Mol. Pharmacol.* **93,** 79-89

17. Young, J.D., Yao, S.Y.M., Baldwin, J.M., Cass, C.E., and Baldwin, S.A. (2013) The human concentrative and equilibrative nucleoside transporter families, SLC28 and SLC29. *Mol. Aspects Med.* **34**, 529-547.

18. Baldwin, S.A., Beal, P.R., Yao, S.Y., King, A.E., Cass, C.E., and Young, J.D. (2004) The equilibrative nucleoside transporter family, SLC29. *Pflugers Arch.* **447**, 735-743.

19. Nivillac, N.M.I., Wasal, K., Villani, D.F., Naydenova, Z., Hanna, W.J.B., and Coe, I.R. (2009) Disrupted plasma membrane localization and loss of function reveal regions of human equilibrative nucleoside transporter 1 involved in structural integrity and activity. *Biochim. Biophys. Acta.* **1788**, 2326-2334.

20. Zhang, C.C., Yan, Z., Li, W., Kuszpit, K., Painter, C.L., Zhang, Q., Lappin, P.B., Nichols, T., Lira, M.E., Affolter, T., Fahey, N.R., Cullinane, C., Spilker, M., Zasadny, K., O'Brien, P., Buckman, D., Wong, A., and Christensen, J.G. (2012) [(18)F]FLT-PET imaging does not always "light up" proliferating tumor cells. *Clin. Cancer Res.* **18**, 1303-1312.

21. Plotnik, D.A., Emerick, L.E., Krohn, K.A., Unadkat, J.D., and Schwartz, J.L. (2010) Different modes of transport for 3H-thymidine, 3H-FLT, and 3H-FMAU in proliferating and nonproliferating human tumor cells. *J. Nucl. Med.* 51, 1464-1471.

22. Paproski, R. J., Ng, A. M. L., Yao, S. Y. M., Graham, K., Young, J. D., and Cass, C. E. (2008) The Role of Human Nucleoside Transporters in Uptake of 3'-Deoxy-3'-fluorothymidine. Mol. Pharmacol. 74, 1372–1380.

23. Casanello, P., Torres, A., Sanhueza, F., González, M., Farías, M., Gallardo, V., Pastor-Anglada, M., San Martín, R., and Sobrevia, L. (2005) Equilibrative nucleoside transporter 1 expression is downregulated by hypoxia in human umbilical vein endothelium. *Circ. Res.* **97**, 16–24

24. Chaudary, N., Naydenova, Z., Shuralyova, I., and Coe, I.R. (2004) Hypoxia regulates the adenosine transporter, mENT1, in the murine cardiomyocyte cell line, HL-1. *Cardiovasc. Res.* **61**, 780-788.

25. Eltzschig, H. K., Abdulla, P., Hoffman, E., Hamilton, K. E., Daniels, D., Schönfeld, C., Löffler, M., Reyes, G., Duszenko, M., Karhausen, J., Robinson, A., Westerman, K. A., Coe, I. R., and Colgan, S. P. (2005) HIF-1–dependent repression of equilibrative nucleoside transporter (ENT) in hypoxia *J. Exp. Med.* **202**, 1493–1505

26. Morote-Garcia, J.C., Rosenberger, P., Nivillac, N.M.I., Coe. I.R., and Eltzschig, H.K. (2009) Hypoxia-inducible factor-dependent repression of equilibrative nucleoside transporter 2 attenuates mucosal inflammation during intestinal hypoxia. *Gastroenterology* **136**, 607-618.

27. Ulaner, G.A., and Schuster, D.M. (2018) Amino Acid Metabolism as a Target for Breast Cancer Imaging *PET Clin*. **13**, 437-444

28. Cha, Y.J., Kim, E.-S., and Koo, J.S. (2018) Amino Acid Transporters and Glutamine Metabolism in Breast Cancer. *Int. J. Mol. Sci.* **19**, 907

29. Jin, L., Alesi, G.N., and Kang, S. (2016) Glutaminolysis as a target for cancer therapy. *Oncogene*. **35**, 3619-3625

30. Schulte, M.L., Fu, A., Zhao, P., Li, J., Geng, L., Smith, S.T., Kondo, J., Coffey, R.J., Johnson, M.O., Rathmell, J.C., Sharick, J.T., Skala, M.C., Smith, J.A., Berlin, J., Washington, M.K., Nickels, M.L., and Manning, H.C. (2018) Pharmacological blockade of ASCT2-dependent glutamine transport leads to antitumor efficacy in preclinical models. *Nat. Med.* **24**, 194-202

31. Patel, S.A., Warren, B.A., Rhoderick, J.F., and Bridges, R.J. (2004) Differentiation of substrate and non-substrate inhibitors of transport system xc(-): an obligate exchanger of L-glutamate and L-cystine. *Neuropharmacology*. **46**, 273-284.

32. Wang, Q., and Holst, J. (2015) L-type amino acid transport and cancer : targeting the mTORC1 pathway to inhibit neoplasia. *Am. J. Cancer Res.* **5,** 1281-1294

33. Oka, S., Okudaira, H., Yoshida, Y., Schuster, D.M., Goodman, M.M., and Shirakami, Y. (2012) Transport mechanisms of trans-1-amino-3-fluoro[1-(14)C]cyclobutanecarboxylic acid in prostate cancer cells. *Nucl. Med. Biol.*; **39**, 109–119

34. Way, J.D., Wang, M., Hamann, I., Wuest, M., and Wuest, F. (2014) Synthesis and evaluation of 2-amino-5-(4-[(18)F]fluorophenyl)pent-4-ynoic acid ([(18)F]FPhPA): a novel (18)F-labeled amino acid for oncologic PET imaging. *Nucl. Med. Biol.* **41,** 660–669

35. Koglin, N., Mueller, A., Berndt, M., Schmitt-Willich, H., Toschi, L., Stephens, A.W., Gekeler, V., Friebe, M., and Dinkelborg, L.M. (2011) Specific PET imaging of xC- transporter activity using a ^{18}F-labeled glutamate derivative reveals a dominant pathway in tumor metabolism. *Clin. Cancer Res.* **17**, 6000-6011

36. Youland, R.S., Kitange, G.J., Peterson, T.E., Pafundi, D.H., Ramiscal, J.A., Pokorny, J.L., Giannini, C., Laack, N.N., Parney, I.F., Lowe, V.J., Brinkmann, D.H., and Sarkaria, J.N. (2013) The role of LAT1 in (18)F-DOPA uptake in malignant gliomas. *J. Neurooncol.* **111**, 11-18.

37. Hu, H., Takano, N., Xiang, L., Gilkes, D.M., Luo, W., and Semenza, G.L. (2014) Hypoxia-inducible factors enhance glutamate signaling in cancer cells. *Oncotarget* **5**, 8853-8868.

Chapter 2

1. DeSantis, C. E., Ma, J., Goding Sauer, A., Newman, L. A., and Jemal, A. (2017) Breast cancer statistics, 2017, racial disparity in mortality by state. *CA. Cancer J. Clin.* **67**, 439–448

2. Kabat, G. C., Ginsberg, M., Sparano, J. A., and Rohan, T. E. (2017) Risk of Recurrence and Mortality in a Multi-Ethnic Breast Cancer Population. *J. Racial Ethn. Health Disparities.* **4**, 1181–1188

3. Tevaarwerk, A. J., Gray, R. J., Schneider, B. P., Smith, M. L., Wagner, L. I., Fetting, J. H., Davidson, N., Goldstein, L. J., Miller, K. D., and Sparano, J. A. (2013) Survival in Patients With Metastatic Recurrent Breast Cancer After Adjuvant Chemotherapy Little Evidence of Improvement Over the Past 30 Years Characteristics of Included Trials. *Cancer* **119**, 1140–1148

4. Bychkovsky, B. L. and Lin, N. U. (2019) Imaging in the evaluation and follow-up of early and advanced breast cancer : When , why , and how often? *The Breast* **31**, 318–324

5. Sun, Y., Yang, Z., Zhang, Y., Xue, J., Wang, M., Shi, W., Zhu, B., Hu, S., Yao, Z., Pan, H., and Zhang, Y. (2015) The preliminary study of 16 α-[^{18}F] fluoroestradiol PET/CT in assisting the individualized treatment decisions of breast cancer patients. *PLoS One* **10**, 1–9

6. Liao, G. J., Clark, A. S., Schubert, E. K., and Mankoff, D. A. (2016) ^{18}F-Fluoroestradiol PET: Current Status and Potential Future Clinical Applications. *J. Nucl. Med.* **57**, 1269–1275

7. Mcguire, A. H., Dehdashti, F., Siegel, B. A., Lyss, A. P., Brodack, J. W., Mathias, C. J., Mintun, M. A., Katzenellenbogen, J. A., and Welch, M. J. (1991) Positron Tomographic Assessment of 16a-[^{18}F] Fluoro-17/3-Estradiol Uptake in Metastatic Breast Carcinoma. *J. Nucl. Med.* **32**, 1526–1531

8. Groheux, D., Cochet, A., Humbert, O., Alberini, J.L., Hindie, E., and Mankoff, D. (2016) ^{18}F-FDG PET/CT for Staging and Restaging of Breast Cancer. *J. Nucl. Med.* **57**, 17S–26S

9. Shen, B., Huang, T., Sun, Y., Jin, Z., and Li, X.F. (2017) Revisit ^{18}F-fluorodeoxyglucose oncology positron emission tomography: 'systems molecular imaging' of glucose metabolism. *Oncotarget* **8**, 43536–43542

10. Alvarez, J. V., Belka, G. K., Pan, T. C., Chen, C. C., Blankemeyer, E., Alavi, A., Karp, J. S., and Chodosh, L. A. (2014) Oncogene pathway activation in mammary tumors dictates FDG-PET uptake. *Cancer Res.* **74**, 7583–7598

11. Kubota, K., Yamashita, H., and Mimori, A. (2017) Clinical Value of FDG-PET/CT for the Evaluation of Rheumatic Diseases: Rheumatoid Arthritis, Polymyalgia Rheumatica, and Relapsing Polychondritis. *Semin. Nucl. Med.* **47**, 408–424

12. Adejolu, M., Huo, L., Rohren, E., Santiago, L., and Yang, W. T. (2012) False-positive lesions mimicking breast cancer on FDG PET and PET/CT. *AJR. Am. J. Roentgenol.* **198**, W304-W314

13. Toyohara, J., Waki, A., Takamatsu, S., Yonekura, Y., Magata, Y., and Fujibayashi, Y. (2002) Basis of FLT as a cell proliferation marker: Comparative uptake studies with [^{3}H]thymidine and [^{3}H]arabinothymidine, and cell-analysis in 22 asynchronously growing tumor cell lines. *Nucl. Med. Biol.* **29**, 281–287

14. Paproski, R. J., Ng, A. M. L., Yao, S. Y. M., Graham, K., Young, J. D., and Cass, C. E. (2008) The Role of Human Nucleoside Transporters in Uptake of 3'-Deoxy-3'-fluorothymidine. *Mol. Pharmacol.* **74**, 1372–1380

15. Young, J.D., Yao, S.Y., Baldwin, J.M., Cass, C.E., and Baldwin, S.A. (2013) The human concentrative and equilibrative nucleoside transporter families, SLC28 and SLC29. *Mol. Aspects Med.* **34**, 529–547

16. Pastor-Anglada, M., Cano-Soldado, P., Errasti-Murugarren, E. & Casado, F. J. SLC28 genes and concentrative nucleoside transporter (CNT) proteins. *Xenobiotica* **38,** 972–994 (2008).

17. Barthel, H., Perumal, M., Latigo, J., He, Q., Brady, F., Luthra, S. K., Price, P. M., and Aboagye E. O., (2005) The uptake of 3′-deoxy-3′-[^{18}F]fluorothymidine into L5178Y tumours in vivo is dependent on thymidine kinase 1 protein levels. *Eur. J. Nucl. Med. Mol. Imaging* **32**, 257–263

18. Semenza, G. L. (2016) The hypoxic tumor microenvironment: A driving force for breast cancer progression. *Biochim. Biophys. Acta - Mol. Cell Res.* **1863**, 382–391

19. Kumar, H. and Choi, D.K. (2015) Hypoxia Inducible Factor Pathway and Physiological Adaptation : A Cell Survival Pathway? **2015**, 1-11

20. Lee, K. E. and Simon, M. C. (2015) SnapShot: Hypoxia-Inducible Factors. *Cell* **163**, 1288

21. Masoud, G. N. and Li, W. (2015) HIF-1α pathway: Role, regulation and intervention for cancer therapy. *Acta Pharm. Sin. B* **5**, 378–389

22. Hamann, I., Krys, D., Glubrecht, D., Bouvet, V., Marshall, A., Vos, L., Mackey, J. R., Wuest, M., and Wuest, F. (2018) Expression and function of hexose transporters GLUT1, GLUT2, and GLUT5 in breast cancer—effects of hypoxia. *FASEB J.* **32**, 5104–5118

23. Eltzschig, H. K., Abdulla, P., Hoffman, E., Hamilton, K. E., Daniels, D., Schönfeld, C., Löffler, M., Reyes, G., Duszenko, M., Karhausen, J., Robinson, A., Westerman, K. A., Coe, I. R., and Colgan, S. P. (2005) HIF-1–dependent repression of equilibrative nucleoside transporter (ENT) in hypoxia *J. Exp. Med.* **202**, 1493–1505

24. Casanello, P., Torres, A., Sanhueza, F., González, M., Farías, M., Gallardo, V., Pastor-Anglada, M., San Martín, R., and Sobrevia, L. (2005) Equilibrative nucleoside transporter 1 expression is downregulated by hypoxia in human umbilical vein endothelium. *Circ. Res.* **97**, 16–24

25. Salman, S. and Nurse, C.A. (2018) Molecular Characterization of Equilibrative Nucleoside Transporters in the Rat Carotid Body and Their Regulation by Chronic Hypoxia. *Adv. Exp. Med. Biol.* **1071**, 43-50

26. Santini, D., Vincenzi, B., Fratto, M. E., Perrone, G., Raymond, L. A. I., Catalano, V., Cass, C., Ruffini, P. A., Spoto, C., Muretto, P., Rizzo, S., Muda, A. O., Mackey, J. R., Russo, A., Tonini, G., and Graziano, F. (2010) Prognostic role of human equilibrative transporter 1 (hENT1) in patients with resected gastric cancer. *J. Cell. Physiol.* **223**, 384–388

27. Mackey, J. R., Jennings, L. L., Clarke, M. L., Santos, C. L., Dabbagh, L., Vsianska, M., Koski, S. L., Coupland, R. W., Baldwin, S. A., Young, J. D., and Cass, C. E. (2002) Immunohistochemical variation of human equilibrative nucleoside transporter 1 protein in primary breast cancers *Clin. Cancer Res.* **8**, 110–116

28. Paproski, R. J., Wuest, M., Jans, H.S., Graham, K., Gati, W. P., McQuarrie, S., McEwan, A., Mercer, J., Young, J. D., and Cass, C. E. (2010) Biodistribution and Uptake of 3'-Deoxy-3'-Fluorothymidine in ENT1-Knockout Mice and in an ENT1-Knockdown Tumor Model *J. Nucl. Med.* **51**, 1447–1455,.

29. Machulla, H.J., Blocher, A., Kuntzsch, M., Piert, M., Wei, R., and Grierson, J.R. (2000) Simplified labeling approach for synthesizing 3'-deoxy-3'-[^{18}F]fluorothymidine ([^{18}F]FLT). *J. Rad. Nuc. Chem.* **243**, 843-846

30. Dehdashti, F. D., Rigsby, P. W. G., Mintun, M. A. M., Lewis, J. S., Siegel, B. A., and Welch, M. J. (2003) Assessing tumor hypoxia in cervical cancer by positron emission tomography with ^{60}Cu-ATSM: Relationship to therapeutic response—a preliminary report. *Int. J. Radiat. Onco.l Biol. Phys.* **55**, 1233–1238

31. Wuest, M., Kuchar, M., Sharma, S.K., Richter, S., Hamann, I., Wang, M., Vos. L., Mackey, J.R., Wuest, F., and Löser, R. (2015) Targeting lysyl oxidase for molecular imaging in breast cancer. *Breast Cancer Res.* **17,** 1–15

32. Robins, M. J., Peng, Y., Damaraju, V. L., Mowles, D., Barron, G., Tackaberry, T., Young, J. D., and Cass, C. E., (2010) Improved syntheses of 5′- S -(2-Aminoethyl)-6- N -(4-nitrobenzyl)- 5′-thioadenosine (SAENTA), analogues, and fluorescent probe conjugates: Analysis of cell-surface human equilibrative nucleoside transporter 1 (hENT1) levels for prediction of the antitumor efficacy of gemcitabine. *J. Med. Chem.* **53**, 6040–6053

33. Griffiths, M., Yao, S. Y. M., Abidi, F., Phillips, S. E. V., Cass, C. E., Young, J. D., and Baldwin, S. A. (1997) Molecular cloning and characterization of a nitrobenzylthioinosine-insensitive (ei) equilibrative nucleoside transporter from human placenta. *Biochem. J.* **328**, 739–743

34. Visser, F., Vickers, M. F., Ng, A. M. L., Baldwin, S. A., Young, J. D., and Cass, C. E. (2002) Mutation of residue 33 of human equilibrative nucleoside transporters 1 and 2 alters sensitivity to inhibition of transport by dilazep and dipyridamole. *J. Biol. Chem.* **277**, 395–401

35. Inic, Z., Zegarac, M., Inic, M., Markovic, I., Kozomara, Z., Djurisic, I., Inic, I., Pupic, G., and Jancic, S. (2014) Difference between Luminal A and Luminal B Subtypes According to Ki-67, Tumor Size, and Progesterone Receptor Negativity Providing Prognostic Information. *Clin. Med. Insights. Oncol.* **8**, 107–111

36. Robertson, S., Stålhammar, G., Darai-ramqvist, E., Rantalainen, M., Tobin, N. P., Bergh, J., and Hartman, J. (2018) Prognostic value of Ki67 analysed by cytology or histology in primary breast cancer. *J. Clin. Pathol.* **71**, 787–794

37. Lewis, J. S. (2007) Cu – ATSM : A radiopharmaceutical for the PET imaging of hypoxia. *Dalton. Trans*. **43**, 4893–4902

38. Moreno-bueno, G., Cano-soldado, P., and Casado, F. J. (2006) Human equilibrative nucleoside transporter-1 (hENT1) is required for the transcriptomic response of the nucleoside-derived drug 50-DFUR in breast cancer MCF7 cells. *Biochem. Pharmacol.* **72**, 1646–1656

39. Playa, H., Lewis, T. A., Ting, A., Suh, B., Muñoz, B., Matuza, R., Passer, B. J., Schreiber, S. L., and Buolamwini, J. K. (2014) Dilazep analogues for the study of equilibrative nucleoside transporters 1 and 2 (ENT1 and ENT2). *Bioorg. Med. Chem. Lett.* **24**, 5801–5804

40. Pastor-Anglada, M. and Pérez-Torras, S. (2015) Nucleoside transporter proteins as biomarkers of drug responsiveness and drug targets. *Front. Pharmacol.* **6**, 1–14

41. Plotnik, D.A., McLaughlin, L.J., Chan, J., Redmayne-Titley, J.N., Schwartz, J.L. (2011) The role of nucleoside/nucleotide transport and metabolism in the uptake and retention of 3'-fluoro-3'-deoxythymidine in human B-lymphoblast cells. *Nucl Med Biol.* **38,** 979-986

42. Ward, J.L., Sherali, A., Mo, Z.P., Tse, C.M. (2000) Kinetic and pharmacological properties of cloned human equilibrative nucleoside transporters, ENT1 and ENT2, stably expressed in nucleoside transporter-deficient PK15 cells. Ent2 exhibits a low affinity for guanosine and cytidine but a high affinity for inosine. *J. Biol. Chem.* **275**, 8375-8381

Chapter 3

1. DeSantis, C. E., Ma, J., Goding Sauer, A., Newman, L. A., and Jemal, A. (2017) Breast cancer statistics, 2017, racial disparity in mortality by state. *CA. Cancer J. Clin.* **67**, 439–448

2. Tevaarwerk, A. J., Gray, R. J., Schneider, B. P., Smith, M. L., Wagner, L. I., Fetting, J. H., Davidson, N., Goldstein, L. J., Miller, K. D., and Sparano, J. A. (2013) Survival in Patients With Metastatic Recurrent Breast Cancer After Adjuvant Chemotherapy Little Evidence of Improvement Over the Past 30 Years Characteristics of Included Trials. *Cancer* **119**, 1140–1148

3. Bychkovsky, B. L. and Lin, N. U. (2019) Imaging in the evaluation and follow-up of early and advanced breast cancer : When , why , and how often? *The Breast* **31**, 318–324

4. Groheux, D., Cochet, A., Humbert, O., Alberini, J.L., Hindie, E., and Mankoff, D. (2016) ^{18}F-FDG PET/CT for Staging and Restaging of Breast Cancer. *J. Nucl. Med.* **57**, 17S–26S

5. Shen, B., Huang, T., Sun, Y., Jin, Z., and Li, X.F. (2017) Revisit ^{18}F-fluorodeoxyglucose oncology positron emission tomography: 'systems molecular imaging' of glucose metabolism. *Oncotarget* **8**, 43536–43542

6. A Alvarez, J. V., Belka, G. K., Pan, T. C., Chen, C. C., Blankemeyer, E., Alavi, A., Karp, J. S., and Chodosh, L. A. (2014) Oncogene pathway activation in mammary tumors dictates FDG-PET uptake. *Cancer Res.* **74**, 7583–7598

7. Kubota, K., Yamashita, H., and Mimori, A. (2017) Clinical Value of FDG-PET/CT for the Evaluation of Rheumatic Diseases: Rheumatoid Arthritis, Polymyalgia Rheumatica, and Relapsing Polychondritis. *Semin. Nucl. Med.* **47**, 408–424

8. Adejolu, M., Huo, L., Rohren, E., Santiago, L., and Yang, W. T. (2012) False-positive lesions mimicking breast cancer on FDG PET and PET/CT. *AJR. Am. J. Roentgenol.* **198**, W304-W314

9. Smith, B,. Schafer, X.L., Ambeskovic, A., Spencer, C.M., Land, H., and Munger, J. (2016) Addiction to Coupling of the Warburg Effect with Glutamine Catabolism in Cancer Cells. *Cell Rep.* **17**, 821–36.

10. Cha, Y.J., Kim, E.-S., and Koo, J.S. (2018) Amino Acid Transporters and Glutamine Metabolism in Breast Cancer. *Int. J. Mol. Sci.* **19**, 907

11. Jin, L., Alesi, G.N., and Kang, S. (2016) Glutaminolysis as a target for cancer therapy. *Oncogene*. **35**, 3619-3625

12. Schulte, M.L., Fu, A., Zhao, P., Li, J., Geng, L., Smith, S.T., Kondo, J., Coffey, R.J., Johnson, M.O., Rathmell, J.C., Sharick, J.T., Skala, M.C., Smith, J.A., Berlin, J., Washington, M.K., Nickels, M.L., and Manning, H.C. (2018) Pharmacological blockade of ASCT2-dependent glutamine transport leads to antitumor efficacy in preclinical models. *Nat. Med.* **24**, 194-202

13. Patel, S.A., Warren, B.A., Rhoderick, J.F., and Bridges, R.J. (2004) Differentiation of substrate and non-substrate inhibitors of transport system xc(-): an obligate exchanger of L-glutamate and L-cystine. *Neuropharmacology*. **46**, 273-284.

14. Wang, Q., and Holst, J. (2015) L-type amino acid transport and cancer : targeting the mTORC1 pathway to inhibit neoplasia. *Am. J. Cancer Res.* **5,** 1281-1294

15. Bartlett, J.M., Thomas, J., Ross, D.T., Seitz, R.S., Ring, B.Z., Beck, R.A., Pedersen, H.C., Munro, A., Kunkler, I.H., Campbell, F.M., Jack, W., Kerr, G.R., Johnstone, L., Cameron, D.A., and Chetty, U. (2010) Mammostrat ® as a tool to stratify breast cancer patients at risk of recurrence during endocrine therapy. *Breast Cancer Res.* **12**, R47-R58

16. Oka, S., Okudaira, H., Yoshida, Y., Schuster, D.M., Goodman, M.M., and Shirakami, Y. (2012) Transport mechanisms of trans-1-amino-3-fluoro[1-(14)C]cyclobutanecarboxylic acid in prostate cancer cells. *Nucl. Med. Biol.*; **39**, 109–119

17. Way, J.D., Wang, M., Hamann, I., Wuest, M., and Wuest, F. (2014) Synthesis and evaluation of 2-amino-5-(4-[(18)F]fluorophenyl)pent-4-ynoic acid ([(18)F]FPhPA): a novel (18)F-labeled amino acid for oncologic PET imaging. *Nucl. Med. Biol.* **41,** 660–669

18. Koglin, N., Mueller, A., Berndt, M., Schmitt-Willich, H., Toschi, L., Stephens, A.W., Gekeler, V., Friebe, M., and Dinkelborg, L.M. (2011) Specific PET imaging of xC- transporter activity using a ^{18}F-labeled glutamate derivative reveals a dominant pathway in tumor metabolism. *Clin. Cancer Res.* **17**, 6000-6011

19. Youland, R.S., Kitange, G.J., Peterson, T.E., Pafundi, D.H., Ramiscal, J.A., Pokorny, J.L., Giannini, C., Laack, N.N., Parney, I.F., Lowe, V.J., Brinkmann, D.H., and Sarkaria, J.N. (2013) The role of LAT1 in (18)F-DOPA uptake in malignant gliomas. *J. Neurooncol.* **111**, 11-18.

20. Semenza, G. L. (2016) The hypoxic tumor microenvironment: A driving force for breast cancer progression. *Biochim. Biophys. Acta - Mol. Cell Res.* **1863**, 382–391

21. Hamann, I., Krys, D., Glubrecht, D., Bouvet, V., Marshall, A., Vos, L., Mackey, J. R., Wuest, M., and Wuest, F. (2018) Expression and function of hexose transporters GLUT1, GLUT2, and GLUT5 in breast cancer—effects of hypoxia. *FASEB J.* **32**, 5104–5118

22. Elorza, A., Soro-Arnáiz, I., Meléndez-Rodríguez, F., Rodríguez-Vaello, V., Marsboom, G., de Cárcer, G., Acosta-Iborra, B., Albacete-Albacete, L., Ordóñez, A., Serrano-Oviedo, L., Giménez-Bachs, J.M., Vara-Vega, A., Salinas, A., Sánchez-Prieto, R., Martín del Río, R., Sánchez-Madrid, F., Malumbres, M., Landázuri, M.O., and Aragonés, J. (2012) HIF2α acts as an mTORC1 activator through the amino acid carrier SLC7A5. *Mol. Cell* **48**, 681-691.

23. Sarikaya, I. (2015) PET imaging in neurology: Alzheimer's and Parkinson's diseases. *Nucl. Med. Commun.* **36,** 775-781.

24. Minn, H., Kemppainen, J., Kauhanen, S., Forsback, S., Seppänen, M. (2014) 18F-fluorodihydroxyphenylalanine in the diagnosis of neuroendocrine tumors. **9**, 27-36.

25. Zhang, J.S., Li, L., Cheng, W. (2016) Single incision laparoscopic 90 % pancreatectomy for the treatment of persistent hyperinsulinemic hypoglycemia of infancy. *Pediatr. Surg. Int.* **32**, 1003-1007.

26. Imperiale, A., Sebag, F., Vix, M., Castinetti, F., Kessler, L., Moreau, F., Bachellier, P., Guillet, B., Namer, I.J., Mundler, O., Taïeb, D. (2015) F-FDOPA PET / CT imaging of insulinoma revisited. *Eur. J. Nucl. Med. Mol. Imaging*. **42,** 409-418.

27. Berndt, M., Schmitt-Willich, H., Friebe, M., Graham, K., Brumby, T., Hultsch, C., Wester, H.-J., Wagner, F. (2013) Method for production of F-18 labeled glutamic acid derivatives. US20130149243A1.

28. Füchtner, F., Angelberger, P., Kvaternik, H., Hammerschmidt, F., Simovc, B.P., Steinbach, J. (2002) Aspects of 6-[18F]fluoro-L-DOPA preparation: precursor synthesis, preparative HPLC purification and determination of radiochemical purity. *Nucl. Med. Biol.* **29**, 477-481.

29. Wuest, M., Kuchar, M., Sharma, S., Richter, S., Hamann, I., Wang, M., Vos, L., Mackey, J.R., Wuest, F., and Löser, R. (2015) Targeting lysyl oxidase for molecular imaging in breast cancer. *Breast Cancer Res.* **13**, 107-132

30. Liu, Y., Beyer, A., and Aebersold, R. (2016) On the Dependency of Cellular Protein Levels on mRNA Abundance. *Cell* **165**, 535–550.

31. Habermeier, A., Graf, J., Sandhöfer, B.F., Boissel, J.P., Roesch, F., and Closs, E.I. (2015) System L amino acid transporter LAT1 accumulates O-(2-fluoroethyl)-L-tyrosine (FET). *Amino Acids* **47**, 335-344.

32. Shennan, D.B., and Thomson, J. (2008) Inhibition of system L (LAT1 / CD98hc) reduces the growth of cultured human breast cancer cells. *Oncol, Rep*. **20**, 885-889

33. Kim, C.S., Cho, S.H., Chun, H.S., Lee, S.Y., Endou, H., Kanai, Y., and Kim, D.K. (2008) BCH, an inhibitor of system L amino acid transporters, induces apoptosis in cancer cells. *Biol. Pharm. Bull.* **31**, 1096–1100

34. Rosilio, C., Nebout, M., Imbert, V., Griessinger, E., Neffati, Z., Benadiba, J., Hagenbeek, T., Spits, H., Reverso, J., Ambrosetti, D., Michiels, J.F., Bailly-Maitre, B., Endou, H., Wempe, M.F., and Peyron, J.F. (2015) L-type amino-acid transporter 1 (LAT1): a therapeutic target supporting growth and survival of T-cell lymphoblastic lymphoma/T-cell acute lymphoblastic leukemia. *Leukemia* **29**, 1253-1266

35. Häfliger, P., Graff, J., Rubin, M., Stooss, A., Dettmer, M.S., Altmann, K.H., Gertsch, J., and Charles, R.P. (2018) The LAT1 inhibitor JPH203 reduces growth of thyroid carcinoma in a fully immunocompetent mouse model. *J. Exp. Clin. Cancer Res.* **37**, 234-249

36. Singh, N., Scalise, M., Galluccio, M., Wieder, M., Seidel, T., Langer, T., Indiveri, C., and Ecker, G.F. (2018) Discovery of Potent Inhibitors for the Large Neutral Amino Acid Transporter 1 (LAT1) by Structure-Based Methods. *Int. J. Mol. Sci.* **20**, 27-53

37. Yang, Y., and Yee, D. (2014) IGF-I regulates redox status in breast cancer cells by activating the amino acid transport molecule xC-. *Cancer Res.* **74,** 2295-2305

38. Habib, E., Linher-Melville, K., Lin, H.X., and Singh, G. (2015) Expression of xCT and activity of system xc(-) are regulated by NRF2 in human breast cancer cells in response to oxidative stress. *Redox. Biol.* **5,** 33-42

39. Iorns, E., Drews-Elger, K., Ward, T.M., Dean, S., Clarke, J., Berry, D., El Ashry, D., and Lippman, M. (2012) A New Mouse Model for the Study of Human Breast Cancer Metastasis. *PLoS One*. **7**, e47995

40. Sato, R., Nakano, T., Hosonaga, M., Sampetrean, O., Harigai, R., Sasaki, T., Koya, I., Okano, H., Kudoh, J., Saya, H., and Arim, Y. (2017) RNA Sequencing Analysis Reveals Interactions between Breast Cancer or Melanoma Cells and the Tissue Microenvironment during Brain Metastasis. *Biomed. Res. Int.* **2017,** 10

41. Baek, S., Choi, C.M., Ahn, S.H., Lee, J.W., Gong, G., Ryu, J.S., Oh, S.J., Bacher-Stier, C., Fels, L., Koglin, N., Hultsch, C., Schatz, C.A., Dinkelborg, L.M., Mittra, E.S., Gambhir, S.S., and Moon, D.H. (2012) Exploratory clinical trial of (4S)-4-(3-[18F]fluoropropyl)-L-glutamate for imaging xC- transporter using positron emission tomography in patients with non-small cell lung or breast cancer. *Clin. Cancer Res.* **18,** 427-437

42. Cheng, M.F., Huang, Y.Y., Ho, B.Y., Kuo, T.C., Hsin, L.W., Shiue, C.Y., Kuo, H.C., Jeng, Y.M., Yen, R.F., and Tien, Y.W. (2019) Prospective comparison of (4S)-4-(3-^{18}F-fluoropropyl)-L-glutamate versus ^{18}F-fluorodeoxyglucose PET/CT for detecting metastases from pancreatic ductal adenocarcinoma: a proof-of-concept study. *Eur. J. Nucl. Med. Mol. Imaging.* **46**, 810-820

43. Stockwell, B.R., Friedmann Angeli, J.P., Bayir, H., Bush, A.I., Conrad, M., Dixon, S.J., Fulda, S., Gascón, S., Hatzios, S.K., Kagan, V.E., Noel, K., Jiang, X., Linkermann, A., Murphy M.E., Overholtzer, M., Oyagi, A., Pagnussat, G.C., Park, J., Ran, Q., Rosenfeld, C.S., Salnikow, K., Tang, D., Torti, F.M., Torti, S.V., Toyokuni, S., Woerpel, K.A., and Zhang, D.D. (2017) Ferroptosis: A Regulated Cell Death Nexus Linking Metabolism, Redox Biology, and Disease. *Cell* **171**, 273-285

44. Sehm, T., Fan, Z., Ghoochani, A., Rauh, M., Engelhorn, T., Minakaki, G., Dörfler, A., Klucken, J., Buchfelder, M., Eyüpoglu, I.Y., and Savaskan, N. (2016) Sulfasalazine impacts on ferroptotic cell death and alleviates the tumor microenvironment and glioma-induced brain edema. *Oncotarget* **7**, 36021-36033.

45. Onishi, Y., Hiraiwa, M., Kamada, H., Iezaki, T., Yamada, T., Kaneda, K., and Hinoi, E. (2019) Hypoxia affects Slc7a5 expression through HIF-2α in differentiated neuronal cells. *FEBS Open Bio.* **9**, 241-247

46. Ogunrinu, T.A., and Sontheimer, H. (2010) Hypoxia increases the dependence of glioma cells on glutathione. *J. Biol. Chem.* **285**, 37716-37724

47. Sato, H., Kuriyama-Matsumura, K., Hashimoto, T., Sasaki, H., Wang, H., Ishii, T., Mann, G.E., and Bannai S. (2001) Effect of Oxygen on Induction of the Cystine Transporter by Bacterial Lipopolysaccharide in Mouse Peritoneal Macrophages. *J. Biol. Chem.* **276**, 10407-10412.

48. Hartmann, O., Kalesse, M. (2014) The structure elucidation and total synthesis of β-lipomycin. *Angew. Chem. Int. Ed. Engl.* **53**, 7335-7338.

49. Horikawa, R., Fujimoto, C., Yazaki, R., and Ohshima, T. (2016) μ-Oxo-Dinuclear-Iron(III)-Catalyzed O-Selective Acylation of Aliphatic and Aromatic Amino Alcohols and Transesterification of Tertiary Alcohols. *Chemistry.* **22**, 12278-12281.

Chapter 4

1. Lin, L., Yee, S.W., Kim, R.B., and Giacomini, K.M. (2015) SLC transporters as therapeutic targets : emerging opportunities. *Nat. Rev. Drug Discov.* **14**, 543-560

2. Eltzschig, H. K., Abdulla, P., Hoffman, E., Hamilton, K. E., Daniels, D., Schönfeld, C., Löffler, M., Reyes, G., Duszenko, M., Karhausen, J., Robinson, A., Westerman, K. A., Coe, I. R., and Colgan, S. P. (2005) HIF-1–dependent repression of equilibrative nucleoside transporter (ENT) in hypoxia J. Exp. Med. **202**, 1493–1505

3 Casanello, P., Torres, A., Sanhueza, F., González, M., Farías, M., Gallardo, V., Pastor-Anglada, M., San Martín, R., and Sobrevia, L. (2005) Equilibrative nucleoside transporter 1 expression is downregulated by hypoxia in human umbilical vein endothelium. *Circ. Res.* **97**, 16–24

4 Paproski, R. J., Ng, A. M. L., Yao, S. Y. M., Graham, K., Young, J. D., and Cass, C. E. (2008) The Role of Human Nucleoside Transporters in Uptake of 3'-Deoxy-3'-fluorothymidine. Mol. Pharmacol. **74**, 1372–1380

5 Paproski, R. J., Wuest, M., Jans, H.S., Graham, K., Gati, W. P., McQuarrie, S., McEwan, A., Mercer, J., Young, J. D., and Cass, C. E. (2010) Biodistribution and Uptake of 3'-Deoxy-3'-Fluorothymidine in ENT1-Knockout Mice and in an ENT1-Knockdown Tumor Model J. Nucl. Med. **51**, 1447–1455,.

6. Youland, R.S., Kitange, G.J., Peterson, T.E., Pafundi, D.H., Ramiscal, J.A., Pokorny, J.L., Giannini, C., Laack, N.N., Parney, I.F., Lowe, V.J., Brinkmann, D.H., and Sarkaria, J.N. (2013) The role of LAT1 in (18)F-DOPA uptake in malignant gliomas. *J. Neurooncol.* **111**, 11-18.

7. Baek S, Choi CM, Ahn SH, Lee JW, Gong G, Ryu JS, Oh SJ, Bacher-Stier C, Fels L, Koglin N, Hultsch C, Schatz CA, Dinkelborg LM, Mittra ES, Gambhir SS, and Moon DH. Exploratory clinical trial of (4S)-4-(3-[18F]fluoropropyl)-L-glutamate for imaging xC- transporter using positron emission tomography in patients with non-small cell lung or breast cancer. Clin Cancer Res 2012;18:427-437

8. Kim, C.S., Cho, S.H., Chun, H.S., Lee, S.Y., Endou, H., Kanai, Y., and Kim, D.K. (2008) BCH, an inhibitor of system L amino acid transporters, induces apoptosis in cancer cells. *Biol. Pharm. Bull.* **31**, 1096–1100

9. Sehm, T., Fan, Z., Ghoochani, A., Rauh, M., Engelhorn, T., Minakaki, G., Dörfler, A., Klucken, J., Buchfelder, M., Eyüpoglu, I.Y., and Savaskan, N. (2016) Sulfasalazine impacts on ferroptotic cell death and alleviates the tumor microenvironment and glioma-induced brain edema. *Oncotarget* **7**, 36021-36033.

10. Häfliger, P., Graff, J., Rubin, M., Stooss, A., Dettmer, M.S., Altmann, K.H., Gertsch, J., and Charles, R.P. (2018) The LAT1 inhibitor JPH203 reduces growth of thyroid carcinoma in a fully immunocompetent mouse model. *J. Exp. Clin. Cancer Res.* **37**, 234-249.